ADSORPTION OF BRANCHED POLYMER CHAINS ONTO SOLID SUBSTRATES

by

Sümeyye Özer

B.S., Teaching Chemistry, Boğaziçi University, 2016

Submitted to the Institute for Graduate Studies in

Science and Engineering in partial fulfillment of

the requirements for the degree of

Master of Science

Graduate Program in Chemistry Boğaziçi University

2019

Aileme…

ACKNOWLEDGEMENTS

This thesis would not have been possible without the help, support and guidance of many people. Firstly, I would like to thank Assoc. Prof. Bülent Akgün for allowing me to work in the research laboratory in the last year of my undergraduate degree and to allow this adventure to continue with the master's degree. I've been motivated to pass all the obstacles in order not to frustrate his trust in me and he was always tolerant and understanding towards me. It is a pleasure for me to express my sincerest gratitude to him for his endless guidance, encouragement, and advice since I met with him.

I would like to thank my thesis committee members Prof. Dr. Duygu Avcı and Prof. Dr. Tarık Eren for giving their valuable time for my thesis. I would also like to thank members of KUYTAM, Koç University namely Assoc. Prof. Uğur Ünal, Dr. Barış Yağcı, Dr. Amir Motallebzadeh and Dr. Ceren Kenar for letting me use various instruments at the center. This opportunity gave me valuable experience and I am always thankful for being able to do this.

I would also thank all the members of Akgün Lab. Especially Ayşe, Emre, and Çağatay for their friendship and help in experiments. Thank you so much for the great work environment, we shared great laughs. It was a precious time that I will never forget.

Besides, I would like to thank my friend Şeyda for always taking care of me in every aspect of my life at every moment. Ebrar and Esma for their numerous visits to the lab to give positive energy and arranging all of our plans according to my experiment schedule. I would like to thank my friend Seda for her lovely support and friendship and Refia for her valuable help during lessons and thesis.

Finally, my biggest appreciations go to my beloved family. I would like to thank my mother Fatma, my father Ali, my sister Zehra and my brother Mehmet for being always there for me. Their unconditional love and endless support let me focus only on my research during this period. Without their support, I would not be able to complete my work.

ABSTRACT

ADSORPTION OF BRANCHED POLYMER CHAINS ONTO SOLID SUBSTRATES

Polymer thin films have a wide range of applications in photovoltaic materials, biomedical coatings, and nanolithography. Thin films are prepared using either solution or melt deposition techniques in which residual stresses are formed during the deposition. Annealing process above glass transition temperature (Tg) of polymers to remove the residual solvent whereas some of the polymer chains to adsorb onto the surface. Presence of adsorbed polymer layer in thin films cause deviations from bulk behavior in physical properties. In earlier studies, segment-substrate interactions are varied to manipulate the enthalpic effect which in general favors adsorption. When each segment pins to the substrate, polymer chains lose conformational entropy which works against adsorption.

In this study, we have elucidated the role of entropic effect by varying the polymer architecture on the structure and growth kinetics of adsorbed layer by ellipsometry, X-ray reflectivity, and atomic force microscopy. Linear polystyrene (PS), 4-arm star PS, comb PS, and centipede PS of similar total molecular weight are used on hydrophilic SiOx and hydrophobic SiH to determine the effect of architecture on adsorption. Quality of the leaching solvent is also investigated for short and long leaching times.

Our results demonstrate that the normalized layer thickness increases as the branching increases. Centipede PS always adsorb to give the thickest layers, whereas linear PS forms the thinnest adsorbed layers. For all the polymers since the enthalpic interactions are the same, the difference is the result of a reduction in the entropic loss for more branched architectures. All polymers yield thicker adsorbed layers on SiH surfaces than on SiOx surfaces due to stronger segment-substrate interactions. Toluene is found to be a better solvent for leaching than chloroform despite the opposite claims in the literature. For the first time, we have shown that just modifying the entropic contribution through polymer architecture opens up a new path to control the formation of adsorbed polymer layers.

ÖZET

DALLANMIŞ POLİMER ZİNCİRLERİNİN KATI ALTTAŞ YÜZEYİNE GERİ DÖNÜŞÜMSÜZ ADSORPSİYONU

İnce polimer filmler fotovoltaik malzemeler, biyomedikal kaplamalar, nanolitografi ve benzeri birçok uygulamada kullanılmaktadır. Filmler hazırlanma sürecinde iken oluşan artık stres ve uzaklaştırılamayan çözücüden kurtulmak için gerçekleştirilen tavlama işlemi bazı polimer zincirleri yüzeye tersinmez olarak adsorbe olmasına ve fiziksel özelliklerin yığın halindeki değerlerinden sapmasına sebep olur. Şimdiye dek yapılan çalışmalarda entalpik etkinin kuvveti değiştirilmiştir. Her bir segment alttaş ile etkileştiğinde polimer zincirleri alttaşa daha fazla mıhlanmakta ve bu sebeple de konformasyonel entropi azalarak adzorplanmaya karşı bir etki oluşturmaktadır.

Bu çalışmada polimer mimarisi sistematik olarak değiştirilerek entropik kaybın adsorbe tabakanın oluşum kinetiği ve yapısını nasıl etkilediği elipsometre, X-ışınları yansıma, ve atomik kuvvet mikroskopu kullanılarak belirlenmiştir. Benzer toplam moleküler ağırlığa sahip lineer polistiren (PS), 4-kollu yıldız PS, tarak PS ve sentiped PS zincirleri hidrofilik SiOx ve hidrofobik SiH yüzeyine adsorbe edilerek polimer mimarisinin adsorbe zincir tabakasına etkileri kısa ve uzun yıkama süreçleri için belirlenmiştir.

Dallanma arttıkça normalize tabaka kalınlığının her iki alttaş yüzeyinde de artması entalpik katkı sabit olduğundan entropik kayıptaki farklara bağlanmıştır. Dallanmış polimerler lineer zincirlere göre yığın halinde daha az konformasyonel entropiye sahip olduğu için kayıpları daha az olmuştur. Tüm polimerler hidrofobik SiH yüzeyinde hidrofilik SiOx yüzeyine göre daha kalın tabakaları daha kısa sürelerde oluşturmuştur. SiH üzerinde adsorbe olmuş tarak PS zincirleri hariç, tüm adsorbe tabakalar yığın yoğunluğuna sahip tek bir tabaka ile modellenmiştir. Toluen'in literatürde belirtilenin aksine adsorbe olmamış zincirleri uzaklaştırmak için kloroformdan daha iyi bir çözücü olduğu tespit edilmiştir. Bu bulguların ışığında dallanma yani sadece entropik faktörler kullanılarak adsorbe tabakanın oluşumunun kontrol edilebileceği ilk defa bu çalışmada gösterilmiştir.

TABLE OF CONTENT

LIST OF FIGURES

LIST OF TABLES

LIST OF ACRONYMS/ABBREVIATION

AFM	Atomic Force Microscopy
ATR-FTIR	Attenuated Total Reflectance - Fourier Transform Infrared
CO_2	Carbon dioxide
D_{eff}	Effective Diffusion Coefficient
DLS	Dynamic Light Scattering
DOAP	Division of Amplitudes Polarimeter
DSC	Differential Scanning Calorimeter
H_2O_2	Hydrogen Peroxide
H_2SO_4	Sulfuric Acid
HF	Hydrofluoric Acid
IAL	Irreversibly Adsorbed Layer
LDS	Local Dielectric Spectroscopy
M_n	Number Average Molecular Weight
M_W	Weight Average Molecular Weight
N	Number of Repeating Unit
NR	Neutron Reflectivity
PDI	Polydispersity Index
PMMA	Poly(methyl methacrylate)
PS	Polystyrene
Ra	Roughness Average
Rg	Radius of Gyration
Rh	Hydrodynamic Radius

Rq	Root Mean Square Roughness
SiH	Passivated Silicon
SiOx	Silicon Oxide
SLD	Scattering Length Density
Tg	Glass Transition Temperature
UV	Ultraviolet
UV / O_3	Ultraviolet / Ozone
XPCS	X-ray Photon Correlation Spectroscopy
XPS	X-ray photoelectron spectroscopy
XR	X-ray

1. INTRODUCTION

1.1. Applications of Thin Polymer Films

Polymers have been used in a wide variety of areas because of their excellent properties such as light weight, high mechanical and dielectric strength, high chemical resistance and low manufacturing cost. These properties can be tuned by altering the molecular building blocks and processing conditions. This unprecedented flexibility in designing materials resulted in the replacement of many traditional metallic or ceramic materials with their polymer counterparts.

Applying polymeric materials in thin film geometry opens up new directions for high-tech materials such as in organic photovoltaic materials [1], water filtration membranes [2], biomedical coatings [3], nanolithography [4], tissue engineering [5] and many others. To create such thin films only micrograms of complex polymeric materials are enough, and this reduces the manufacturing cost dramatically.

Controlling the dynamics and stability of thin films in nanoscale devices has a vital importance to obtain maximum efficiency and maintain their performance over a long time period. It is well known that physical properties of polymer thin films deviate from their bulk behavior due to existence of adsorbed polymer chains on the substrate. Therefore, in recent years, there is a huge interest to understand formation and structure of adsorbed polymer layers from solution and melt.

1.2. Formation of Adsorbed Layer

In the above-mentioned applications, thin polymer films are coated on substrates using solution casting, spin coating, or spraying. To reach equilibrium and to eliminate residual stresses and solvents, films are annealed above their glass transition temperature (T_g). During the annealing process, some of the polymer chains within the film irreversibly

adsorb onto substrate. Adsorption does not only happen for films in the melt state. On the contrary, most of the early literature has dealt with the adsorption of polymer chains from solution at room temperature. When a substrate is placed in a polymer solution, if dissolved polymer chains have more favorable surface-segment interaction with the particles or the substrate than the solvent, chains will adsorb to the surface. Irreversibly adsorbed layers (IAL) can be obtained either in solution or in melt. For linear polymers, formation of IAL follows the same thermodynamic principles in both media. However, in solution the number of components involved is larger and additional Flory-Huggins interaction parameters play an important role. In solution chains adsorb and desorb faster and IAL reaches dynamic equilibrium much faster than that in melt.

Polymer adsorption in solution is a well-studied topic both theoretically and experimentally. From theoretical perspective, it was hard to take into account all contributions such as solvent-polymer interactions, chain-chain contribution and especially segment distribution near to substrate. Earlier theoretical work used assumptions to make simplifications in the calculations such as using dilute and good solvent conditions. Therefore, they claimed there is no reason to take polymer-polymer interactions into account. However, formation of an adsorbed layer necessitates the polymer-polymer interactions within the layer. Theories of Silberberg [6] and Hoeve [7] considered the interactions between the polymer chains but they had specific assumptions about the segment density distribution which neglect the contribution of tails. Later Roe [8] has developed more sophisticated theory and calculated the segment density profile near the surface but his theory simplified the contributions from each segment to be equal independent of the distance from the substrate and he did not calculate distribution of different conformations.

The most complete theoretical model is developed by Schuetjens and Fleer [9]. In this theory, polymer adsorption is presented using quasi-crystalline lattice model. They were able to calculate number of chains in train, tail and loop conformations in equilibrium. These conformations are shown in Figure 1.1. Adsorbed segments of the polymer chain are called as trains and the non-adsorbed segments between the pinned segments are called as loops. Free ends of the chains are called as tails. They found that the segment density decays exponentially close to the substrate and the decay is much slower as the distance from the

substrate becomes larger. They explained the segment density distribution with large fraction of dangling tails in the adsorbed layer.

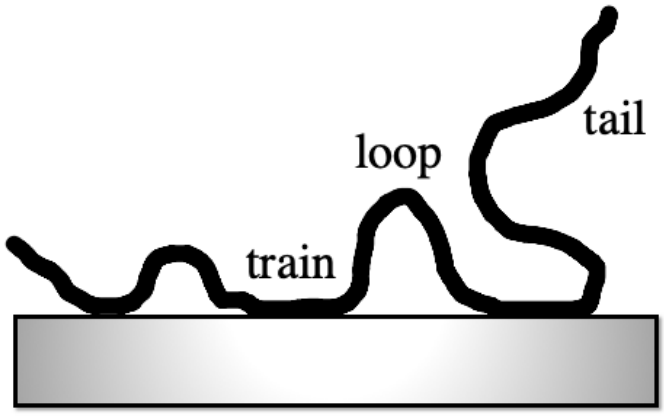

Figure 1. 1. Conformations of an adsorbed polymer chain on a solid substrate.

There are two main factors that govern the adsorption process; enthalpic gain and entropic loss[10]. Polymer chains can only adsorb to the substrate if the segment–surface interactions are stronger than solvent-substrate interactions in solution or if there are attractive interactions between polymer segments and substrate in melt. However, when the chain segments are pinned to the substrate, chain movements are restricted and as a result polymer chains cannot search all the available conformations in bulk. This causes a decrease in the conformational entropy of the chains. Therefore, the balance between entropic loss and enthalpic gain mandates the equilibrium structure of the adsorbed polymer layer. If segmental adsorption energy is low, adsorbed segments may gain enough energy by thermal motion or solvent-polymer interaction and desorb from the substrate. Polymer desorption happens in solution and at equilibrium, rates of adsorption and desorption are equal. In melt, desorption is more difficult to observe unless another miscible polymer with stronger segment-substrate interaction is brought into contact with the adsorbed polymer layer for a long period of time above the T_g of both polymers.

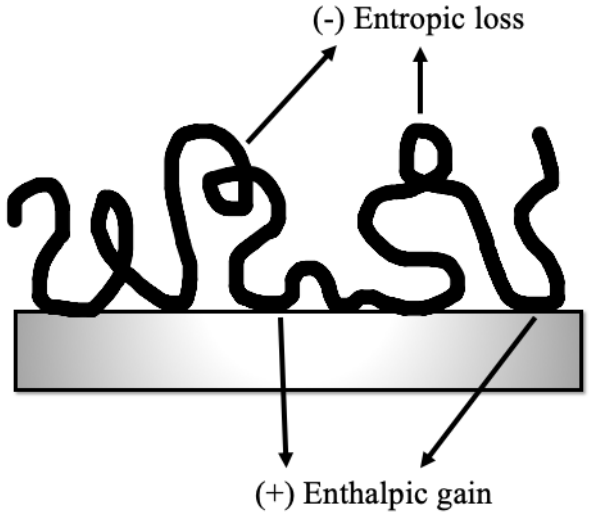

Figure 1. 2. Representation of balance between enthalpic gain and entropic loss for an adsorbed chain.

Polymer adsorption occurs either through chemisorption or physisorption. In physisorption, polymer chains are attracted to the surface via weak intermolecular interactions. Usually, the strength of the segment-substrate interaction energy (adsorption energy) is around a few k_BT, where k_B is the Boltzmann constant and T is the temperature, and a single segment-substrate interaction can easily be broken by thermal fluctuations. However, when linear polymer chains adsorb, they make $N^{1/2}$ contacts with the substrate and the total adsorption energy is the sum of all the individual segment-substrate interaction energies. Considering the number of monomer groups in a polymer chain, the adsorption energy becomes so high that thermal fluctuations cannot break all these interactions simultaneously and therefore these layers are called IAL. This does not imply that these chains cannot be removed under any conditions, but it demonstrates at room temperature these layers are very stable.

Adsorption energy depends on the monomer unit and the functional groups on the substrate surface. For example, adsorption energy for poly(methyl methacrylate) (PMMA) on SiOx surface is around $4k_BT$ per segment due to strong hydrogen bonding whereas the adsorption energy of PS on SiOx surface is around $1k_BT$ per segment [11]. Therefore, adsorption energy can be tuned either by changing the monomer structure or functional

groups on the substrate . In general, it is easier to control the hydrophilicity/hydrophobicity of the substrate.

Since chemisorption requires the formation of a chemical bond between the segments of a polymer chain and the functional groups on the substrate surface, activation barrier is larger than that for physisorption. Chemisorption is simply irreversible, and it creates a chemical bond between only two units. This results in a rather uniform chain structure throughout the layer. However, in physisorption, depending on the arrival time of the different polymer chains, one can obtain different chain conformations throughout the layer. Early arriving chains find completely empty substrate sites and they try to make as many segment-substrate interactions they can and this cause flattening of chains with train conformation. Once many of the substrate sites are filled then the late comers cannot make many segmental contacts due to excluded-volume barrier [12]. They can only make a few contacts, and this causes the formation of mostly tail and loop conformations. Thickness of the adsorbed layer depends on the relative fraction of chains with different conformations. If adsorbed layer mostly composed of chains with train conformation, then the thickness of the layer would be small. However, if loops and tails are contributing most to the adsorbed polymer chains then the layer thickness would be larger.

Accurate estimation of adsorption energies is not straightforward. The most widely accepted method introduced by Cohen-Stuart et al. [13] requires desorption experiments and simultaneous collection of adsorption isotherms. In this method, two Flory-Huggins interaction parameters are used to determine thermodynamic properties of the mixture; one is for the free energy of mixing polymer and solvent and the other is free energy of polymer-surface segmental contacts. High molecular weight adsorbed polymer chains on the surface are desorbed and they are replaced by low molecular weight identical polymers. Through rigorous calculations they showed that it is possible to determine segmental adsorption energy.

Desorption of adsorbed polymers was studied experimentally by Granick and coworkers in solution. They used protonated polystyrene (PS-h) and deuterated polystyrene (PS-d) with similar molecular weights and polydispersities. Enthalpic gain from the PS-h segment silica surface interaction was 1.8 k_BT [14]. Adsorption of PS-d is slightly favored

compared to PS-h with 0.04 k_BT more enthalpic gain per segment [12]. When adsorbed mass reached equilibrium for PS-h (Mw = 575 kg/mol), solution is replaced with PS-d (Mw = 550 kg/mol) solution of the same concentration. Surface coverage was monitored in-situ using attenuated total reflection Fourier-transform infrared spectroscopy (ATR-FTIR). Displacement of PS-h with PS-d was observed on the surface [15]. In this case, such a small enthalpic gain per segment when PS-d adsorbs cause the desorption of PS-h since many segments interact at the same time with the underlying substrate to reduce the overall energy of the system.

1.3. Effect of Adsorbed Layer on Physical Properties of Thin Polymer Films

Adsorption of polymers onto solid substrates does not have to happen only in dilute solution, instead it can happen in melt state as well. Although theory of polymer adsorption in dilute solution is studied in detail since 1980s, adsorption from melt has only attracted interest in the last 10 years due to experimental challenges in characterization of a few nm thick polymer layers with buried interfaces. Adsorption from melt pulled so much interest since presence of adsorbed polymer chains in thin films causes deviation of physical properties from bulk such as diffusion [16], crystallization [17], viscosity [18], hydrophobicity [19] and T_g [20].

Since many segments of adsorbed chains in flattened layer with train conformation pins to the substrate one would expect that the mobility of these chains are dramatically reduced so that they have been called as dead layers for a long while in the literature. Due to significant reduction of mobility in this layer, it is also expected that the non-adsorbed chains may entangle with the adsorbed chains and the mobility of neighboring chains are also slowed. Therefore, diffusion of polymer chains in the film should be slower. This hypothesis was tested by Jiang and coworkers [16]. They have studied the effect of irreversibly adsorbed chains in thin polymer films on diffusion in super critical carbon dioxide ($ScCO_2$) (T_c =36 °C and P_c = 8.2 MPa) with bilayer films of h-PS/d-PS using neutron reflectivity (NR) [16]. Sorption of CO_2 molecules has shown to plasticize glassy polymers and decreases T_g value by enhancing chain mobility [21]. At the ridge condition Koga and coauthors showed that the sorption of CO_2 reaches a maximum and even at 36 ℃ one can

observe diffusion in bilayer films of PS [22]. They demonstrated that vertical diffusion constant (D_{eff}) depends on distance of the interface between the layers from the substrate. Diffusion of PS chains is reduced an order of magnitude compared to that of PS in bulk for 0.6 Rg thick bottom layers. As the film thickness of the bottom layer increases, the diffusion coefficient increases, and the bulk value is recovered for $3R_g$ thick bottom layers. Since the thickness of the adsorbed chain layer is less than $1R_g$, they have concluded that the mobility of adsorbed chains is limited significantly, and this reduction disappears slowly as the non-adsorbed chains are further away from the adsorbed chains. In the last few years this view is challenged by Napolitano and coworkers by measuring the thermal expansion coefficient of adsorbed PS layers with various thickness on SiOx using in-situ spectroscopic ellipsometry measurements [23]. They found that the adsorbed layers with thicknesses less than 10 nm showed an increase in thermal expansion compared to bulk and this implies that the layer is not dead. They explained this observation with the packing frustrations due to increase in free volume at the interface.

Napolitano and coworkers have elucidated the effect of film thickness on the crystallization of poly(L-lactide) films capped between two conductive aluminum layers by dielectric relaxation spectroscopy. Film thicknesses varied between 8 nm and 300 nm [17]. They have followed the time dependent changes in dielectric loss modulus for different film thicknesses and found that the decrease in mobility as the films get thinner. This effect could be either originated by the finite size (confinement) effects on crystallization or the adsorption of polymer chains on the metal layers. They have resolved the contribution of these two effects by careful investigation of Havriliak-Negami parameters. For film thicknesses down to 25 nm they found that crystallization time (t_c) is a function of $1/h_c$ where h_c is the film thickness. This behavior indicates the dominant contribution is the finite size effect since overall sample volume decreases. However, for film thicknesses below 25 nm they showed that the slope of t_c vs h_c curves increases significantly because of the contribution from chain adsorption. For layers thinner than 10 nm crystallization is inhibited for the time scale of the experiment [14][20]. They also found a gradient of mobility from the substrate to roughly 15 to 20 nm away from the substrate at which the bulk value is recovered. This behavior is also qualitatively consistent with the Koga and coworkers' earlier results [13-24].

Viscosity of polymer thin films is studied by various research groups for years and different results are reported using different measurement techniques. In general, conclusions are drawn from the T_g measurements and depending on the direction of the Tg shift either viscosity claimed to be higher or lower than the bulk value. It is believed that a thin film consists of two layers; highly mobile liquid-like top layer which follows Arrhenius dynamic closer to the free surface and bulk-like inner region just above the solid substrate [25]. Solid substrate slows down dynamics by restricting configurational space available for chains whereas free surface enhances segmental motion even below glass transition temperature of polymer and dominate physical properties especially in thinner films. Physical properties of thin films, including viscosity, change depending on balance between these two competing effects. Effect of film thickness on viscosity is investigated using PS thin films ranging from 2.3 nm to 79 nm. It is found that viscosity decreases especially at lower temperatures as film thickness decreases and for films thicker than 50 nm viscosity matches with bulk value [25]. Local viscosity of thin films is also studied by Koga and coworkers using gold nanoparticles embedded 57 nm thick PS films above their bulk Tg [18]. X-ray photon correlation spectroscopy (XPCS) measurements showed that local viscosity at the center of the film is always higher compared to surface of the film. This is explained with presence of irreversibly adsorbed polymer chains with limited mobility. These hardly mobile chains restrict the mobility of neighboring chains through entanglements and create a gradient of viscosity from substrate to the air surface.

Adsorbed polymer chains may also cause switch in hydrophilic/hydrophobic character of thin polymer films. Moisture absorption capacity of poly(vinyl acetate) (PVAc) (Mw = 350 kg/mol, $R_g \sim 17$ nm) with thickness ranging from 21 to 128 nm is characterized with local dielectric spectroscopy (LDS) [19]. It is found that as adsorbed layer thickness increases, water uptake decreases although PVAc is a hydrophilic polymer. Because high interfacial monomer density in adsorbed layer reduces free volume and creates less permeable environment for water molecules.

T_g value for thin films is also affected by the presence of adsorbed polymer chains. It can be higher or lower than the bulk value depending on polymer/surface interactions. Reduction of T_g in thin films is generally explained with presence of free surfaces. Priestley and coworkers observed 10 orders of magnitude faster structural relaxation at a region 3 nm

below the free surface compared to bulk [26]. However, observation of a T_g reduction even for capped films of poly(4-tert-butylstyrene) where free surface does not exist implies that the excess free volume at the substrate side where polymer chains adsorb can make an impact on T_g value [27]. In addition, T_g of thin 8-arm star PS films is found to be higher than the bulk value due to better packing of star polymers at the interface compared to linear chains [28]. These results clearly show that free surface is an important factor but not enough to explain the change in T_g as a function of film thickness by itself. Free volume holes diffusion model is suggested to explain interesting shifts in the T_g value of thin films. As the adsorbed layer forms at the beginning, because of packing frustrations there is an excess free volume near the substrate, and this cause a reduction in T_g [29]. Once the layer is annealed for long time period, these holes diffuse to the air surface and annihilates. As the adsorbed layer reaches an equilibrium to reach bulk density one should not see any T_g shift and this has been proven by Napolitano and coworkers [30].

Tacticity of PMMA have a drastic effect on the T_g value of spin-cast film. Grohens et al. [31] investigated the Tg of thin PMMA films by spectroscopic ellipsometry using isotactic PMMA (i-PMMA) and syndiotactic PMMA (s-PMMA). They found that there is a correlation between the density of the adsorbed layer at the substrate and measured T_g value. i-PMMA adsorbs with higher density than s-PMMA. This change in the density of the adsorbed layer causes an increase in T_g of i-PMMA film and decrease in the T_g value of s-PMMA film.

1.4. Growth Kinetics and Structure of Adsorbed Polymer Layer

Deviations from the bulk behavior in thin films clearly show the presence of adsorbed layer as explained in the previous section in details. Considering all these facts into account, it is possible to tune material properties to the desired level by controlling the thickness and density of the adsorbed layer. This can be achieved if the adsorbed layer formation mechanism is resolved in detail. Although, adsorption of polymers from solution and melt is extensively studied, we have only learnt so far how the enthalpic interactions can be varied since almost all of the studies use different linear polymers on various substrates. [32]. It is still not clear if we can gain control through variations in entropic contribution. Our main target is to fill this large gap in the literature.

Gin et al. [34] reported conformation of chains adsorbed onto the solid substrate from the melt using initially 50 nm thick PS (Mw = 170 kg/mol) films on hydrogen passivated silicon. They followed Guiselin method to prepare the adsorbed layer [35]. After annealing spun-cast films above T_g under vacuum, thin films are washed with toluene to extract non-adsorbed chains and characterized using NR and X-ray reflectivity (XR). Thickness of the adsorbed PS layer found to be function of annealing time. At early times the growth of the layer is linear with annealing time and once the surface sites are mostly occupied then the growth becomes logarithmic. XR data demonstrated that there is a high-density region just above the substrate with mostly train conformation and above this layer there is a layer with bulk-like density composed of mostly loops and tails. Early arriving chains create flattened conformation because of the trains and late arriving chains form loosely adsorbed layer due to loops and tails.

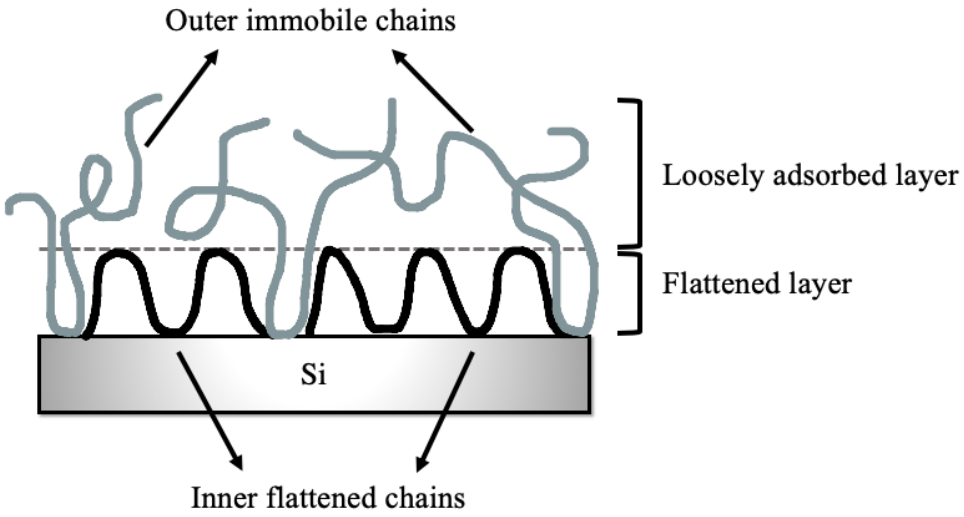

Figure 1. 3. The interfacial sublayer consists of the loosely adsorbed chains and flattened chains with different chain conformations.

Napolitano developed a kinetic model [32] for the growth of adsorbed PS chains on SiOx. Experimental data indicated that there are two regimes as explained before and he has fitted the experimental data with the following equations.

$$h_{ads} = \begin{cases} h_0 + \upsilon t & \text{for } t < t_{cross} \\ h_{cross} + \Pi \log t/t_{cross} & \text{for } t > t_{cross} \end{cases} \qquad \text{(Eq. 1)}$$

In these equations, t_{cross} is crossover time, it corresponds the time when early stages of chain pinning are completed, similarly h_{cross} is the thickness at which surface coverage is completed. v and Π are growth rates at linear and logarithmic regimes, respectively. His model is valid for different molecular weights as well. However, the effect of annealing temperature is not taken into account. When PS (Mw = 955 kDa) films are annealed at 140 °C and 160 °C, the structure of the equilibrium adsorbed layer does not change but growth rates of linear and logarithmic regimes increases as temperature rises [33]. Strength of the intermolecular interactions between polymer segments and substrate are not included but it is expected growth rate is influenced. Equation suggests and infinite growth however it is experimentally known that the growth of the adsorbed layer reaches an equilibrium value and stops. These are the main drawbacks of the model.

Durning et al. [34] showed that adsorbed layer growth kinetic is affected by molecular weight of the polymer. Two different molecular weights of PMMA (M_w = 70 kg/mol and 345 kg/mol) are spin coated on silanol-bearing quartz surface and leached with benzene to remove non-adsorbed chains. Time scale to reach equilibrium (τ_{eq}) thickness is power-law dependent to molecular weight, $M_{w0.9}$. There is a steeper growth curve for smaller molecular weight and equilibrium adsorbed layer thickness (h_{dry}) is greater for higher molecular weight. h_{dry} is correlated with $N_{1/2}$ in accordance with random walk model.

1.4. Aim of The Study

Adsorption of polymer chains onto solid substrates is mainly investigated using linear chains from solution and recently in melt. The type of polymers and the surface energy of the substrate were varied in these studies to change the contribution of enthalpic gain. However, it is not clear how the contribution of entropic loss can be controlled. One way of changing the entropy of the polymers without changing enthalpic interactions is to modify the topology of the polymer. For example, linear PS and star-shaped PS chains have different conformational entropies. Presence of a junction point and stretching of polymer segments near the junction point yields lower conformational entropy for star polymers compared to their linear analogs. When a star polymer is adsorbed on a substrate, it is expected to lose less conformational entropy compared to linear polymer chain of same total molecular weight. Since entropic loss term will be smaller one would expect a larger relative gain for each segmental interaction and enhanced adsorption. Kosmas et al. calculated that number of contacts on the surface is proportional with the $N_{1/2}$ for a linear chain, but it increases with the number of arms for star polymers of the same total molecular weight[35]. Comb chains behave like linear chains if ratio of molecular weights of side chain over the backbone becomes closer to 1. If this ratio becomes large, they act like higher functionality star polymers [35]. Ring polymers are in between star polymers with functionality of 3-4 and 5-6. But this simulation is valid only for a single chain adsorption on substrate, effect of chain-chain interactions is neglected.

Earlier work of Kawaguchi [36] focused onto adsorption of linear and comb polymer chains of identical molecular weight from cyclohexane solution at theta temperature to chrome plate using ellipsometry. They elucidated the adsorption and extension of these polymers on the surface. Comb polymer forms a denser adsorbed layer but the linear chains in adsorbed layer extends further into solution than comb polymers. Higher segment density on the substrate for the comb polymer agrees well with the results of Kosmas [30]. Self-consistent field theory calculations also predicted that comb polymers should form thinner adsorbed layers than linear polymers since they do not have dangling tails [37]. They assumed that the adsorption happens through the side chains not through backbone and this is still a question that should be verified experimentally.

In this work, our aim is to elucidate the effect of polymer architecture on the structure and formation of adsorbed layer. We have used linear, 4-arm star, comb, and centipede PS chains of roughly equal molecular weight to create adsorbed layers on hydrophilic and hydrophobic surfaces. Growth kinetics and the structure of the equilibrium adsorbed layer are characterized using ellipsometry and XR respectively. Understanding the role of polymer architecture will enable us to modify the entropic contribution so that the formation and structure of the adsorbed layer can be tuned. Hence, this study will open new pathways to control the structure and properties of adsorbed layers.

2. EXPERIMENTAL

2.1. Materials

Toluene (99.7 %, Merck), chloroform (99.7%, J. T. Baker), sulfuric acid (H_2SO_4) (51%, Merck), hydrogen peroxide (H_2O_2) (30%, Merck), and hydrofluoric acid (HF) (48%, T. J. Baker) are used as received. Phosphorus doped n-type silicon wafers with 100 mm diameter and 0.6 mm thickness are purchased from El-Cat Inc. Silicon wafers are cleaned with piranha solution and UV/Ozone (UV-O_3) treatment to obtain hydrophilic surface and treated further with 2.5 vol. % HF solution to get hydrophobic surface.

Branched polystyrene (PS) chains are synthesized by David Uhrig using anionic polymerization at the Center for Nanophase Materials Sciences (CNMS) at Oak Ridge National Laboratory. All polymers have very narrow molecular weight distribution with polydispersity index (PDI) values in between 1.03 and 1.08. Bulk glass transition temperature (T_g) of each polymer is measured by differential scanning calorimeter (DSC). Radius of gyration (R_g) values in melt state are either calculated using theoretical equations from literature or hydrodynamic radius (R_h) in good solvent condition is measured using dynamic light scattering and then scaled to melt condition to obtain R_g. Physical properties of the branched PS chains used in this work are shown in Table 1.

Table 1. Physical properties of branched and linear PS chains

.	$M_{n,total}$ (kg/mol)	$M_{n,arm}$ (kg/mol)	PDI	R_g (nm)	T_g (°C)
Linear PS	484	-	1.05	15.4	107.0
Centipede PS	543	30	1.07	14.5	107.0
Comb PS	741	60	1.06	17.5	107.5
4-arm star PS	483	120	1.03	13.8	107.5

Even though, equilibrium adsorbed layer thicknesses are normalized with the size of the polymers, absolute molecular weights of the polymers chosen to be close to each other. Linear PS (MW=484 kg/mol) and 4-arm star PS (MW=483 kg/mol) have identical total molecular weights. Centipede PS (Mw=543 kg/mol) has in average 4.5 branch points with molecular weight of side chains are 30 kg/mol. Therefore, molecular weight of centipede backbone is 270 kg/mol. Comb PS (Mw=741 kg/mol) has two times longer side chains which are 60 kg/mol, and backbone is 356 kg/mol.

2.2. Cleaning of Silicon Substrates

Surface science requires clean work environment, clean substrates and use of nearly pure materials since very tiny amounts of contaminants can totally ruin the results for a few nm thick layers. Therefore, substrate cleaning has to be performed effectively. Quality and efficiency of cleaning should be optimized for the substrate and contaminant type on the surface. There are many techniques for substrate cleaning, and they can be categorized into two groups; wet cleaning and dry cleaning. Piranha treatment is chosen as a wet cleaning technique, and UV-Ozone (UV/O_3) treatment is used as dry-cleaning technique. Both of these treatments make the surface of a silicon wafer highly hydrophilic.

2.2.1. Piranha Cleaning

Piranha treatment is very reliable and effective method to remove organic molecules from the surface of the solid substrates and it leaves hydroxylated surface behind. There are multiple recipes in the literature [38][39]. In this work concentrated sulfuric acid (H_2SO_4) is mixed with hydrogen peroxide (H_2O_2) with 7:3 volume ratio, respectively.

Great care and several precautions are required while handling with piranha solution because it is highly corrosive. The reaction between H_2SO_4 and H_2O_2 is very exothermic but once solution is stable then it is heated up to 90 to 100 °C to keep it active. Bubbles are observed during the piranha treatment due to the oxidization of organic contaminants to CO_2 as final product.

Even though the exact cleaning mechanism is not established yet, it has been speculated that there are two stages in piranha cleaning; dehydration and oxidation. In the fast dehydration step hydrogen and oxygen are expected to be removed as water molecules and organic residues on the surface are carbonized. Then the carbonized residues are oxidized to CO_2 in the oxidation step.

2.2.2. UV-Ozone Treatment

UV-Ozone (UV-O_3) cleaning is a dry, easy, and inexpensive cleaning technique for wide variety of substrates such as quartz, silicon, gold, nickel, aluminum, mica and glass. It is effective to clean organic contaminants like oils, residual solvent, and hydrocarbons. However, it is not useful to remove inorganic contaminants (dust and salts) and thick polymer films, thus pre-cleaning is required using solvents, soap solutions or anything that can remove inorganic contaminants before UV-O_3 treatment. It is not possible to remove thick polymer films using UV-O_3 due to crosslinking upon UV exposure. The details of how UV-O_3 cleaning works given by Vig et al. [40] and the mechanism of UV-O_3 cleaning is explained briefly below.

A low-pressure mercury discharge lamp generates UV radiation with 184.9 nm and 253.7 nm wavelengths. At each of these wavelengths different processes occur. At 184.9 nm oxygen molecules (O_2) are dissociated first into oxygen atoms (Eq. 2) and in the subsequent step oxygen atoms react with oxygen molecules to yield ozone (O_3) (Eq. 3). These two steps together are called as ozone generation.

$$O_2 \rightarrow O + O \qquad \text{(Eq. 2)}$$

$$O + O_2 \rightarrow O_3 \qquad \text{(Eq. 3)}$$

At ozonolysis step, 253.6 nm UV light decomposes O_3 molecules to O_2 and activated oxygen O^* (Eq. 4) which is highly energetic and hence very reactive.

$$O_3 \rightarrow O_2 + O^* \qquad \text{(Eq.4)}$$

Activated oxygen is a very strong oxidizing agent and reacts with the organic contaminants on the substrate surface. For polymers, chain scission occurs, and hydrocarbons are converted to simple volatile byproducts. This is the last step where decomposition of organic matters occurs.

After UV-O_3 treatment, silicon substrate is hydrophilic since surface is covered with 1 nm to 2 nm thick oxide layer. Hydrophilicity of the surface can be verified via contact angle measurements. A well cleaned, hydrophilic surface enables water droplet to spread almost completely and give contact angle close to zero. Contaminated surface yields higher contact angle values.

UV-O_3 cleaning requires fine adjustment of key process parameters such as the amount and the type of contaminant, distance between the source and sample, exposure time, efficiency of precleaning, and the atmosphere between the source and the sample surface. It is shown that UV- O_3 treatment produces a clean surface less than 1 minute if sample is pre-cleaned[40]. In this study, UV- O_3 cleaning is performed for 30 minutes at 10 mm away from the UV source.

1.2.3. Hydrofluoric (HF) Acid Etching

Surface energy of the substrate is one of the key parameters for this study since adsorption of polymers depends strongly on the surface-segment interaction energy. In order to investigate the impact of surface energy on adsorption, surface energy of the silicon substrate is varied by tuning the hydrophobicity. Piranha or UV-O_3 cleaned silicon wafers are hydrophilic and they have high surface energy. HF etching modifies the silicon surface from hydrophilic to hydrophobic nature. Even though HF is a weak acid (pKa = 3.15), it is an excellent etchant to remove native oxide (SiO_x) layer and widely used to create ultraclean surfaces in semiconductor industry. HF etching yields relatively smooth surface with root-mean-square (rms) surface roughness (σ_{rms}) around 6 Å [41]. Burrows et al. using X-ray photoelectron spectroscopy (XPS) and ion scattering spectroscopy measurements

demonstrated that silicon surface after HF treatment is mainly terminated by hydrogen and fluorine content is minimal [42].

Piranha treated silicon wafers are kept in 2.5% volume percent HF solution in distilled water for 30 seconds. All HF treatments are made using freshly prepared solutions with the same HF concentration and treatment time to obtain consistent results. HF etched silicon wafers are coated with polymer solutions using spin-coating as soon as HF treatments are finished to ensure no appreciable amount of native oxide layer is regrown. This time between the HF treatment and spin-coating is in general less than 30 seconds.

2.3. Adsorbed Layer Preparation

All the branched polymers are dissolved in toluene which is a good solvent for PS [43]. After polymers are completely dissolved, solutions are filtered using 0.22 μm or 0.45 μm syringe filters to remove any dust. Piranha or HF-cleaned silicon wafers are placed into spin coater and held steady with vacuum. Then solutions are dropped onto the wafers using glass pipette and spun cast for a minute between 2000 revolution per minute (rpm) and 3500 rpm depending on the target film thickness. Spin coating is a well-known technique to deposit uniform thin polymer layers on solid substrates where Newtonian fluid rotates with constant angular velocity. Fast evaporation of volatile solvent leaves a polymer layer on the flat surface due to viscous force and surface tension [44]. Thickness of thin polymer films can be controlled via rotation speed, evaporation rate and solution concentration. Meyerhofer's equation (Eq. 5) [45] indicated that, increase in viscosity (or concentration) of the solution results in an increase in layer thickness whereas increase in rotation speed causes thickness decrease.

$$\frac{dh}{dt} = -\frac{2\rho\omega^2 h^3}{3\eta} - E \qquad \text{(Eq. 5)}$$

Here, w represents angular speed, ρ is mass density, η stands for viscosity, h is thickness of fluid layer (not dry) and E is evaporation rate. In this study, rotation time is kept constant for 60 seconds, solution concentrations are varied in accordance with desired initial

film thickness. For each polymer, solution concentration versus film thickness plot is established at a fixed rotation speed using four different concentration values and then film thicknesses are controlled based on the concentration.

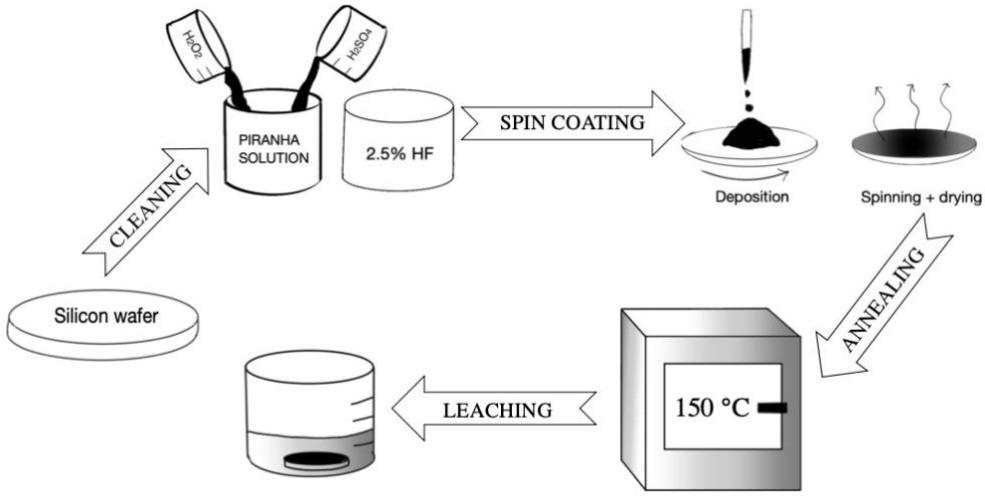

Figure 2. 1. Schematic representation of experimental procedure for the preparation of an adsorbed layer.

After spin coating, polymer thin films are annealed under vacuum at 150 °C between 30 minutes and 192 hours. Long annealing process above the T_g of the polymer in general ensures complete chain relaxation and eliminates residual stress and residual solvent remaining from the deposition process. Here annealing is used to promote adsorption of polymer chains to the substrate. Upon completion of annealing, samples are removed from the oven and quenched on an aluminum plate to room temperature very rapidly. Then samples are kept in toluene for 10 minutes and dried. This leaching process is repeated 5 times with fresh toluene in each step. During leaching non-adsorbed chains are removed from the substrate so that samples only contain adsorbed polymer chains. Once toluene leaching is finalized samples are annealed again under vacuum at 130 °C for 2 hours to remove residual toluene in the film. At this step samples are characterized and later the same leaching protocol is followed using chloroform to remove loosely adsorbed PS chains from flattened chains if there are any [46].

2.4. Characterization of Bulk Polymers and Adsorbed Layers

T_g value of a polymer is a very crucial parameter for determining the temperature at which annealing should be done to ensure complete chain relaxation. Bulk T_g values for each PS architecture are determined using differential scanning calorimeter (DSC). Radius of gyration (R_g) values are used for normalization of equilibrium adsorbed layer thickness so that different PS architectures with different molecular weights can still be compared. R_g values are calculated using well-known formulas from the literature and also R_g of polymer chains are estimated from the R_h values measured in good solvent condition using MALVERN ZS – ZETASIZER at Koç University Surface Science and Technology Center (KUYTAM).

Quantitative characterization of adsorbed polymer layers that have 1 nm to 20 nm thickness is quite challenging. In order to follow the growth kinetics of the adsorbed layers ellipsometry (Film Sense-1 Multi-Wavelength Ellipsometer, Version 1.50, Bogazici University) is used. The thickness, roughnesses at the air surface and the substrate interface, and the density of the adsorbed layers are determined by X-ray reflectivity (XR) (Bruker D8 Advance X-Ray Diffractometer, Koç University Surface Science and Technology Center (KUYTAM)) measurements. Atomic force microscopy (AFM), (Bruker Dimension Icon AFM, Koç University Surface Science and Technology Center (KUYTAM)), is used to examine surface morphology of the adsorbed layers.

2.4.1. Differential Scanning Calorimetry

Differential scanning calorimeter (DSC) is an instrument to measure thermal properties of polymers such as melting temperature (T_m), crystallization temperature (T_c), T_g and enthalpy changes associated with these transitions. The principle of DSC measurements is summarized briefly here.

There are 2 aluminum pans, one of them is a reference pan which is kept empty and the other one is a sample pan that is filled with polymer and then pressed. The mass of the polymer in the sample pan is recorded to DSC software for calculations. The main principle

is maintaining the temperature of sample and reference pans the same upon heating or cooling. When polymers undergo a physical transition such as first-order phase transition depending on the enthalpy change either more or less heat is required to maintain the temperature. For endothermic changes (i.e. melting) more heat is needed and heat flows to the sample pan whereas for exothermic changes (i.e. crystallization) less heat is required so heat flow to the sample pan is reduced. The difference in the heat flow between sample and reference pans yields a curve of heat flux versus temperature. By multiplying calorimetric constant (K) and the area of peaks for a given transitions, the enthalpy of transition can be derived.

The TA Instruments Q2000 DSC is used to measure Tg for linear, comb, centipede and 4-arm star polystyrene samples. In the first heating step, samples are heated from room temperature to 150 ℃ with a rate of 10 ℃/min to remove the thermal history. After the first heating, samples are cooled back to the room temperature with the same rate. The second heating run is performed using the same temperature range and heating rate as in the first heating run. T_g of polymers are obtained from the plot of heat flow versus temperature curve in second heating run. At the glass transition temperature cooperative segmental motions begin and a glassy polymer gets into melt state. The heat capacity of the polymer changes during this transition and T_g is determined from the middle point of the tangent that connects the two straight lines drawn from the beginning and end of the transition.

2.4.2. Dynamic Light Scattering

Dynamic light scattering offers a quick determination of polymer and nanoparticle sizes in solution from a little amount of sample volume. Incident laser beam illuminates the polymer solution and as a result light is scattered in every direction. This scattering yields a speckle pattern due to wave interferences. At each shot a speckle pattern is collected and speckle patterns obtained at different times are correlated using an autocorrelator. Diffusion coefficient of particles and relaxation times can be obtained from the decay of autocorrelation function. Since diffusion of the particles or polymers in solution is directly related to the size, hydrodynamic radius (R_h) is obtained from DLS measurements. Small

particles diffuse faster and creates fast decaying intensity fluctuations whereas large particles exhibit slower diffusion and slow decaying autocorrelation functions.

Incoming laser light passes through the attenuator and hits the solution. DLS measurements are done using a Malvern Zetasizer equipped with 4 mW He-Ne laser with 633 nm wavelength. Scattered light passes through focusing lenses and reaches the detectors located at 90º or 173º from the incident laser beam, to detect backscattering. Intensity fluctuations are observed from the computer connected to detectors by comparing intensity fluctuation of the beam with itself within microseconds. Intensity distribution is calculated from data signal processor (correlator) and number/ volume/ intensity distribution of particles is found.

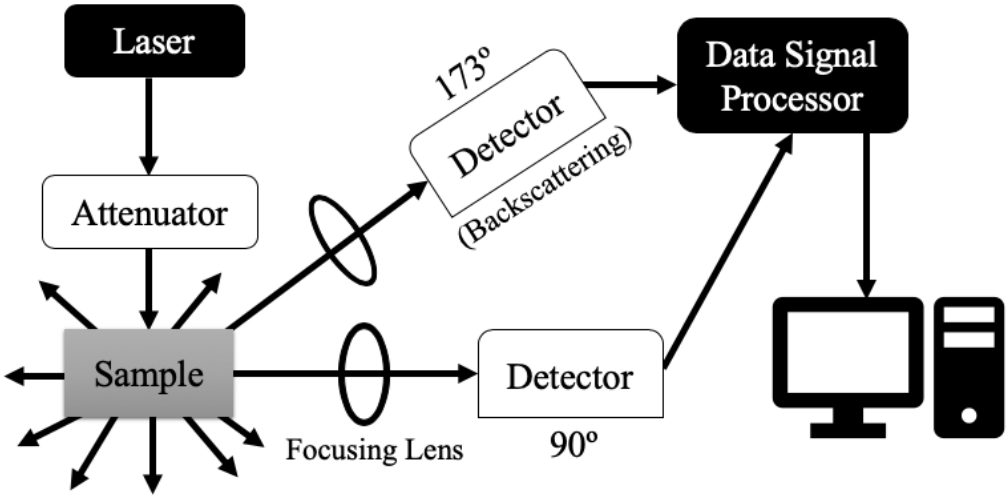

Figure 2. 2. Schematics of DLS set up and measurement.

Once hydrodynamic radiuses are determined by DLS measurements, R_g values are estimated from the R_h values. The ratio of R_g/R_h in general provides information about shape of the samples; 0.78 for spherical nanoparticles, between 1.5 and 2.1 for coils and bigger than 2 for nanotubes [47].

2.4.3. Ellipsometry

As a well-established optical measurement technique, ellipsometry is a fast and non-destructive method to measure thickness and refractive index of thin films. The change in polarization state of light beam reflected from the sample is measured and this change in beam polarization depends on film thickness. In this study, Film Sense FS-1 Multi-Wavelength Ellipsometer is used. Ellipsometric data is acquired using 4 different wavelengths at 465 nm (blue), 525 nm (green), 590 nm (yellow), and 635 nm (red) simultaneously. Wavelength and polarization state of incident beam is set, polarization state of reflected beam is measured with a method called DOAP (Division-of-amplitude photopolarimeter). This method can be expressed as a matrix equation in Equation 6,

$$I = AS \qquad \text{(Eq. 6)}$$

where I is a 4x1 matrix showing four different intensities measured by detector, A is 4x4 instrument calibration matrix and S is a 4x1 vector consist of stokes parameters, where polarization of light is expressed by four different stokes parameters S_0, S_1, S_2 and S_4.

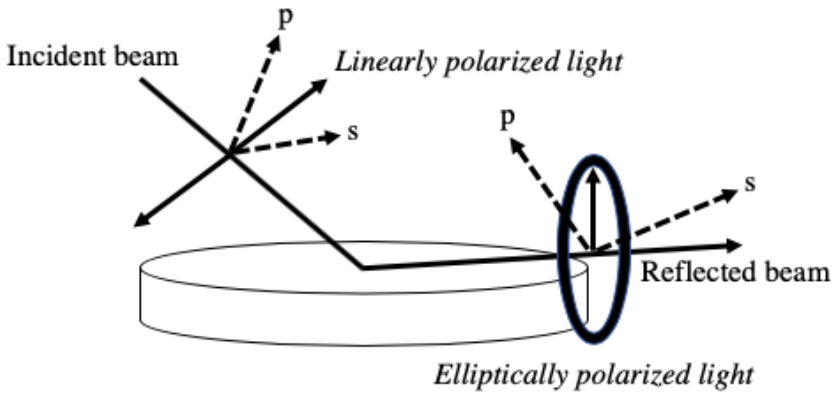

Figure 2. 3. Interaction of incident light with sample and resulting polarization change in an ellipsometry measurement.

Ellipsometry data is quantitatively analyzed using a model-based fitting. A multilayer model is created in which the refractive index information for substrate and polymer layers are used as inputs and the thickness of the layers are used as fit parameters. Marquardt-Levenberg algorithm is used to find the global minimum during the fit process. The difference between fit and measured data is denoted as fit difference and this difference is kept as small as possible.

2.4.4. X-ray Reflectivity

Specular X-ray reflectivity (XR) is a nondestructive surface characterization technique. It provides information about the structure of thin films in perpendicular direction to the film surface. Thickness and density of layers as well as roughnesses at various interfaces can be obtained with high accuracy and spatial resolution.

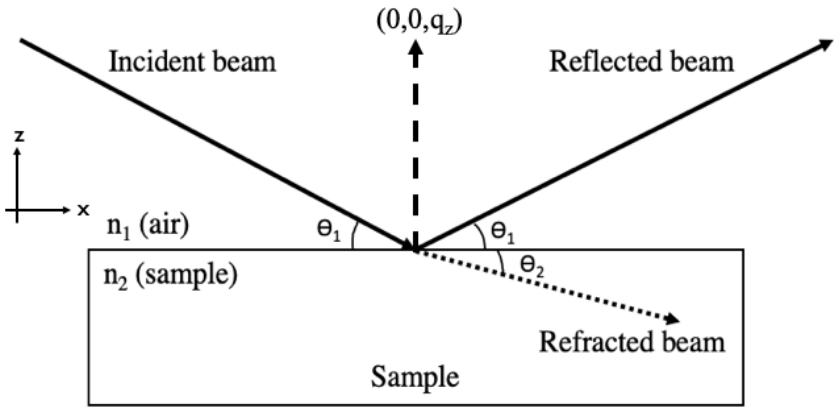

Figure 2. 4. Geometry of an specular X-ray reflectivity experiment.

When the incidence angle of the X-ray beam is equal to the reflection angle it is called specular reflectivity. In this case there is only one component of the momentum transfer wave-vector which is in the z-direction (q_z). Hence the collected structural information yields the electron density variation in the perpendicular direction to the film surface. Structural information in x- and y-directions is averaged out during the measurement. Technique is capable of discriminating very minor changes in the shape of electron density profile and therefore it is very sensitive for structural changes in the z-

direction. Q_z depends on the incidence angle (θ) as well as the wavelength (λ) of the X-ray source as shown in the following formula;

$$q_z = \frac{4\pi \, Sin\theta}{\lambda} \qquad \text{(Eq. 7)}$$

In a typical XR measurement wavelength is fixed and reflectivity is measured as a function of q_z by increasing the incident and reflection angles simultaneously. Reflectivity is defined as the number of reflected X-ray photons collected by a scintillation counter divided by the number of incident X-ray photons over the sample. At incidence angles below the critical angle (θ_c), all the X-ray photons are totally externally reflected, and the reflectivity ratio is equal to 1. At angles above θ_c, X-ray beam starts to penetrate into the sample and reflectivity ratio decreases first sharply then with close to q^{-4} dependence. This dependence is valid for smooth surfaces based on Porod's Law [48]. As the incident angle increases, penetration depth increases very rapidly around critical angle and above q_c it can reach micrometers. In addition to penetration depth, probed length scale also decreases with increasing incidence angle. Since the X-ray instruments utilizes fixed beam height, the footprint of the beam on the sample decreases as the incidence angle increases. Therefore, it is important to have isotropic and uniform samples for the measurements.

If a thin film consists of layers with different electron densities, a phase difference related to the thickness of the layer occurs between the reflected beams from different interfaces. Refracted beams are reflected from each layer/layer interface as well as air surface/layer and layer/substrate interfaces. All these reflected beams constructively and destructively interfere with each other to create Kiessig fringes as shown in Figure 2.5. The period of Kiessig fringes (Δq_z) is related to the phase difference and hence yields information about the thickness of the layer. Film thickness can be determined using fringe spacing between neighboring maxima and minima. There is an inverse relationship between the thickness of the layer, d_L, and the fringe spacing as is shown in equation 8.

$$d_L = \frac{2\pi}{\Delta q_z} \qquad \text{(Eq. 8)}$$

As the fringe spacing becomes smaller, then the layer becomes thicker or vice versa. This simple equation does not take into account the dynamic effects in the vicinity of the critical angle and to obtain more precise thickness information without a detailed fit one needs to use Bragg's equation[49].

$$\sin^2 \theta_i = \theta_c^2 + (n_i + \Delta n)^2 \, \lambda^2 \, / \, 4d^2 \qquad \text{(Eq. 9)}$$

where θ_i is the position of the maximum or minimum of the ith interference fringe, θ_c is the critical angle, n is an integer, Δn = 1/2 and 0 for the maximum and minimum, respectively. Finally, λ is the X-ray wavelength (1.54 nm) and d is thickness.

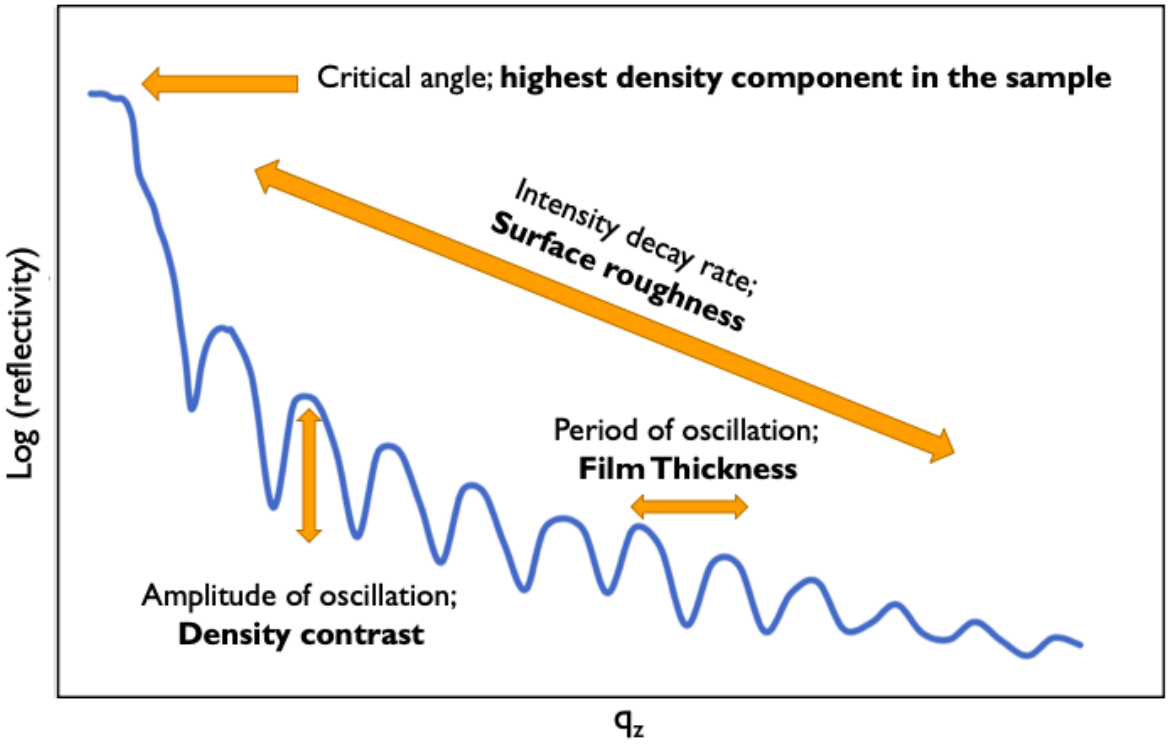

Figure 2. 5. A typical X-ray reflectivity profile that summarizes the model parameters and what they determine in a measurement.

Another important information can be extracted from a reflectivity measurement is the electron density of the layers. Electron density is directly related to the mass density and the number of electrons in the molecule. As can be seen from equation 10, as the number of electron or mass density increases, the electron density of the molecule increases as well.

$$\mathrm{SLD} = \frac{\sum_{i=1}^{N} b_i}{V_m} \qquad \text{(Eq. 10)}$$

Scattering length contributions (b_i) are summed for individual atoms, N is the number of atoms in unit cell and division by volume of unit cell gives scattering length density (SLD). SLD value is proportional to electron density. Qualitatively, observing the critical angle value and the amplitude of the Kiessig fringes give hints about the electron density of the layers within the film. The critical angle is determined by the layer with the highest electron density in the sample. Quite often thicker polymer layers on silicon wafers yield also small oscillations before the critical angle for the silicon and these oscillations give information about the critical angle for the polymer layers and therefore their electron densities. When the Kiessig fringe amplitude is large, the electron density difference between the layers (contrast) is large as well. When the contrast becomes weaker, Kiessig oscillations are damped.

Critical angle for total reflection, where intensity starts to decay, gives an idea about density of the film and amplitude of oscillation provide information about density contrast within the film. Smaller amplitude of oscillation means density difference is less and bigger amplitude implies there is great density contrast in the film. Physical density can be directly correlated with electron density of the film for XR measurements because scattering derives from electron density in the film. There is a relation between SLD of the film and the critical angle.

$$q_c = (16\,\pi\,\mathrm{SLD})^{1/2} \qquad \text{(Eq. 11)}$$

In our measurements, SLD value for the layer reveals the packing of the chains next to the substrate, if there is a mixture of components then the relative fraction of each component. Therefore, SLD value obtained from XR measurements is very critical for our work. XR measurement depends on the roughness at the air surface and buried interfaces. An rms roughness much greater than 5 nm can kill all the Kiessig fringes and therefore make the measurement useless. Below 5 nm XR measurement is very sensitive to the changes in roughness and through fitting roughness values at each interface can be determined with

accuracy. In general, fast decay of the curve indicates the presence of rough interface or surface whereas decay proportional to q^{-4} indicates sharp and very smooth interfaces.

2.4.5. Atomic Force Microscopy

Atomic force microscopy (AFM) is a well-established method for determining the morphology of thin films. 3-Dimensional topology of the surface reveals microstructures on the surface such as nucleation and growth, presence of ordered patterns and surface roughness. In certain cases, the thickness of the films can also be obtained by forming a scratch and obtaining an AFM image around the scratch.

In this study AFM is used in intermittent-contact (tapping) mode, where cantilever oscillates vertically around its resonance frequency. Resonance frequency is set in accordance with tip properties. Cantilever frequency changes during oscillation because tip is exposed to attractive and repulsive forces with the sample surface. To keep the amplitude and drive frequency identical, the distance between tip and sample is adjusted during scanning.

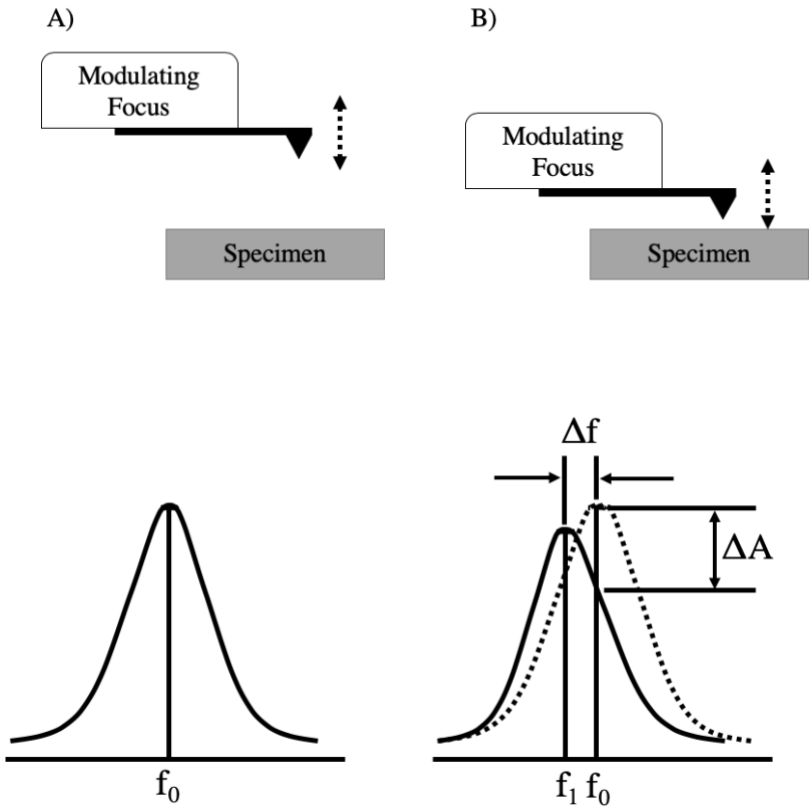

Figure 2. 6. A representation of AFM measurement in tapping mode.

Vertical resolution of AFM instrument is around 1 Å and technique yields precise surface morphology. However, the lateral resolution depends on the radius of the tip and in general it is around 10 nm. Resolution of the AFM is limited by mechanical vibration and random electrical fluctuations. These noises are eliminated using a vibration isolation stage.

Roughness of thin films influences wetting, lubrication, friction and adhesion properties for many technological applications. In this project, surface roughness of the branched thin polymer films is measured using AFM and XR measurements. Roughness is evaluated quantitively by amplitude values in z-direction in AFM measurement and there are several roughness definitions in the analysis software. The most commonly used definitions are roughness average (σ_{av}), and σ_{rms} [50]. Roughness from the XR measurements are obtained by fitting the XR data as mentioned earlier. REFLFIT software provides full width at half maximum (fwhm) values which are 2.35 times the value of σ_{rms}.

Even though σ_{av} is widely used roughness analysis because it is arithmetic average of the absolute values of height deviations from the mean line, in this work we have reported σ_{rms} values to be able to make comparison with XR results. σ_{av} is calculated by the following formula,

$$\sigma_{av} = \frac{1}{L}\int_0^L |Z(x)|\, dx \qquad \text{(Eq. 12)}$$

L is the length of the profile on the x-axis used for measurement and Z(x) is the variation of the height from the profile line for each data point.

σ_{rms} is the root mean square of deviations from the mean height. Since the square of the amplitude is used for the calculation, it is more sensitive for valley and peak deviations compared to σ_{av}. σ_{rms} values are always larger than σ_{av} values.

$$\sigma_{rms} = \sqrt{\frac{1}{L}\int_0^L |Z^2(x)|dx} \qquad \text{(Eq. 13)}$$

AFM and XR measurements yield rms roughnesses but it is very rare these values are in exact agreement. There are many reasons for that but the most important one is that the band widths of these two techniques are different. Since XR technique has a larger frequency band width it tends to yield larger rms roughness values compared to the AFM measurements [51]. In general, XR technique probes a larger area on the sample due to large coherence values of the technique whereas AFM probes smaller local areas. Our measurement also show that XR roughness is always higher compared to AFM roughness.

3. RESULTS AND DISCUSSION

3.1. Growth kinetics of adsorbed layers

Growth kinetics of adsorbed branched PS layers at 150 ℃ for various annealing times is followed by ellipsometry. Adsorbed layer and normalized (d_{ads}/R_g) adsorbed layer thicknesses for initially 50 nm thick linear PS (Mn=484 kg/mol) chains on SiH substrate is shown in Figure 3.1 as a function of annealing time. After each sample is annealed for given amount of time, they are all leached in toluene for 10 minutes (min) and this leaching process is repeated five times with fresh toluene. Therefore, measured thickness values are obtained after 50 min leaching in toluene. Adsorbed layer thickness increases rapidly as annealing time increases till 8 hours (h), but then no change in thickness is observed. Average thickness after 8 h is calculated as 12.4 nm. R_g value for this linear chains is measured as 15.4 nm using DLS and this yields normalized equilibrium adsorbed layer thickness ($d_{ads,eq}/R_g$) as 0.8. This value is in agreement with the literature [52].

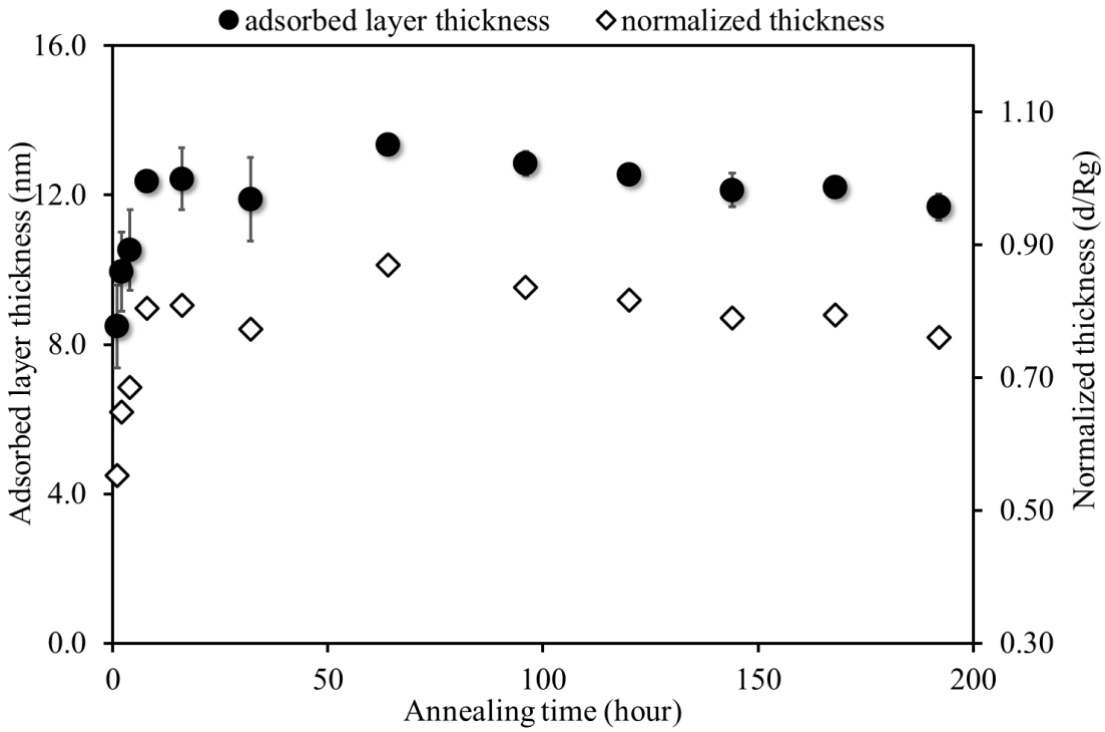

Figure 3.1. Adsorbed layer (filled spheres) and normalized adsorbed layer thickness (empty diamonds) as a function of annealing time for linear PS chains on SiH substrate.

To investigate the effect of surface energy, same experimental procedure is repeated on SiO_x surface for linear PS. The results shown in Figure 3.2 indicates that the growth kinetics of linear PS chains on hydrophilic surface is quite different than that on hydrophobic surface. Initially, there is no sharp increase as in the case of hydrophobic surface. Adsorbed layer thickness gradually increases upon increasing annealing time, and it saturates around 96 h. Equilibrium adsorbed layer thickness is 4.1 nm which is one third of the $d_{ads,eq}$ on hydrophobic surface. Normalized thickness reaches at most 0.3 and this value is slightly lower than reported values for the same system in the literature. Results from these two figures together demonstrates interaction energy between hydrophobic PS chains and hydrophilic surface is smaller than that on hydrophobic substrate.

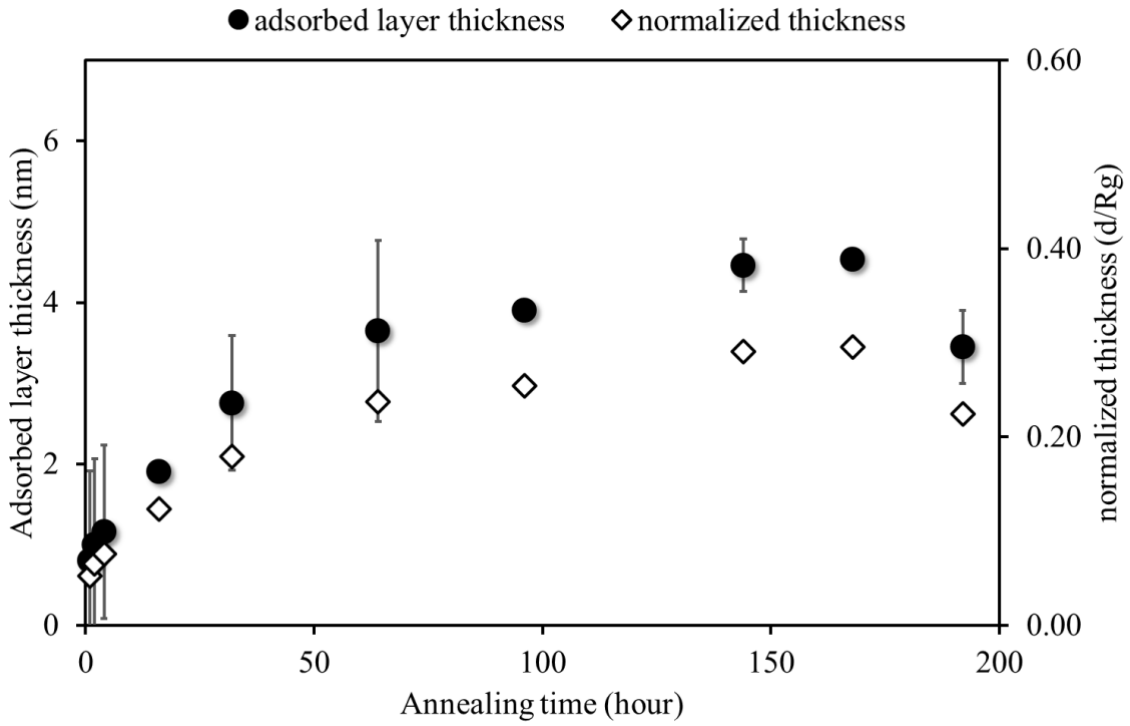

Figure 3. 2. Adsorbed layer thickness (filled spheres) and normalized thickness (empty diamonds) as a function of annealing time for linear PS chains on SiOx substrate.

Once adsorbed layer growth for linear PS chains is validated then the same methodology is applied to different PS architectures. Initially 50 nm thick 4-arm star PS (Mn=483 kg/mol) films spun-cast on SiH surface are annealed at 150 ℃ under vacuum for

various times and leached with toluene. Since both polymers have identical total molecular weight, it is reasonable to draw conclusions on the effect of branching. Adsorbed layer thickness for 4-arm star PS increases from 8.7 nm to 13 nm rapidly in the first 8 h and then no remarkable change is observed (Figure 3.3). The shape of the growth curve is very similar to the shape of the growth curve for linear PS on SiH which suggests a similar growth kinetics. Equilibrium thickness is found as 12.8 nm and $d_{ads,eq}/R_g$ value is 0.89. This value is slightly higher than that of linear PS chains.

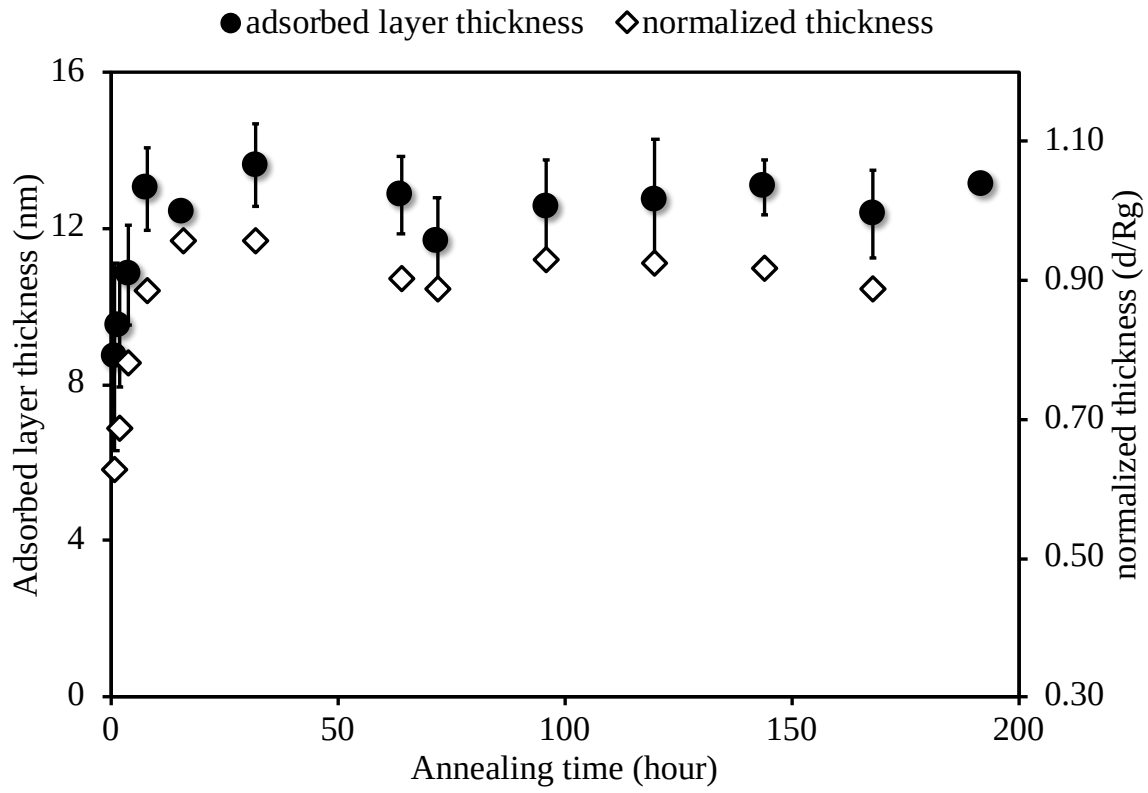

Figure 3.3. Adsorbed layer (filled spheres) and normalized thickness (empty diamonds) as a function of annealing time for 4-arm star PS chains on SiH substrate.

When the same 4-arm PS layer is adsorbed on a SiO_x substrate, our expectation is to find a similar growth pattern as in the case of linear PS on SiO_x surface. These two polymers are expected to have the same enthalpic interaction energy due to segment–substrate contacts. However, the entropic penalty will be different in each case since linear chains will lose more conformational entropy per chain for pinning of each segment than the corresponding star polymers. In a 4-arm star PS, 4 linear PS chains merge at the core. Around

the core, chains repel each other and they are stretched near the junction point similar to polymer brushes. The conformation of the chains are far from Gaussian coil conformation. As the end of the chain is far away from the junction point, the stretching decreases. This is the main reason for lower conformational entropy for star chains in general. When the star polymers are adsorbed and their segments pin to the surface, the reduction in conformational entropy is not as severe as for linear chains and adsorption should be more favorable for star polymers. Kinetic growth of adsorbed layer for 4-arm star PS on SiO_x is shown in Figure 3.4. Adsorbed layer grows gradually till 120 h and then the thickness value remains same. The shape of the growth curve is similar to that of linear PS on SiO_x surface. Equilibrium adsorbed layer thickness is around 6.5 nm which is larger than that of linear PS on SiO_x. Normalized equilibrium thickness is calculated as 0.46. This value is 50% higher than that for linear PS chains.

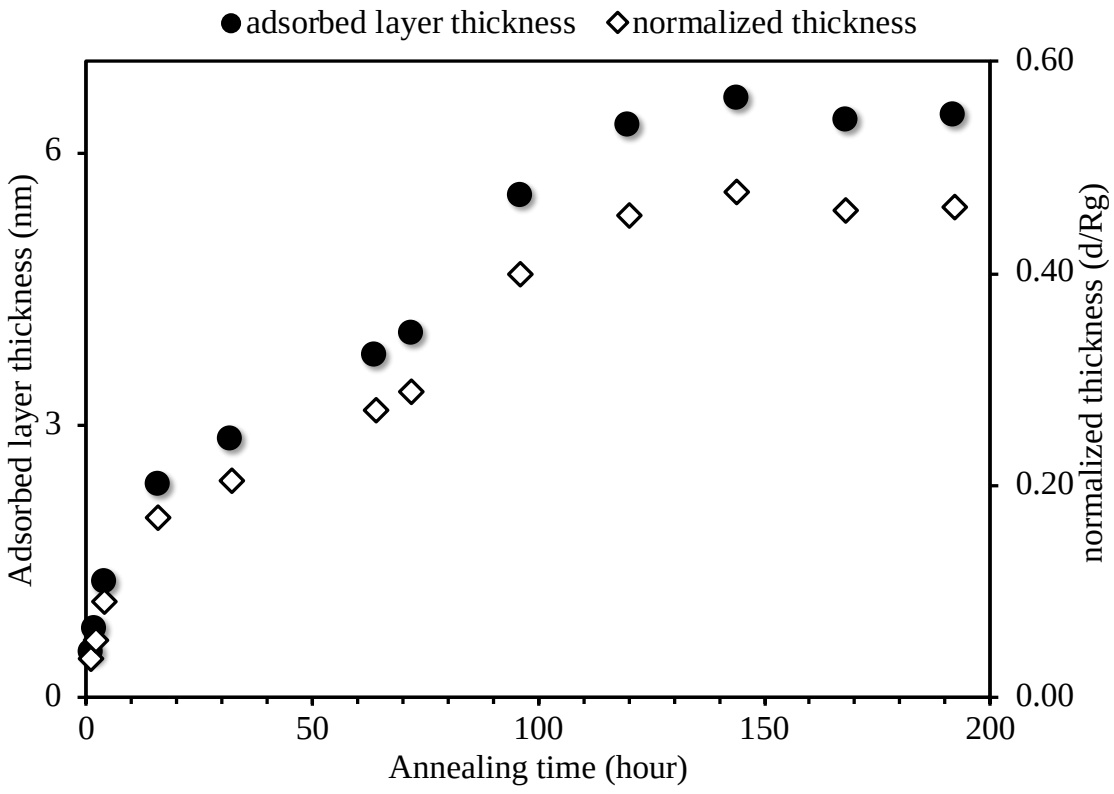

Figure 3.4. Adsorbed layer (filled spheres) and normalized thickness (empty diamonds) as a function of annealing time for 4-arm star PS chains on SiO_x.

Star polymers are branched polymers with one junction point. There are other types of branched polymers for which the number of junction points is larger than 1. For example, comb and centipede polymers may have multiple junction points and investigation of their adsorption can possibly tell us the importance of number of junction points. Of course, depending on the density of junction points the conformation of comb and centipede will change and backbone stretching will contribute as well. Adsorption of comb PS (Mn=734 kg/mol) on SiH surface is illuminated following the same experimental protocol. Comb PS with total M_n of 734 kg/mol and $M_{n,arm}$ of 58.5 kg/mol is synthesized and used for the adsorption studies as well. It has 6.3 branches and the M_n of the backbone was 365 kg/mol. Adsorbed layer thickness results obtained by ellipsometry are plotted in Figure 3.5. Thickness of the adsorbed layer starts from 9.7 nm at 1 hour and rises to 15.7 nm at 32 h of annealing. Adsorbed layer thickness does not change much beyond 32 h of annealing and equilibrium adsorbed layer thickness is 16.2 nm. The value of $d_{ads,eq}/R_g$ is calculated as 0.93 which is larger than that of linear PS and 4-arm star PS chains.

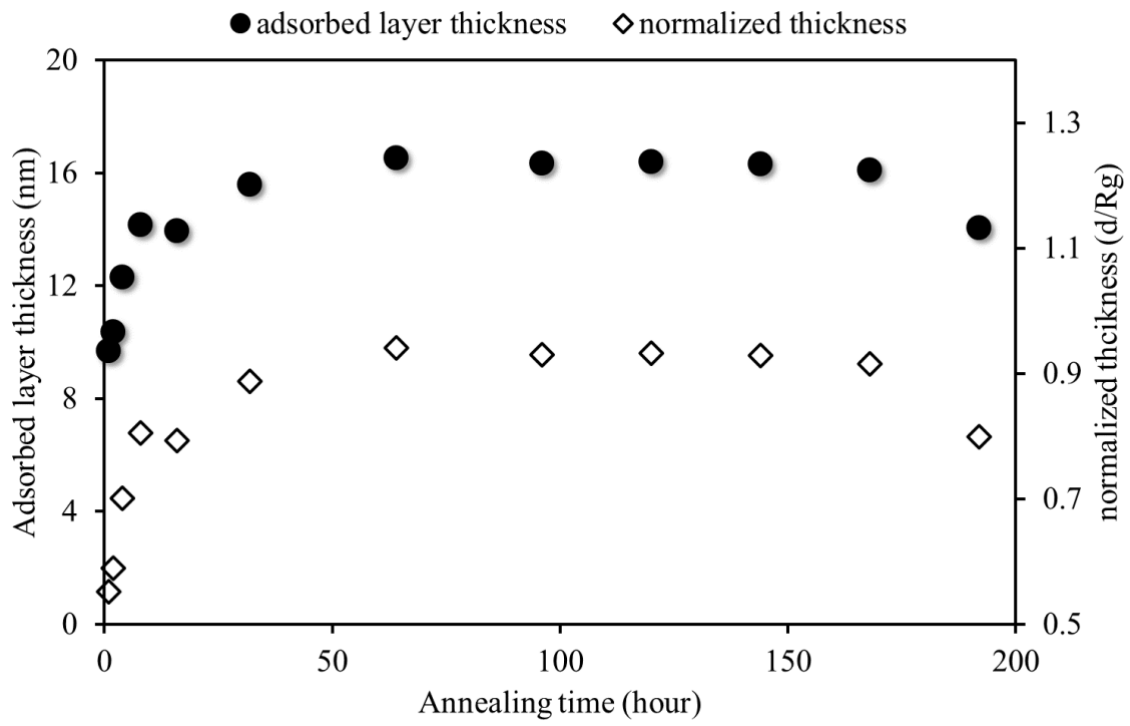

Figure 3.5. Adsorbed layer (filled spheres) and normalized thickness (empty diamonds) as a function of annealing time for comb PS chains on SiH.

When the same comb PS is adsorbed onto SiO_x surface, adsorbed layer reached its equilibrium thickness of 8.5 nm which yields $d_{ads,eq}/R_g$ value of was 0.49 (Figure 3.6). Adsorb layer thickness reached its equilibrium value in 64 h and this was faster than linear PS and 4-arm star PS.

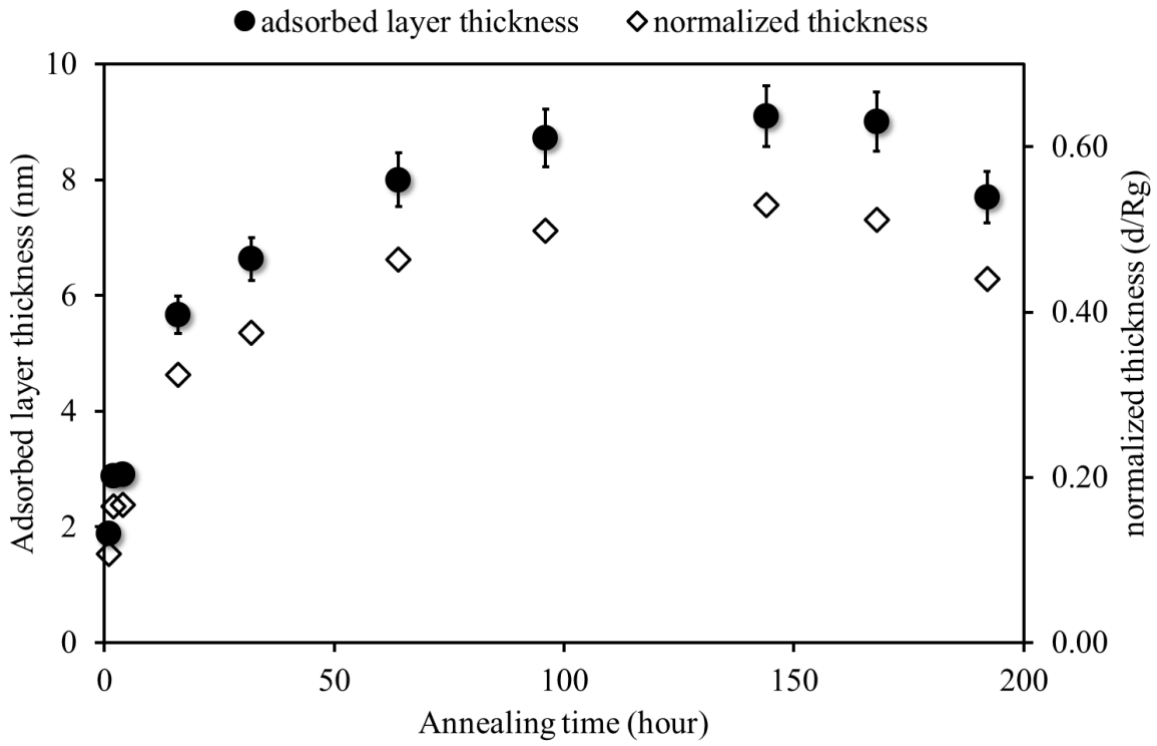

Figure 3.6. Adsorbed layer (filled spheres) and normalized thickness (empty diamonds) as a function of annealing time for comb PS chains on SiO_x.

Centipede PS with total M_n of 540 kg/mol and $M_{n,arm}$ of 28.1 kg/mol is synthesized and used for the adsorption studies as well. It has 4.5 branches and arms are paired on both sides of the main backbone. Therefore, the M_n of the backbone was 287 kg/mol. Backbone and arms of centipede PS are shorter than comb PS. Hence, centipede PS has a higher branching density than the comb PS. Figure 3.7 shows at 32 h centipede PS adsorbed layer formation reaches its first plateau around 13.6 nm and then there is a small increase at 120 h to attain average equilibrium thickness of 15.3 nm. R_g is estimated as 14.5 nm using DLS and normalized thickness of 1.04 is the highest among these four different PSs on SiH surface.

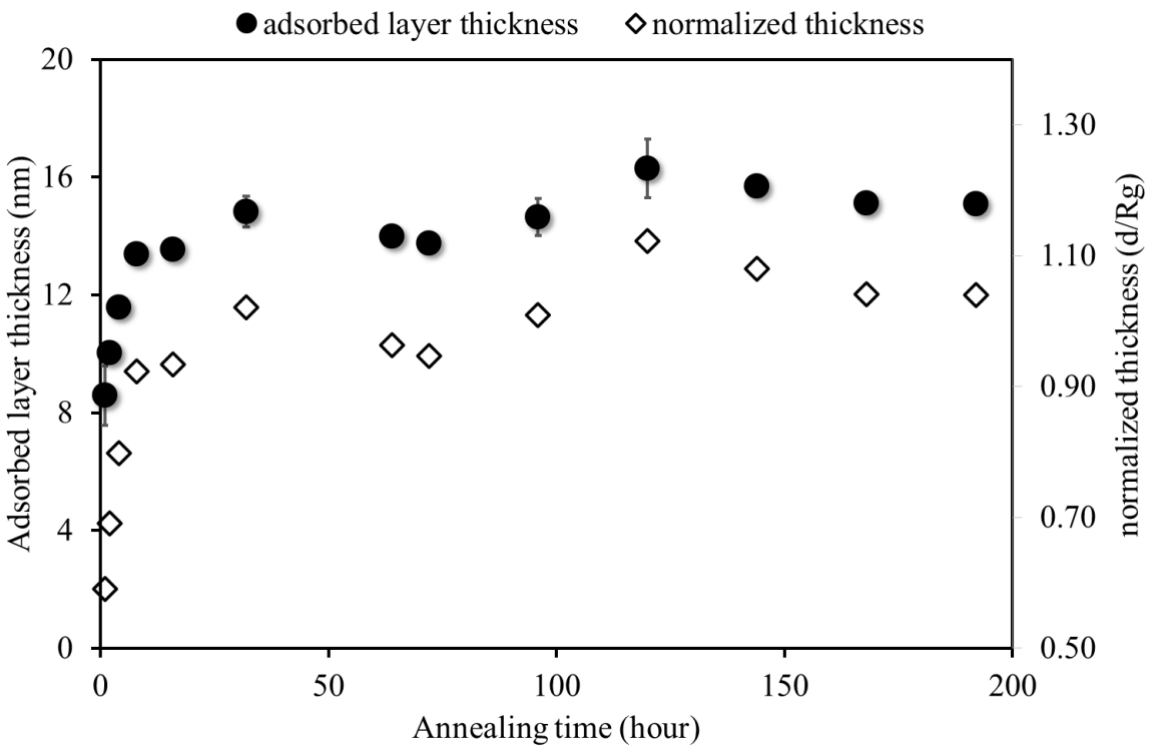

Figure 3.7. Adsorbed layer (filled spheres) and normalized thickness (empty diamonds) as a function of annealing time for centipede PS chains on SiH.

Adsorption of centipede PS on SiO_x surface is also measured with ellipsometry and thickness values after toluene leaching are summarized in Figure 3.8. Adsorbed centipede PS layer on SiO_x surface grows to its average value more gradually than on SiH which is similar to other PS samples. However, the time it takes to reach equilibrium value was almost same on both surfaces. This behavior is different than the other samples. Equilibrium adsorbed layer thickness is obtained as 9.1 nm after 96 h. Normalized thickness of 0.6 is the highest between all samples and factor of 2 larger than the linear PS on SiO_x.

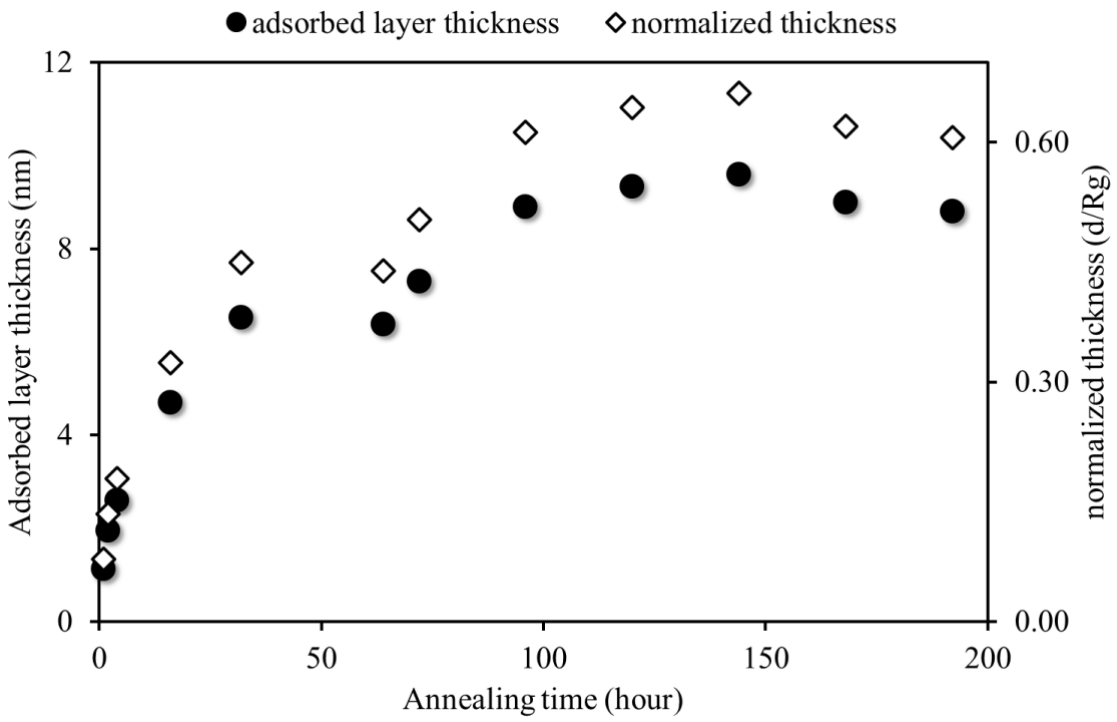

Figure 3.8. Adsorbed layer (filled spheres) and normalized thickness (empty diamonds) as a function of annealing time for centipede PS chains on SiO_x.

Figures 3.9 and 3.10 demonstrate the normalized thickness values for all PS samples together on both surfaces and the most important result from the ellipsometric measurements is that normalized thickness of the adsorbed layer increases as the branching of the polymer increases. Since normalized thickness value is already taking size differences between different PS samples into account, we could claim that the differences in entropic contribution play an important role in adsorption and one can alter the growth of adsorbed layer by tuning the entropic factor through change in polymer architecture.

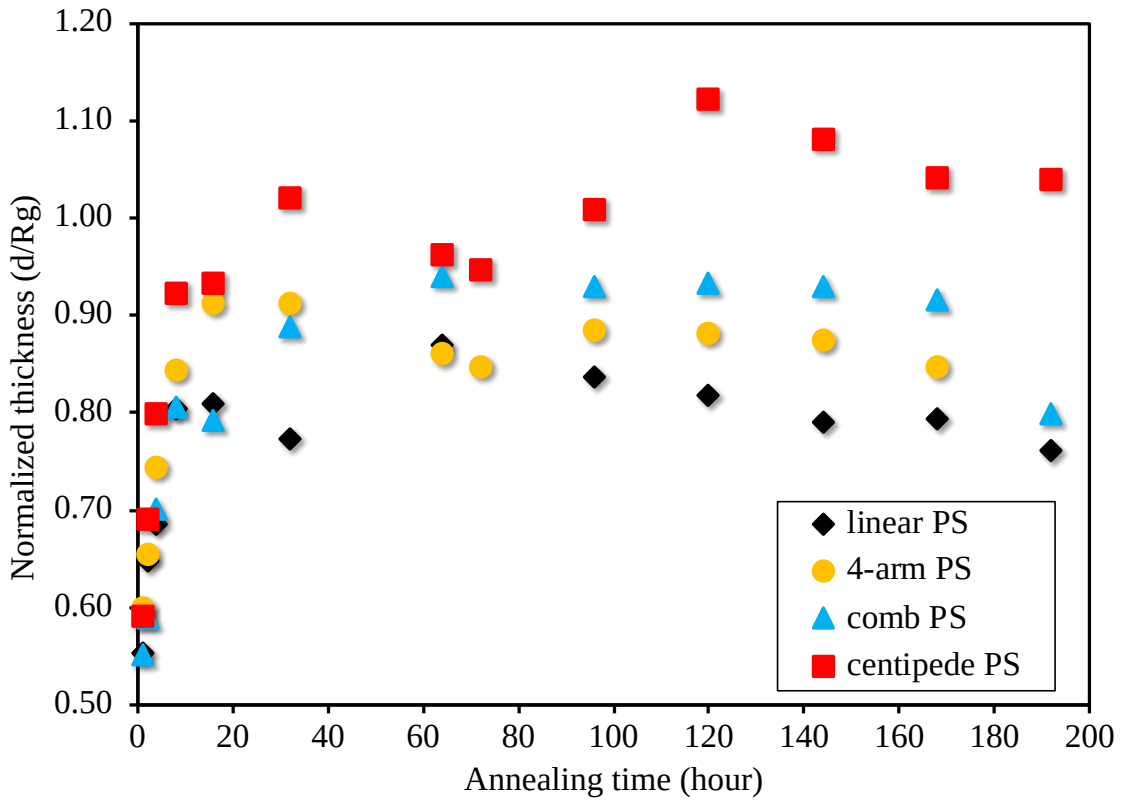

Figure 3.9. Normalized thicknesses as a function of annealing time for linear PS, 4-arm star PS, comb PS and centipede PS chains on SiH.

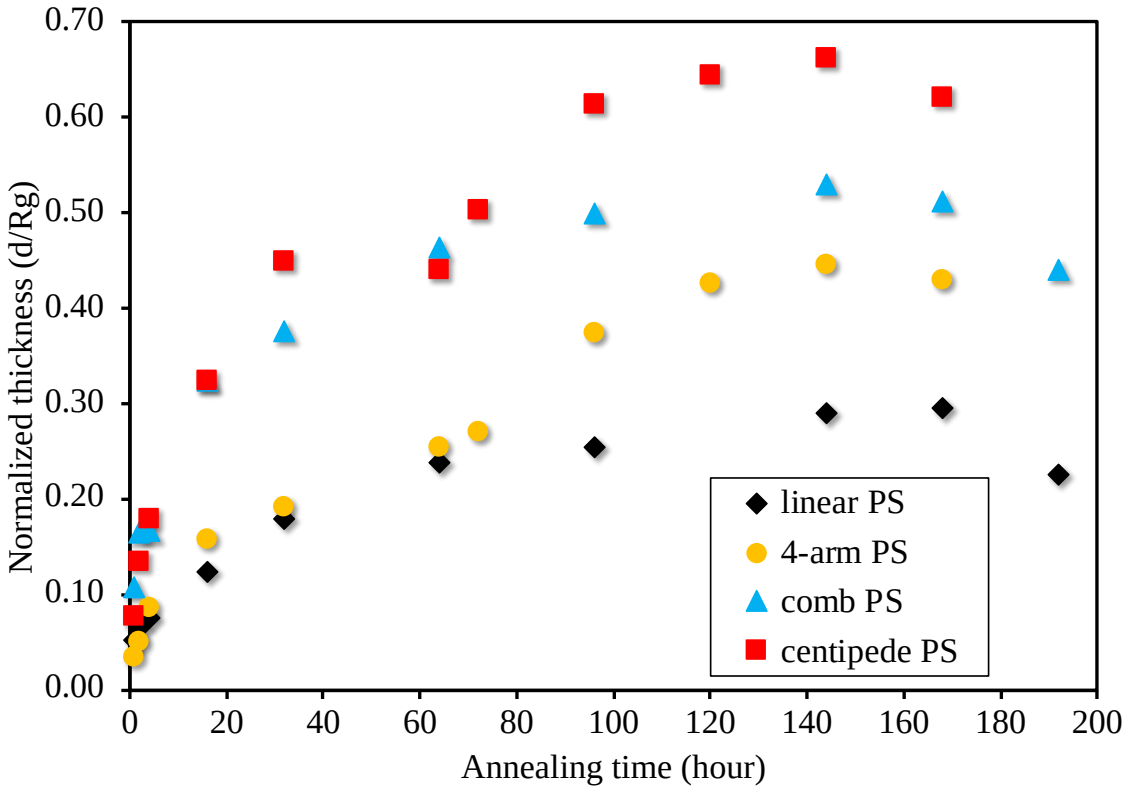

Figure 3.10. Normalized thicknesses as a function of annealing time for linear PS, 4-arm star PS, comb PS and centipede PS chains on SiO_x.

3.2. Layer Structure of Adsorbed Layers

3.2.1. Branched Adsorbed PS layers on SiH

The layer structure of adsorbed PS films was investigated using X-ray reflectivity (XR) measurements, and the surface morphology was monitored by atomic force microscopy (AFM). The information about the layer thickness, interface and surface roughnesses, and the electron density vs depth profile are obtained by fitting the XR data using REFLPAK software [53]. REFLPAK uses XR scattering length density (SLD) values instead of electron density values. Both electron density and SLD values are related to the mass density of the polymer and number of electrons that the repeating unit has. Therefore, the distribution profile of mass density in the perpendicular direction can be derived. SLD value of PS in bulk, SiO_x and Si are calculated as 9.6×10^{-6} Å^{-2}, 1.88×10^{-5} Å^{-2}, and 2×10^{-5} Å^{-2}, consecutively. SLD values of Si and SiO_x are kept constant through fitting process. However, SLD value of branched PS layers are used as a fit parameter and the value is obtained from the best model fit.

Logarithm of reflectivity is plotted against momentum transfer wave-vector in z-direction (q_z) for linear PS adsorbed layers on SiH as a function of annealing time (Figure 3.11). Annealing time for each reflectivity profile is given next to the curve. Real data points are shown as empty circles and the reflectivity from the best fit models are shown with solid lines. The agreement between these two demonstrates the goodness of the fit. Minima of Kiessig fringes shift gradually towards lower q_z-values as the annealing time increases to 16 h. Lower q_z values in reciprocal space corresponds to larger length scale in real space. Hence, the thickness of the adsorbed layer increases up to 16 h. Between 16 h and 192 h, the minima values shift slightly towards right or left, and this indicates that the thickness of the layer does not change much around an average value. The absence of damping in fringe amplitude shows that the roughness does not increase with increase in annealing time. One can calculate the thickness of the adsorbed layer from the spacing between the consecutive minima or maxima. For example, the thickness of the adsorbed layer after 192 h annealing

calculated to be 10.6 nm from this rather crude calculation. However, more accurate modeling analysis yields 10.8 nm. This demonstrates that even simple calculations from the raw data can give pretty accurate thickness values.

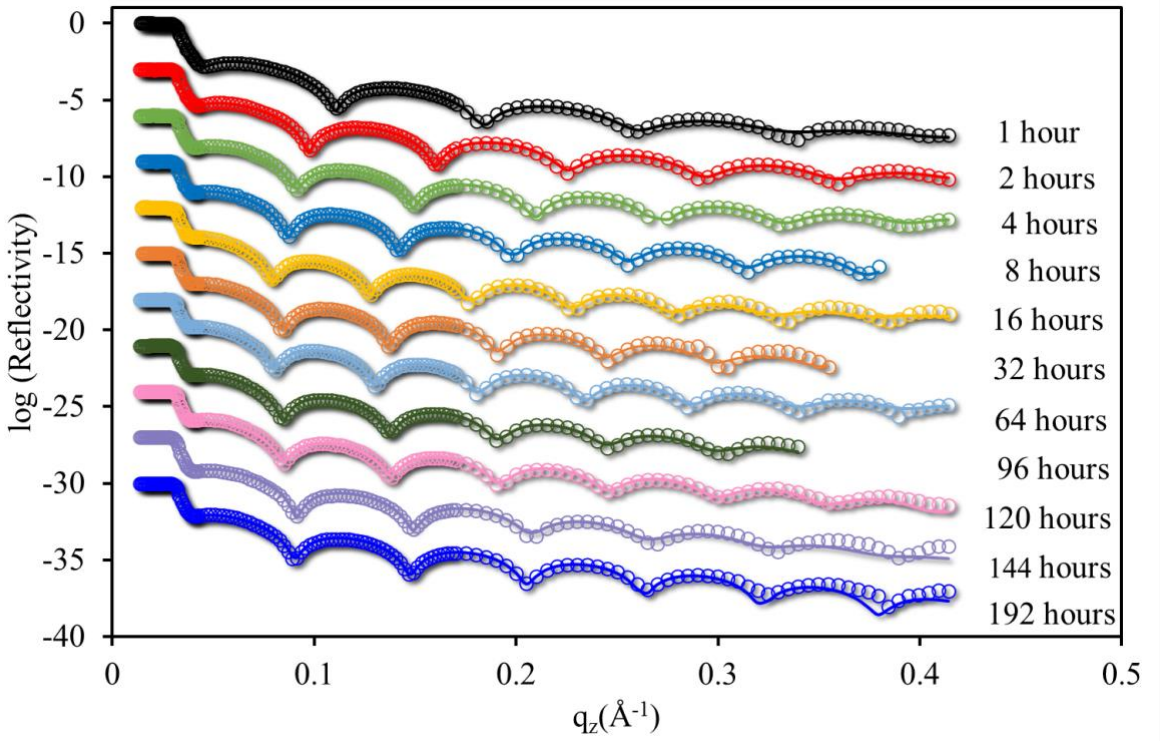

Figure 3.11. XR data (open symbols) and best fit model curves (lines) as a function of momentum transfer wave vector in the perpendicular direction to the surface, (q_z), for linear PS on SiH from 1 h to 192 h of annealing at 150°C. Adjacent curves have been shifted vertically by $\log(10)^{-3}$ for clarity.

It is not possible to obtain quantitative information about roughness and SLD values, instead only qualitative information about these parameters can be acquired from the visual inspection of the raw reflectivity curve. SLD values of the layers and the roughness values at each interface can only be determined from the fitting. SLD profiles obtained from the real space models which provided the best fits are plotted as a function of depth in Figure 3.12. An SLD profile demonstrates the change in mass density along the z-direction. We can see layers with different densities in Figure 3.12. SLD profile for 1 h annealing indicates that the model has three different layers. Between depth of -2 nm and 2 nm, there is a semi-infinite Si slab for which the SLD value is 2×10^{-5} $Å^{-2}$. Then there is a layer with SLD value

of 1.6 x 10^{-5} $Å^{-2}$. The SLD value for native SiO_x layer is 1.88 x 10^{-5} $Å^{-2}$ and obviously this layer is not a pure SiO_x layer. However, the SLD value of the layer is extremely high for a polymer layer as well. Koga and coworkers [54] found that the flattened PS chains form a layer denser than that of chains in bulk and the density difference is around 20% at most. This gives an upper bound for the SLD value of PS chains around 1.2 x 10^{-5} $Å^{-2}$ which is markedly lower than the apparent SLD value of the layer. The SLD value of 1.6 x 10^{-5} $Å^{-2}$ indicates the possibility of a layer composed of both linear PS chains and SiO_x. Even though SiO_x layer is etched by HF treatment, it is very well known that SiO_x layer regrows rather quickly if the substrate is exposed to oxygen or air for a prolonged time. The initial linear PS films were spun-cast within 20 to 30 seconds after the HF treatment. Hence, we are not expecting SiO_x layer formation during this period.

Most likely explanation for the presence of the SiO_x in the layer is that during the early annealing times for the spun-cast layer, adsorbed PS chains do not cover the whole substrate. There are bare Si regions on the surface which are exposed to air after toluene leaching and SiO_x layer regrows in these regions. Since apparent SLD value obtained by fitting is a linear combination of the SLD values of SiO_x and the PS, we have calculated the volume fraction of PS in this layer as 0.4 after 1 h annealing. Finally, there is a layer of PS between the depths of 3 nm and 11.5 nm, which yields thickness of 8.5 nm. The dashed horizontal line indicates the bulk SLD value of 9.6 x 10^{-6} $Å^{-2}$ for PS. This PS layer has almost bulk-like SLD. The same model fits the data quite well for measurements up to 8 hours of annealing. There are two layers composed of adsorbed polymer chains. One is next to the substrate and it is mixed with regions of SiOx and the second one on top of this layer consists of only adsorbed PS chains.

As the coverage of the adsorbed chains increase, it is expected to find much less SiO_x since there will be smaller regions for it to regrow. SLD profile for 16 h annealing demonstrates a decrease in the SLD of the mixed layer and concurrent increase in thickness. This decrease in SLD suggests a decrease in the volume fraction of SiOx and an increase in the volume fraction of the adsorbed PS chains. If we assume again that the literature value for the flattened PS layer from Koga's work is correct than the volume fraction of the adsorbed PS chains in this layer becomes 1. If we were able to fit all the reflectivity data for

longer annealing times using the same model, then the model would be satisfactory. However, this two-layer model is not necessary for data after 64 h annealing. A single layer model is able to provide excellent fits to the data with adsorbed PS chains having bulk SLD value. If the SLD value of the adsorbed PS chains assumed to be same as bulk SLD in the mixed layer, then the volume fraction of PS chains become 0.3 for 1h annealing and 0.74 for 16 h annealing. Overall, our model shows a single layer of adsorbed PS chains on SiH substrate which is not consistent with results of Koga and coworkers [54].

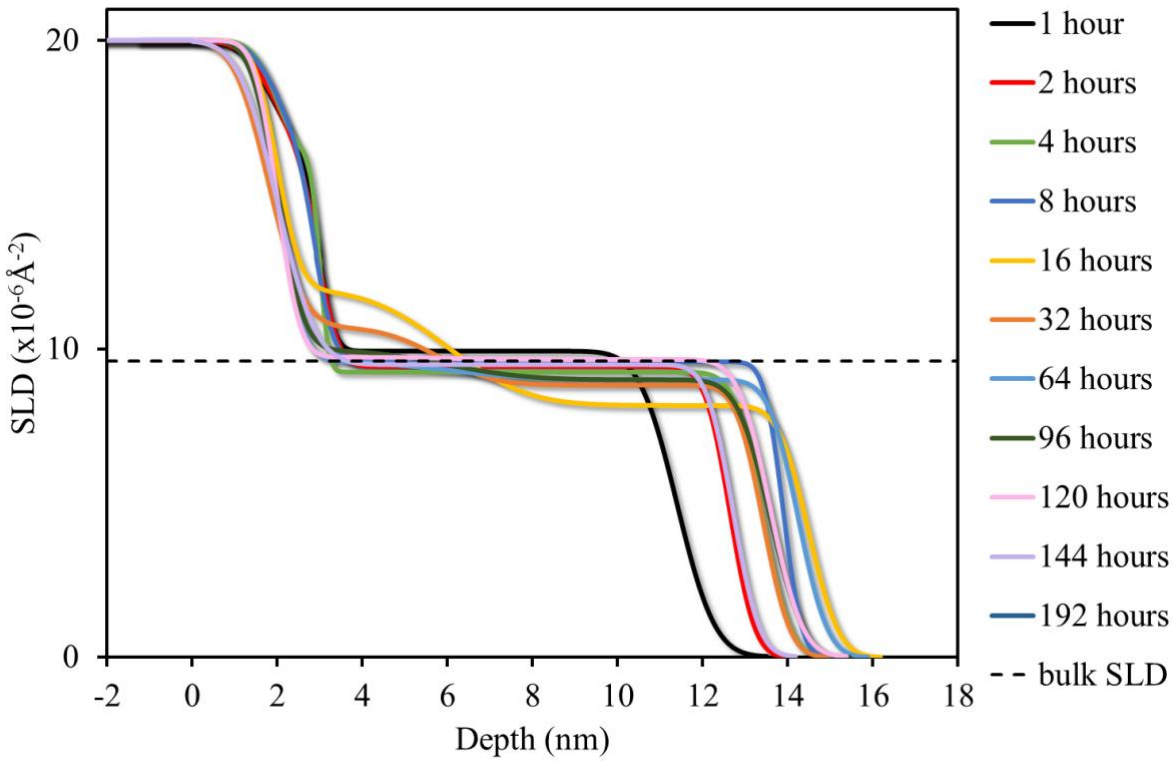

Figure 3.12. Scattering length density (SLD) as a function of depth for linear PS from 1 h to 192 h of annealing at 150 ℃ on SiH.

Adsorbed layer thicknesses obtained by the best fits are compared with the ones obtained from ellipsometry measurements in Figure 3.13 for linear PS. There is an excellent agreement between the two techniques and the difference between the two is at most 10 %.

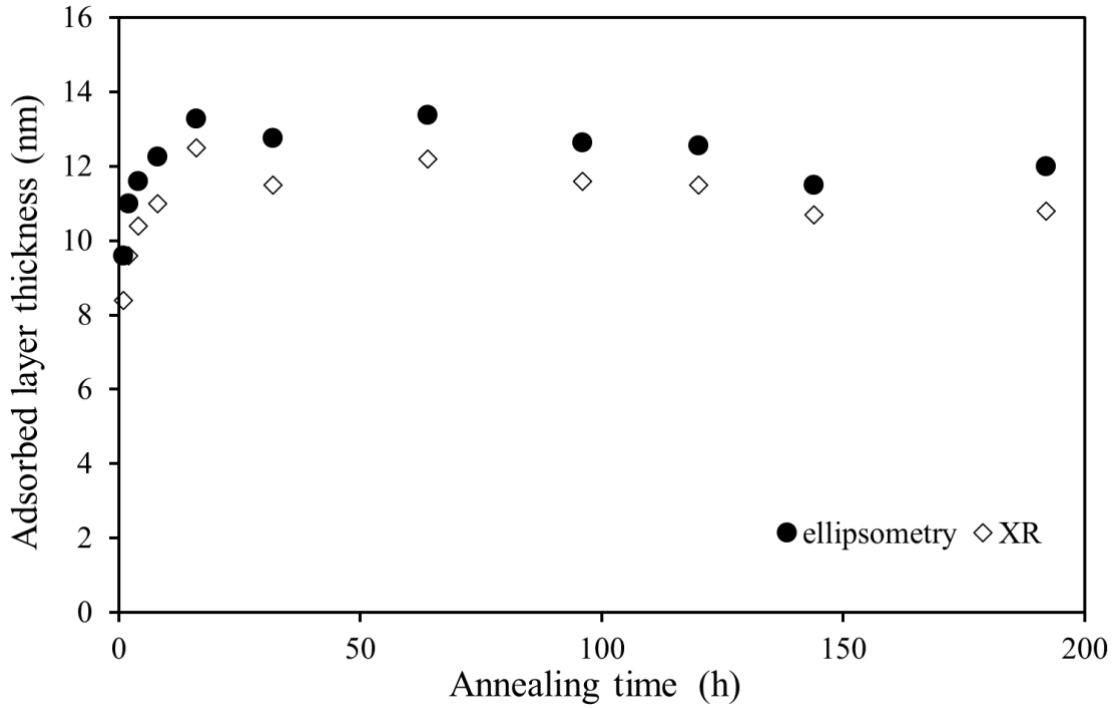

Figure 3.13. Adsorbed layer thickness as a function of annealing time measured by ellipsometry (filled spheres) and XR (empty diamonds).

XR curves measured for the adsorption of 4-arm star PS on SiH substrate at 150 ℃ are shown in Figure 3.14 for various annealing times and corresponding SLD profiles are shown in Figure 3.15. Spacing of Kiessig fringes shows an increase in the thickness of the adsorbed layer up to 32 h and then a slight decrease followed by no change after 72 h.

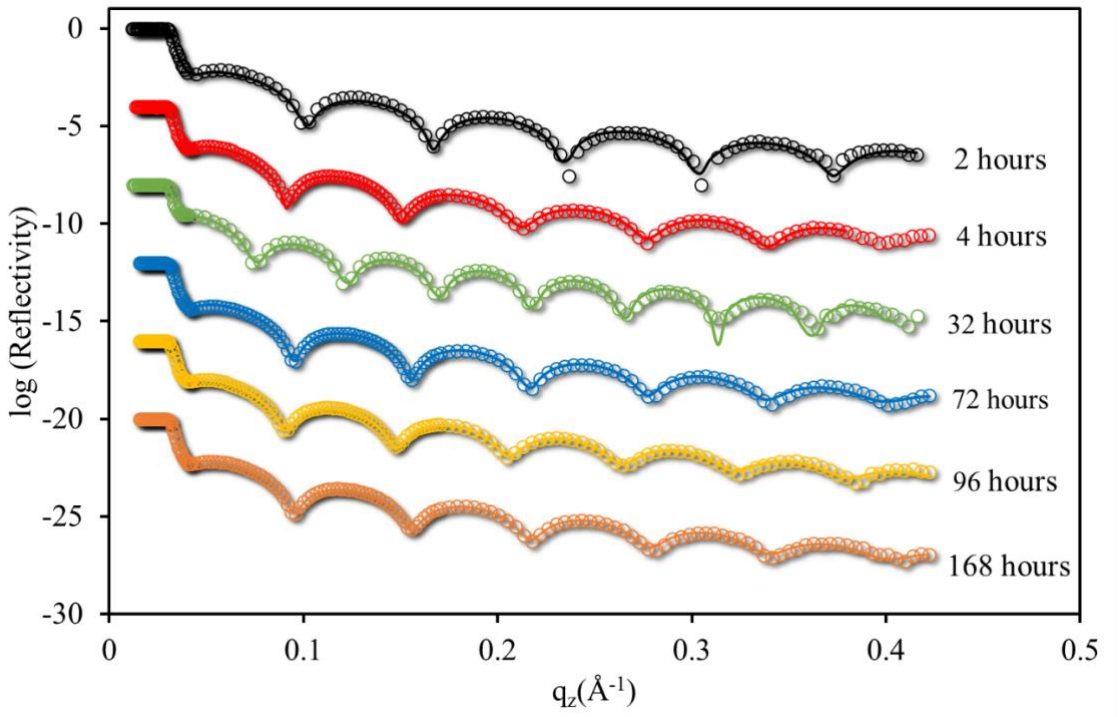

Figure 3.14. XR data (open symbols) and best fit model curves (lines) as a function of q_z for 4-arm star PS on SiH from 2 h to 168 h of annealing at 150°C. Adjacent curves have been shifted vertically by log (10)$^{-4}$ for clarity.

SLD profile for 4-arm star PS adsorption measurements on SiH substrate demonstrates similar structural features with the linear PS. At very early stages of annealing there are two layers one with the regions of adsorbed 4-arm star PS and empty areas filled by regrowing SiO_x and another layer on top composed of adsorbed 4-arm star PS chains. Volume fraction of 4-arm star PS chains in the mixed layer is 0.2 after 2 h of annealing and then it increases to 0.3 at 4 h of annealing. Once all the substrate surface is covered by the adsorbed chains and no SiO_x exists then a single layer model gives reflectivity curves overlaps well with experimental curves. The SLD of this single polymer layer is around the bulk SLD value for the 4-arm star PS chains. After the adsorbed layer thickness reaches an equilibrium, single layer with bulk density is sufficient to define the structure. This layer is quite smooth with rms roughness value, $\sigma_{rms,XR}$, of 0.4 nm.

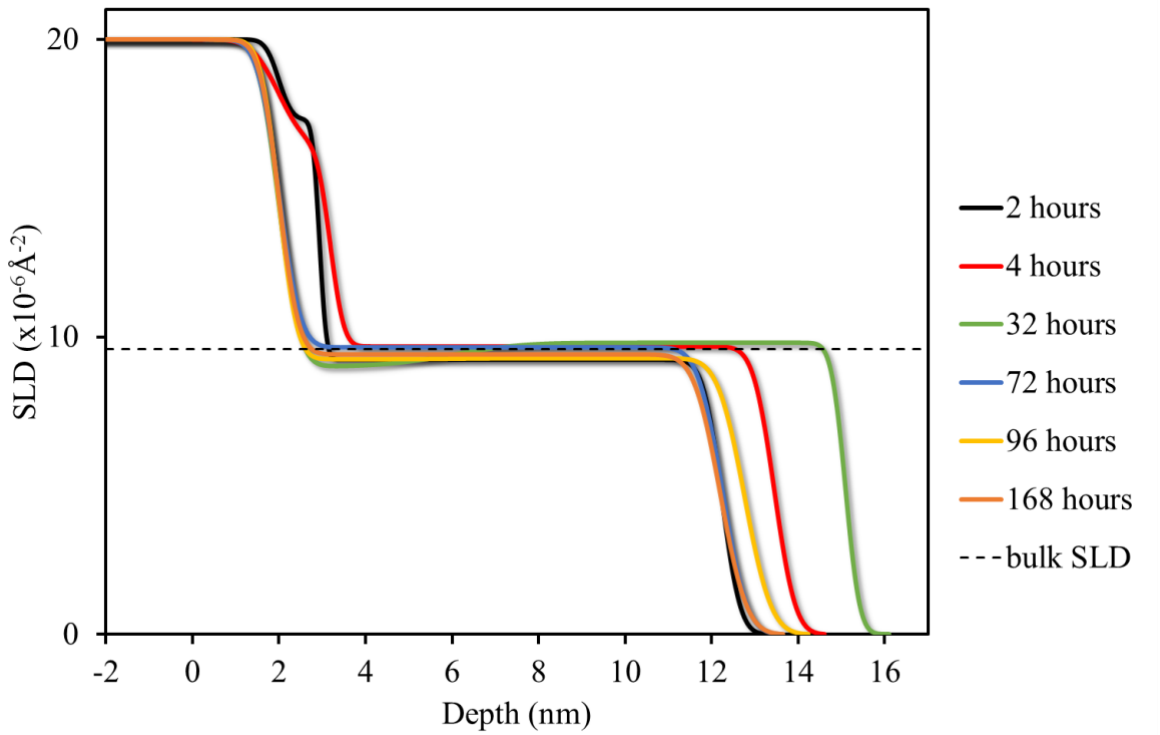

Figure 3.15. The SLD as a function of depth for 4-arm star PS from 2 h to 168 h of annealing at 150 ℃ on SiH.

The similarities of the adsorbed layer structure for 4-arm star PS and linear PS suggest that the architecture affected only equilibrium adsorbed layer thickness, not the layer structure. To gain more insight about the impact of architectural changes on the layer structure, adsorption of comb PS on SiH surface at 150 ℃ is investigated. Reflectivity profiles at various annealing times between 1 h and 120 h are illustrated in Figure 3.16. Initial thickness of the film is 10.6 nm after an hour and at equilibrium adsorbed layer thickness is 17.4 nm. In terms of absolute thickness, comb PS forms the thickest adsorbed layer. However, it has the highest molecular weight and therefore the largest R_g value between the branched PSs and its normalized thickness is not the highest. The normalized thickness of adsorbed layer at equilibrium is 1. Reflectivity curves show Kiessig fringes at high q_z-values are dampened more compared to linear and 4-arm star PS adsorbed layers. Even though comb PS adsorbed layer has the highest $\sigma_{rms,XR}$ value between all the samples it is 0.6 nm and the layer is considered to be quite smooth.

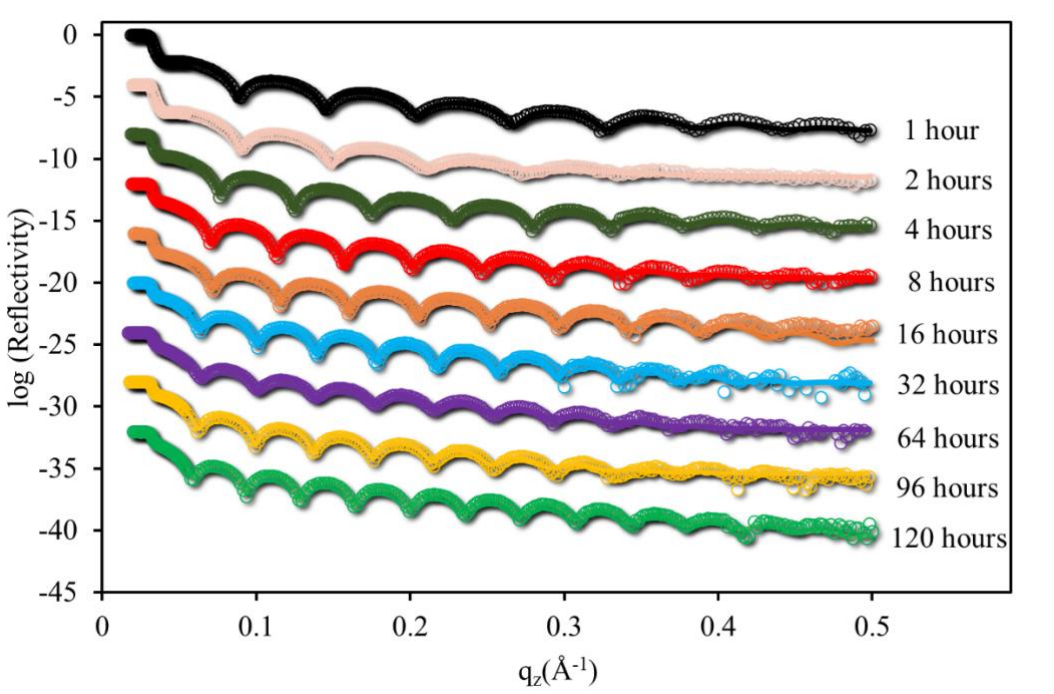

Figure 3.16. XR data (open symbols) and best fit model curves (lines) as a function of q_z for comb PS on SiH from 1 h to 120 h of annealing at 150°C. Adjacent curves have been shifted vertically by log (10)$^{-4}$ for clarity.

From 1 to 4 h of annealing, adsorbed layer has bilayer structure, there is a 1.2 nm thick region with SLD value of 1.6x10^{-5} Å^{-2} as previously observed for linear and 4-arm star PS on SiH. At 8 h, there is a bilayer structure, but bottom layer has a smaller SLD value (1.06x10^{-5} Å^{-2}) compared to earlier annealing times. Adsorbed layer has single layer structure starting from 16 h. It means that almost all the surface sites are covered by adsorbed PS chains between 8 h to 16 h. For a single layer model structure SLD values for the adsorbed PS chains are very close to bulk SLD value.

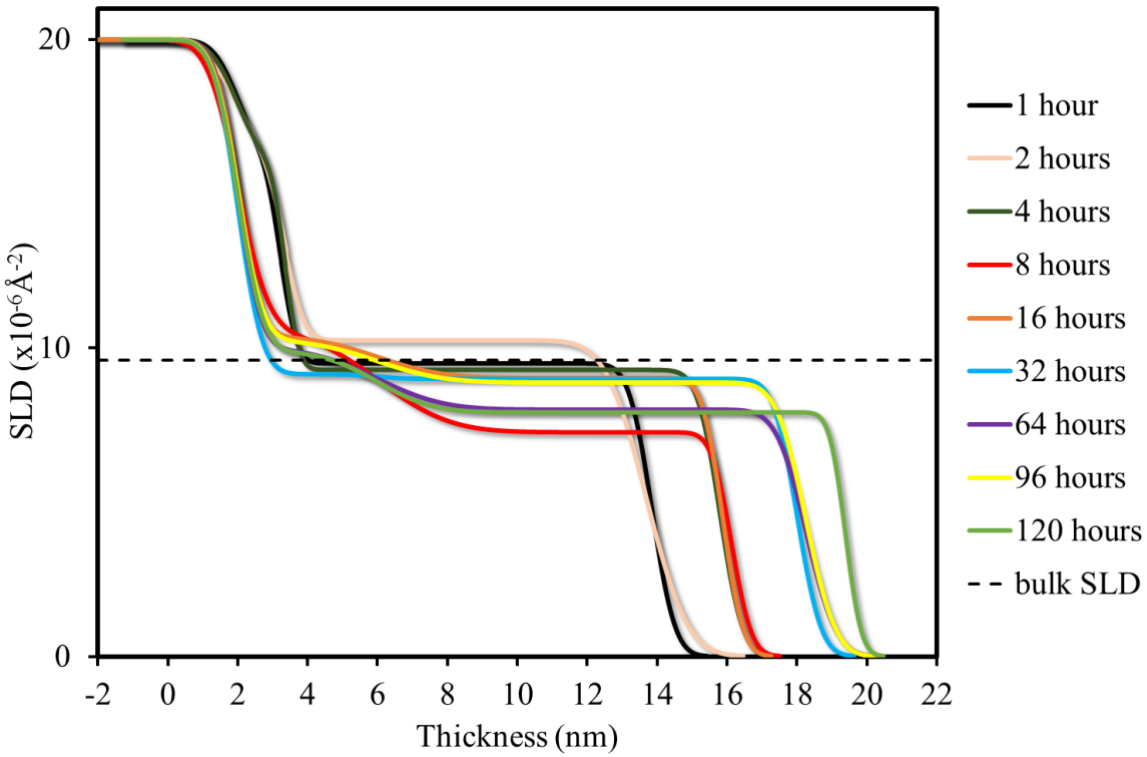

Figure 3.17. SLD as a function of depth for comb PS from 1 h to 120 h of annealing at 150 ℃ on SiH.

XR curves for centipede PS on SiH are shown in Figure 3.18. Adsorbed layer thickness increases rapidly in the first 8 h of annealing and then fluctuate around 16 nm as can be seen from the shift of the fringe minima. Since the molecular weight of centipede PS is smaller than the comb PS, the normalized thickness for equilibrium adsorbed centipede PS layer is the highest. Surface of the centipede PS adsorbed layers found to be smooth with $\sigma_{rms,XR}$ value in average 0.54 nm.

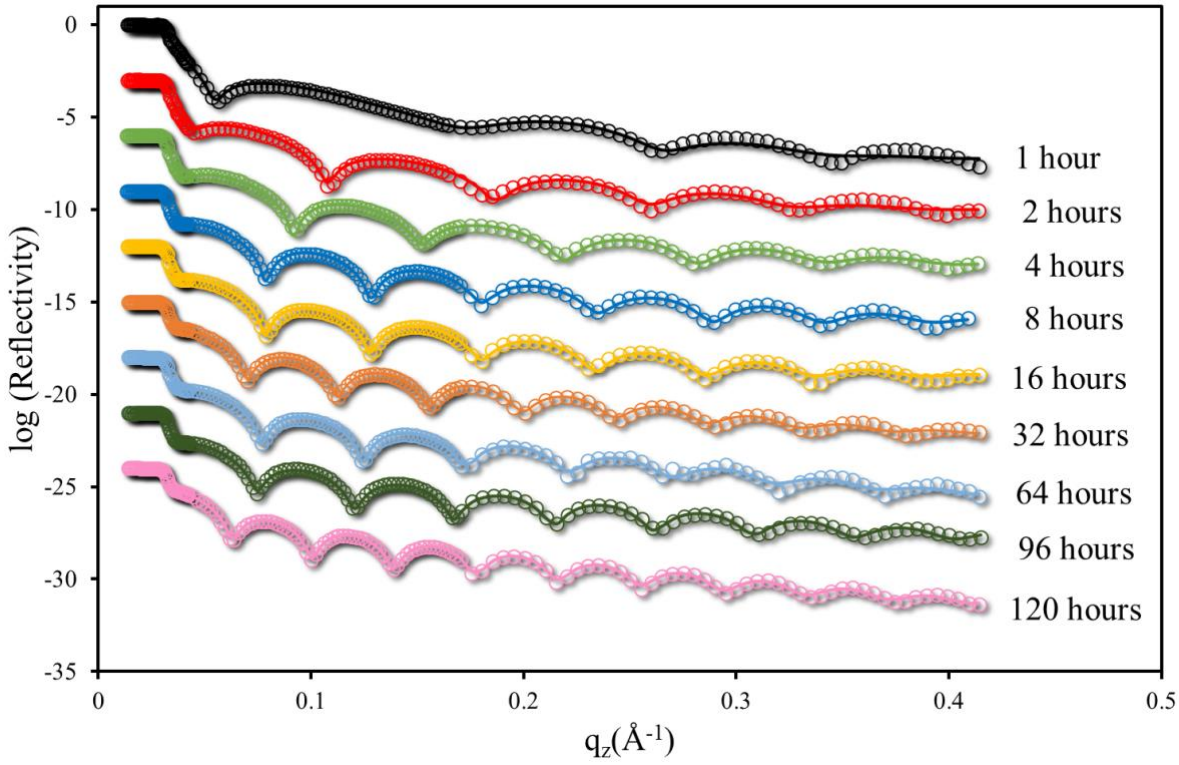

Figure 3.18. XR data (open symbols) and best fit model curves (lines) as a function of q_z for centipede PS on SiH from 1 h to 120 h of annealing at 150°C. Adjacent curves have been shifted vertically by log (10)$^{-3}$ for clarity.

SLD profiles belong to adsorbed centipede PS layers plotted in Figure 3.19 demonstrates a familiar picture to linear and 4-arm star PS SLD profiles. In the first 16 h of annealing there is a bilayer structure. Bottom layer is the mixture of adsorbed centipede PS chains and SiO_x regions and the top layer is composed of adsorbed centipede PS chains with bulk density. At 1 h, bottom layer is 2.5 nm thick and has a SLD value of 1.76 x 10^{-5} Å^{-2}. This SLD value corresponds to volume fraction of 0.14 for adsorbed centipede PS chains in the bottom layer. The amount of adsorbed polymer chains in the bottom layer is the lowest for centipede PS. Upon increasing annealing time, bottom layer thickness and SLD decreases and layer structure can be fit by a single layer with bulk SLD value at 32 h of annealing. This annealing time coincides well with the time it takes to reach equilibrium adsorbed layer in ellipsometry measurements.

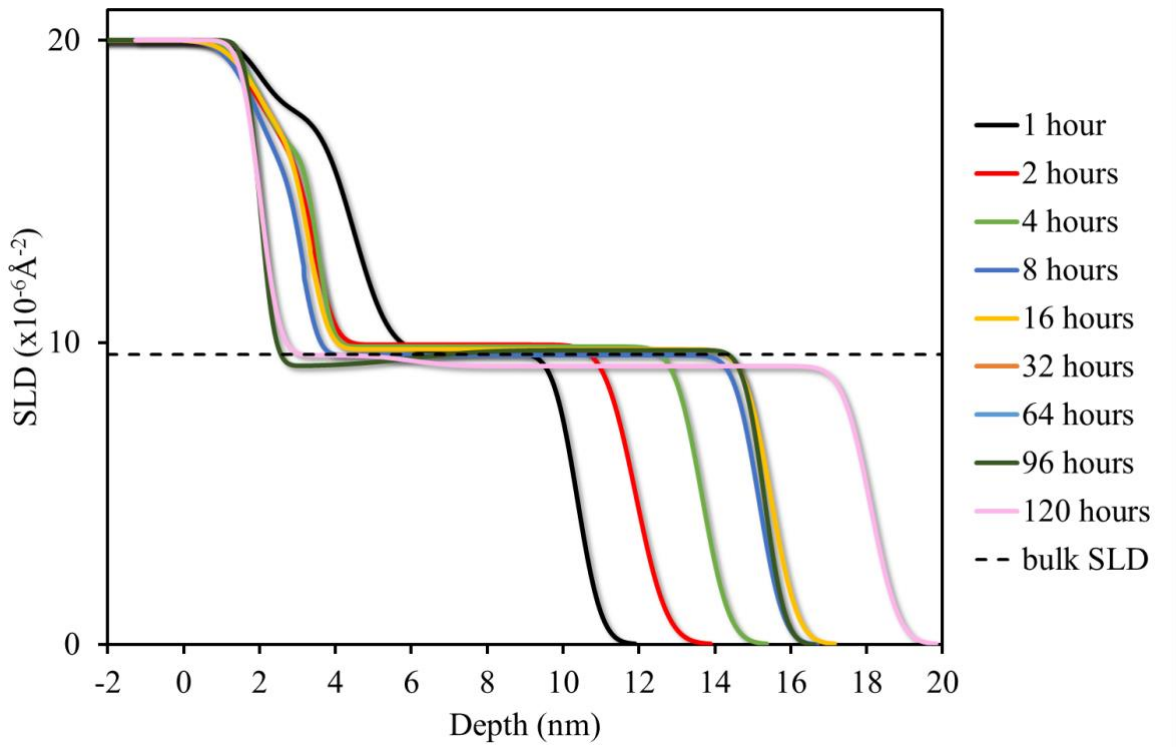

Figure 3.19. SLD profiles for centipede PS from 1 h to 120 h of annealing at 150 ℃ on SiH.

XR measurements indicates that the formation and structure of adsorbed layers composed of different branched PS chains are similar. Normalized thickness varies depending on the architecture, but the layer structure is not affected much. AFM measurements on the surface morphologies of 120 h annealed, toluene leached linear PS, 4-arm star PS, and centipede PS adsorbed layers on SiH showed $\sigma_{rms,AFM}$ of 0.275 nm, 0.511 nm and 1.26 nm respectively. The agreement between AFM and XR measurements for linear and 4-arm star PS is good however there is a discrepancy for centipede PS. Since both techniques are sensitive to different bandwidths, and measurements are done on different length scales, it is not surprising to have a difference between the two.

a)

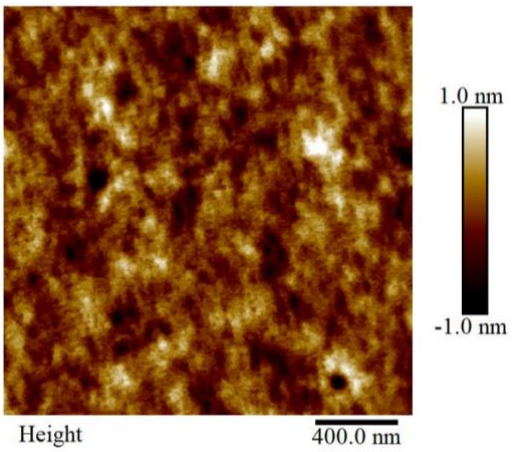

b)

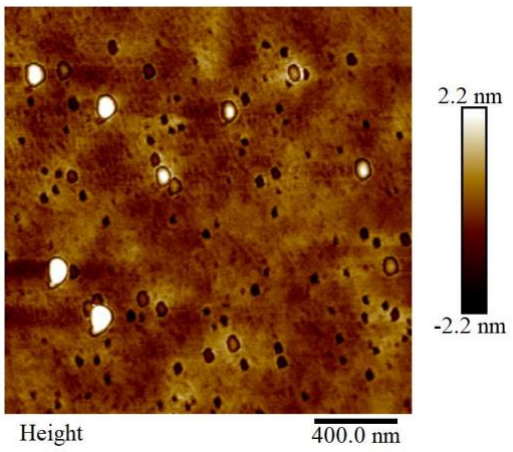

c)

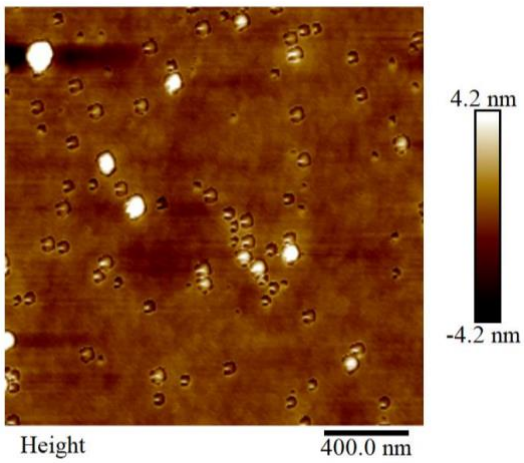

Figure 3.20. AFM height images for a) linear PS, b) 4-arm star PS, and c) centipede PS after they are annealed for 120 h at 150 ℃ and toluene leached.

3.2.2. Layer Structure of Adsorbed Polymer Chains on SiO_x

As explained in the introduction, the interaction energy between the polymer segments and the surface plays an important role in the formation of the adsorbed layer. It is possible to change either the polymer or the type of surface to form a different adsorbed layer. We have used Si surfaces covered with native oxide to understand the role of enthalpic interactions on the structure of adsorbed layer. Experimental adsorption protocol used for SiH substrates are repeated for linear PS, 4-arm PS, comb PS and centipede PS on hydrophilic SiO_x surface. Since PS is a hydrophobic polymer with advancing contact angle of 99°, one would expect that the interaction energy per segment between PS and SiO_x surface is much less compared to that between PS and SiH surface. For linear polymers, thickness of the adsorbed layer found to be lower on SiOx surface than on SiH surface. Assuming entropic contribution will not change dramatically, our expectation is to see thinner adsorbed layers on SiO_x surface. The layer structure of adsorbed layers is characterized using XR. Due to time constraints XR data is only collected for a few samples for each PS architecture.

XR curves collected for the adsorption of linear PS on SiO_x after 4 h, 32 h, and 196 h annealing at 150 ℃ are shown in Figure 3.21. When the XR data is compared with that belong to SiH surface, the most important difference is the frequency of Kiessig fringes and therefore the thickness of the layers. Adsorbed linear PS chains on SiO_x surface form thinner layers than on SiH surface. At 168 h of annealing the thickness of the adsorbed layer is 5 nm which corresponds to normalized thickness of 0.32 However, at the same annealing time on SiH surface (Figure 3.15) adsorbed layer is 12.2 nm thick and this value gives normalized thickness of 0.79. SLD profiles in the inset shows that the adsorbed linear PS chains are occupying single layer with SLD value increasing with annealing time. This suggests that the layer initially is not formed completely and only around 32 h all the empty surface sites are filled by the polymer. As the chains continue to adsorb density of the layer increases and the surface roughness of the adsorbed PS layer decreases.

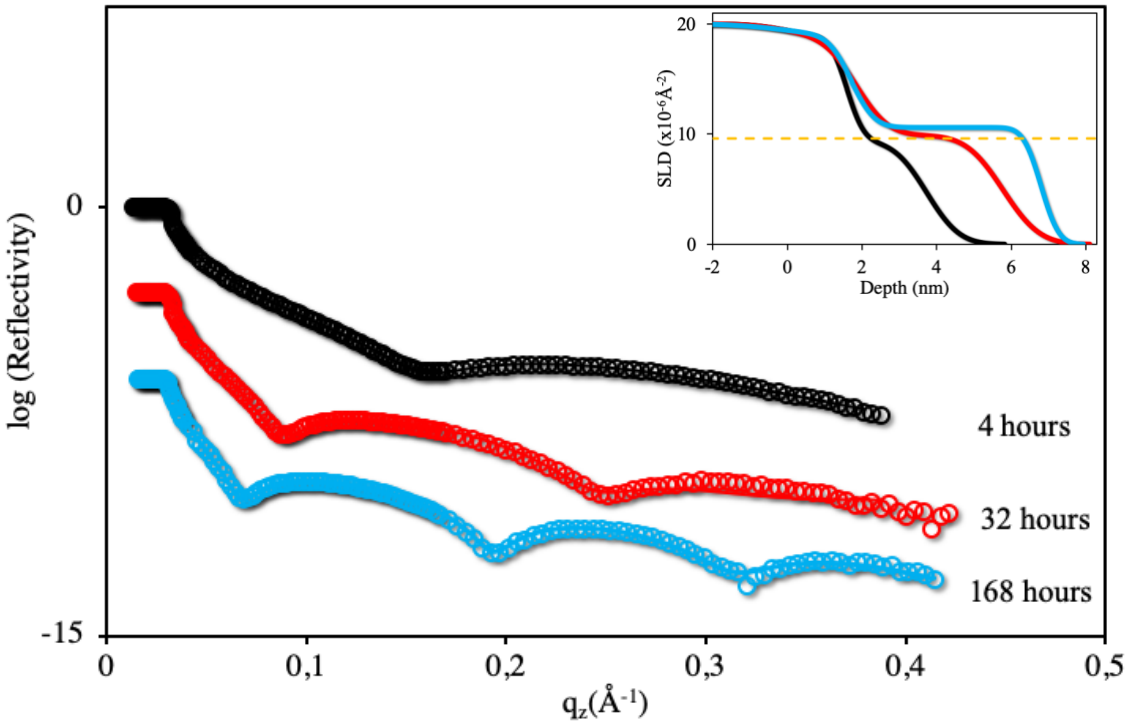

Figure 3.21 XR data (open symbols) and best fit model curves (solid curves) as a function of q_z for linear PS on SiOx for 4 h (black), 32 h (red), and 168 h (blue) of annealing at 150°C. Adjacent curves have been shifted vertically by log(10)$^{-3}$ for clarity. SLD profiles obtained from the best fits for 4h (black), 32 h (red) and 168 h (blue) are shown in the inset.

XR data for adsorption of 4-arm star PS chains on SiOx surface and corresponding SLD profiles (inset) are shown in Figure 3.22. 4-arm star PS chains have a silane core and the number of free ends is 4. As is evident from the XR data, increase in number of free ends from 2 (linear) to 4 gives rise to a thicker layer at 168 h. Again, at early times the SLD of the adsorbed 4-arm star PS layer is less than the bulk value and the layer is quite rough. These two important information points out an incomplete layer. At the beginning there is not a continuous layer instead there are patches of polymer and empty spaces in between these patches. SLD value of the layer reaches bulk SLD value for PS at 32 h and the roughness at the air surface decreases. Hence, at this point we can imagine that the layer is

completely formed and there are no more patches. SLD profile for 168 h indicate that the layer thickness increases without any change in the SLD value and surface roughness.

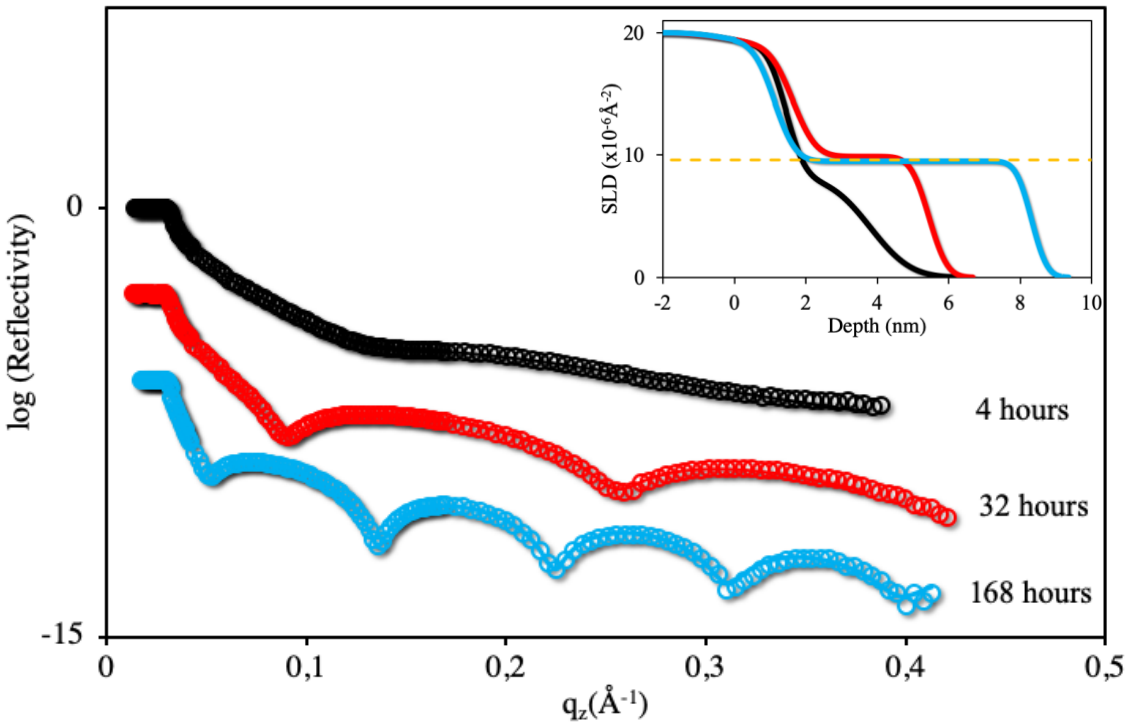

Figure 3.22. XR data (open symbols) and best fit model curves (solid curves) as a function of q_z for 4-arm PS on SiOx for 4 h (black), 32h (red) and 168 hours (blue) of annealing at 150°C. Adjacent curves have been shifted vertically by log(10)$^{-3}$ for clarity. SLD profiles obtained from the best fits for 4 h (black), 32 h (red) and 168 h (blue) are shown in the inset.

When more branched comb PS is adsorbed, there is a major difference at early annealing times. Adsorbed layer after 4 h of annealing already reached its bulk SLD value as shown in the inset of Figure 3.23. This implies that the stronger adsorption of comb PS on SiO_x surface compared to linear and 4-arm star PS architectures. Theoretical work of Kosmas et al. [35] indicated that the number of contacts a chain can make during the adsorption depends on the architecture. Linear polymers can make the less number of contacts, then star polymers with 3-or 4-arms. Ring polymers can make more contacts than these two and star polymers with higher functionality can pin with a greater number of contacts. In this scale of number of contacts comb polymers can be anywhere depending on a ratio of branch molecular weight over backbone molecular weight. As this ratio gets closer

to zero, number of contacts will be close to linear chains and as this number becomes larger, number of contacts will be similar to star polymers with higher functionalities. For the comb PS used in this study, the ratio is 0.16. This value is not large, but we do not have tabulated values to know exactly where this value will be placed on the scale. However, our data shows that the thickness of the adsorbed comb PS layer at 4 h is larger than both linear and 4-arm star PS. Adsorbed comb PS layer has already formed completely in the first 4 h of adsorption and the thickness remains to be larger than that of linear and 4-arm star PS throughout all the adsorption times.

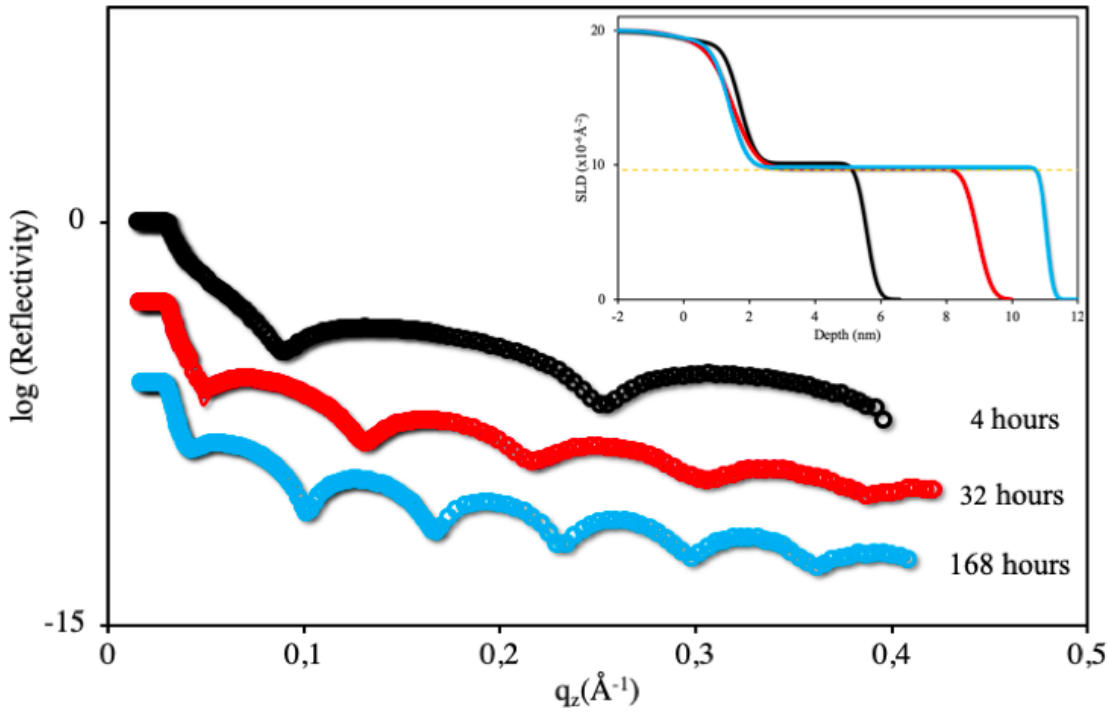

Figure 3.23 XR data (open symbols) and best fit model curves (solid curves) as a function of q_z for comb PS on SiO_x for 4 h, 32 h and 168 h of annealing at 150°C. Adjacent curves have been shifted vertically by log $(10)^{-3}$ for clarity. SLD profiles obtained from the best fits for 4 h (black), 32 h (red) and 168 h (blue) are shown in the inset.

Adsorption of centipede PS on SiO_x surface follows a very similar path to adsorption of comb PS. Even at 4 h there is a complete layer and this layer is slightly thinner than the comb PS adsorbed layer. However, for the longest annealing time of 168 h, centipede PS

layer becomes thicker than the comb PS adsorbed layer. At this point we should emphasize that the total molecular weight of comb PS is 1.5 times larger than that of centipede PS. Therefore, normalized thickness of centipede PS adsorbed layer is even larger than the absolute thickness value. SLD values at longer annealing times are lower than the bulk SLD value for PS. This decrease in SLD after 4 h suggests the rearrangement of the chains on the surface and increase in the loop and tail conformations and decrease in train conformation.

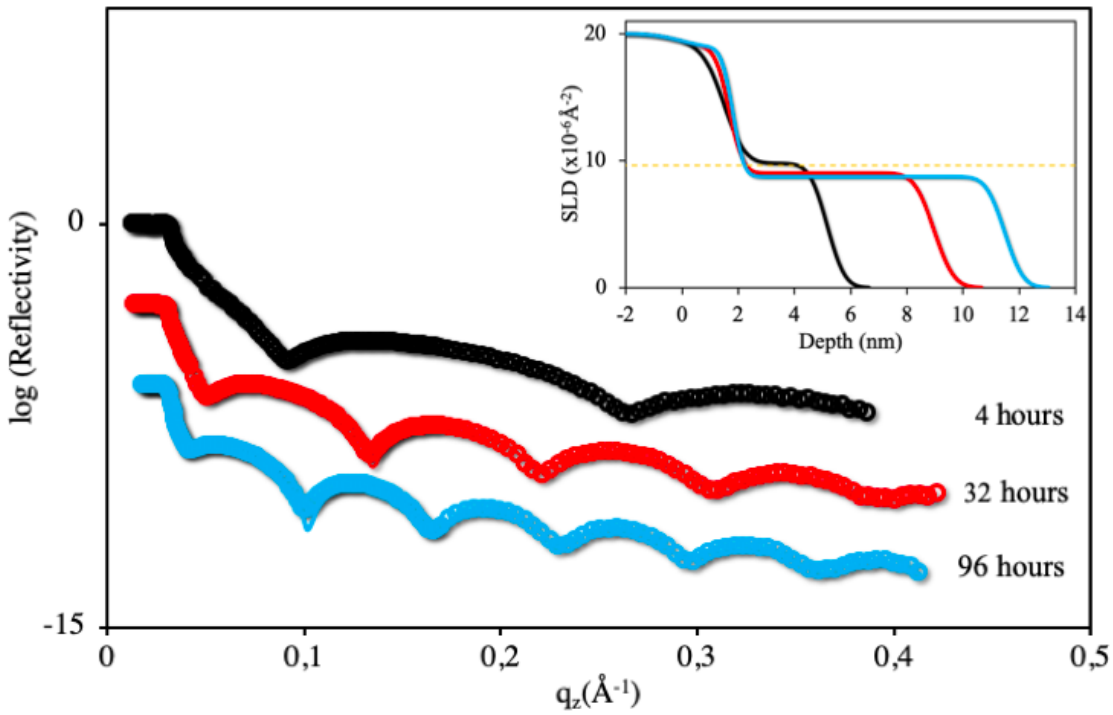

Figure 3.24. XR data (open symbols) and best fit model curves (solid curves) as a function of q_z for centipede PS on SiOx for 4 h (black), 32 h and 168 h of annealing at 150°C. Adjacent curves have been shifted vertically by log(10)$^{-3}$ for clarity. SLD profiles obtained from the best fits for 4 h (black), 32 h (red) and 168 h (blue) are shown in the inset.

In summary, at early times there is an incomplete layer formation for linear and 4-arm star PS on SiH and SiOx surfaces. Simultaneous SiOx growth on SiH substrate during adsorption obscures the expected low SLD value for PS layer in the SLD plots. However, volume fraction values around 0.15 to 0.3 for the first adsorbed layer indicates these layers are far from being complete. As the adsorption time increases, adsorbed layer continues to grow and complete layers with bulk-like density form. The same is true for comb and

centipede PS chains as well with one important difference at earlier adsorption times. Both polymers are adsorbed with bulk-like densities within the first 4 h of annealing. Later on, adsorbed comb and centipede layers grow in z-direction without a change in their mass densities.

Examining ellipsometry and XR data proves surface energy is one of the main parameters that dictates the extent of polymer adsorption. In each case, hydrophobic PS chains of different architectures adsorb to form thicker layers on SiH substrate. AFM height images of adsorbed polymer layers on different surfaces confirm this finding. AFM height images of initially 50 nm thick linear PS films that are annealed at 150 °C for 168 h and leached with toluene using same washing conditions show smoother surface on SiO_x compared to SiH. The value of $\sigma_{rms,\ AFM}$ is 0.26 nm on SiO_x, whereas it is 0.45 nm on SiH surface.

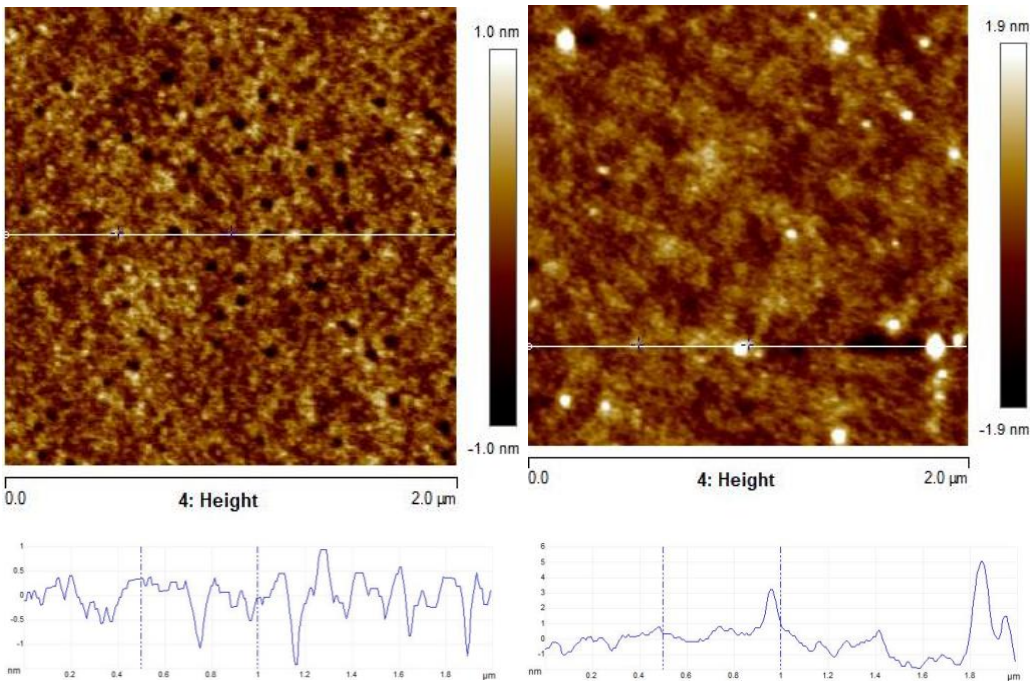

Figure 3.25. AFM height images in intermittent-contact mode for adsorbed linear PS layers after 168 h annealing and toluene leaching on SiO_x (left), and on SiH (right).

Surface morphologies of 4-arm star PS adsorbed layers on SiO_x and on SiH are shown in Figure 3.26. Overall, on both surfaces the surface roughness of the adsorbed layer

is very small. On SiH, the layer has lot of small holes but none of them extends deeper than 2 nm. The reason for the formation of holes is not clear. One may imagine these holes may indicate very early stages of dewetting. However, the fact that PS sticks better to SiH surface due to net attractive interaction as well as large molecular weight of PS chains weakens this hypothesis.

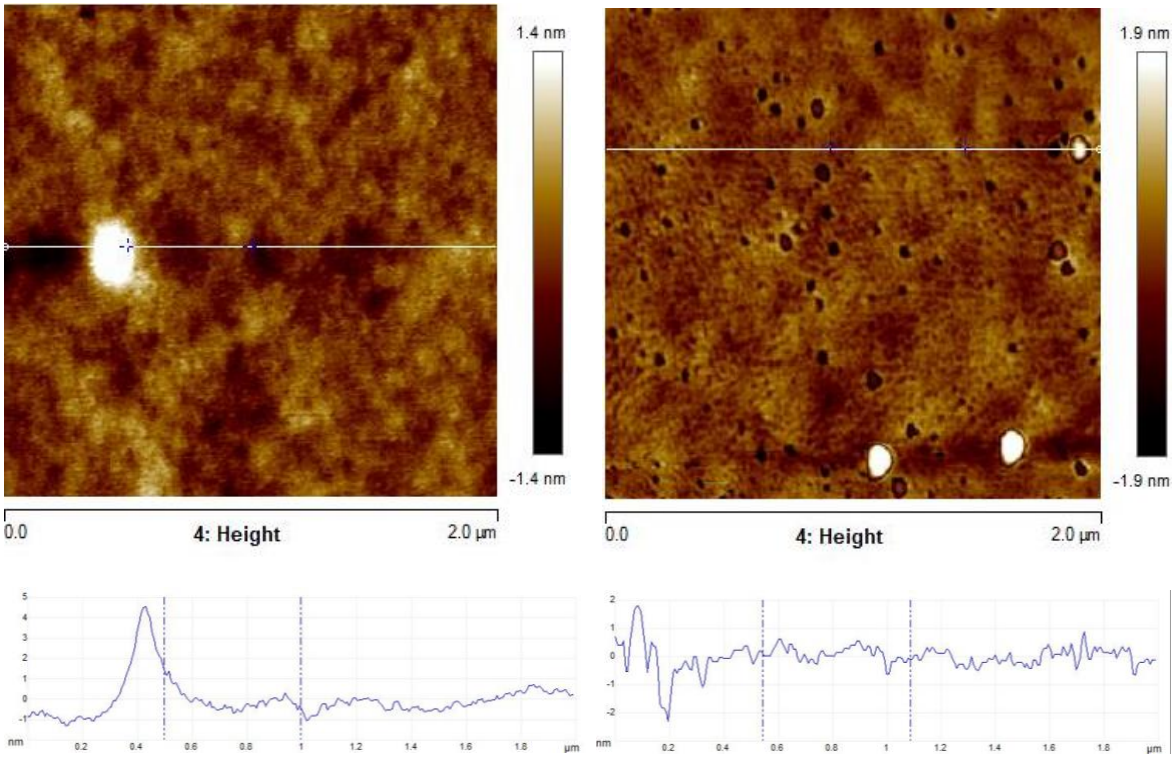

Figure 3.26 AFM height images in intermittent-contact mode for adsorbed 4-arm star PS layers after 120 h annealing and toluene leaching a) on SiO_x (left), and b) on SiH (right).

AFM height images for the adsorption of centipede PS chains on SiO_x and SiH are shown in Figure 3.27. Adsorbed layer for centipede PS after 120 h annealing on SiO_x has a very smooth surface but on SiH there are many bumps which makes the surface rough.

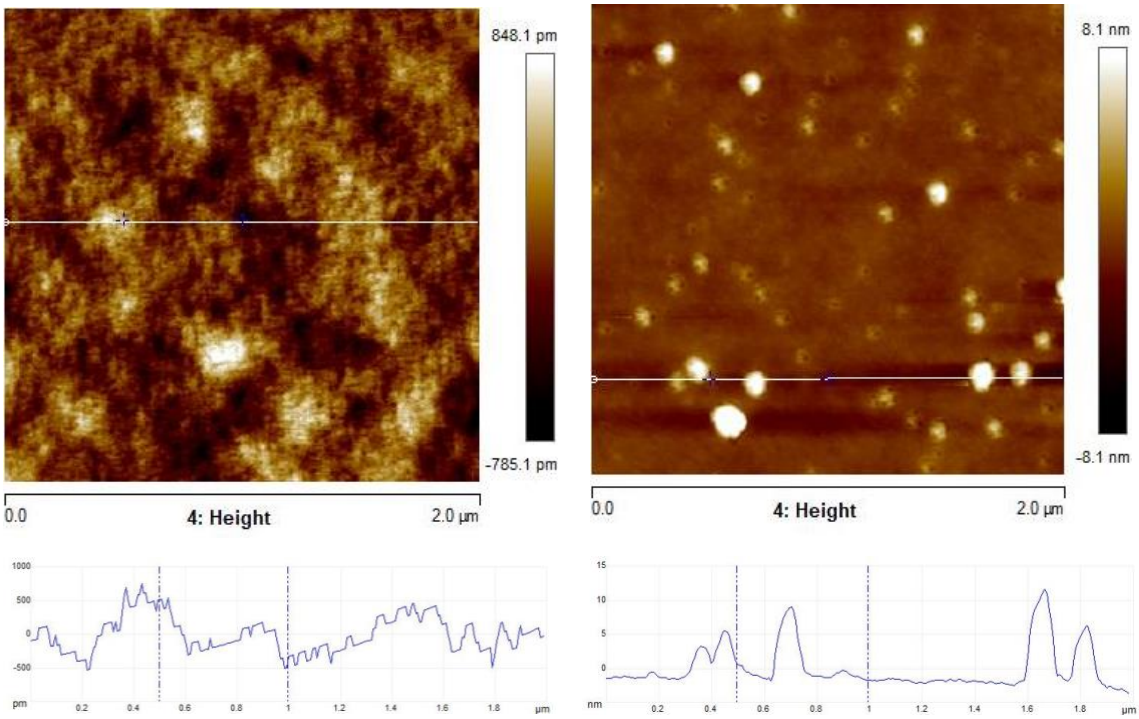

Figure 3.27 AFM height images in intermittent-contact mode for adsorbed layer of centipede PS after 120 h annealing and toluene leaching a) on SiO_x (left), and b) on SiH (right).

3.3. Effect of Solvent Leaching

Solvent polymer interactions play a crucial role for extracting non-adsorbed and loosely adsorbed chains during leaching process. Although PS is accepted as a non-polar polymer with small dipole moment [55] (Table 2) when solvent molecules penetrate into the film, polar interactions as well play an important role. Chloroform and toluene are the most used solvents for leaching studies of linear PS thin films in the literature. Chloroform is a more polar solvent and its polarity causes spinodal dewetting of adsorbed PS layers much earlier compared to toluene leaching [56]. However, Koga and coworkers claimed that to be able to remove all the loosely adsorbed chains to probe flattened layer chloroform leaching is essential [57].

Table 2. Dipole moments of materials used.

	Dipole Moment (π/D)
Polystyrene	0.375 ± 0.0010
Toluene	1.04 ± 0.02
Chloroform	1.75 ± 0.03

Flory-Huggins interaction parameter between chloroform and PS, $\chi_{PS\text{-}CHCl3}$, is smaller than that between toluene and PS. Hence, chloroform is known to be a better solvent for PS as compared to toluene. Surface morphology and layer structure are expected to be affected by solvent-polymer interactions. Despite the calculated values Unni et al. experimentally demonstrated that the toluene is a better solvent for leaching studies done on adsorbed linear PS layers.

We have tested the effectiveness of these two solvents on our adsorbed layers. Same leaching procedure is applied on adsorbed centipede PS layer after 96 h annealing on SiH using chloroform and toluene. After annealing is finished, samples are rapidly quenched to room temperature and leached with fresh solvent for 10 minutes and this process is repeated 5 times. XR curves show that there is a 13.3 nm thick residual adsorbed layer remained after toluene leaching of initially 50 nm thick film. Air surface seems to be smooth with rms roughness of 0.97 nm. Whereas, same leaching experiment with chloroform left 16.2 nm thick centipede PS adsorbed layer with rms roughness of 1.6 nm. SLD profile indicates no difference between the SLD values of the adsorbed layers obtained after different solvent leaching.

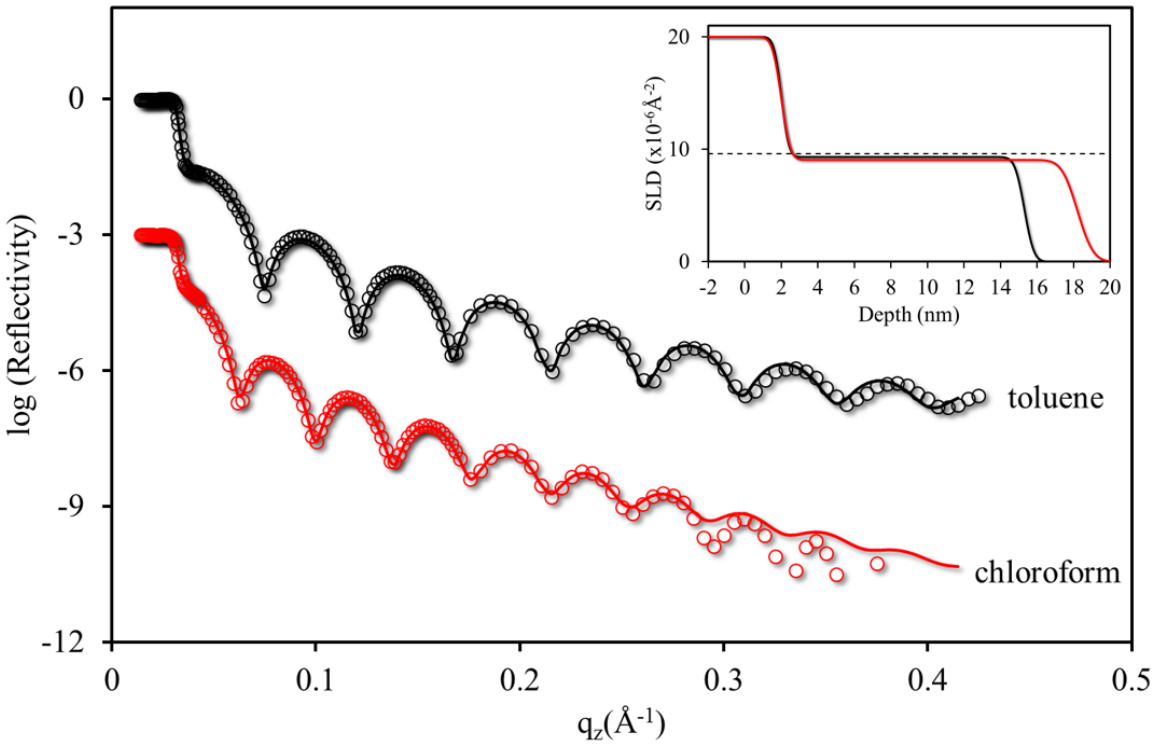

Figure 3.28. XR data (symbols) and best fit model curves (solid curves) as a function of q_z for adsorbed centipede PS layer on SiH after 96 h of annealing at 150°C and washed with toluene (black) and chloroform (red) leached. Adjacent curves have been shifted vertically by log (10)$^{-3}$ for clarity.

Thickness change after each leaching step is followed by ellipsometry and results are plotted in Figure 3.30. Leaching the annealed polymer films 5 times with fresh solvent and for 10 minutes is a standard protocol in the literature. However, data in Figure 3.30 reveals that most of the non-adsorbed chains are washed away in the first leaching step and in consecutive leaching steps thickness of the layer decreases very slightly. Another important difference to note is that toluene leaching removes more adsorbed chains than chloroform leaching.

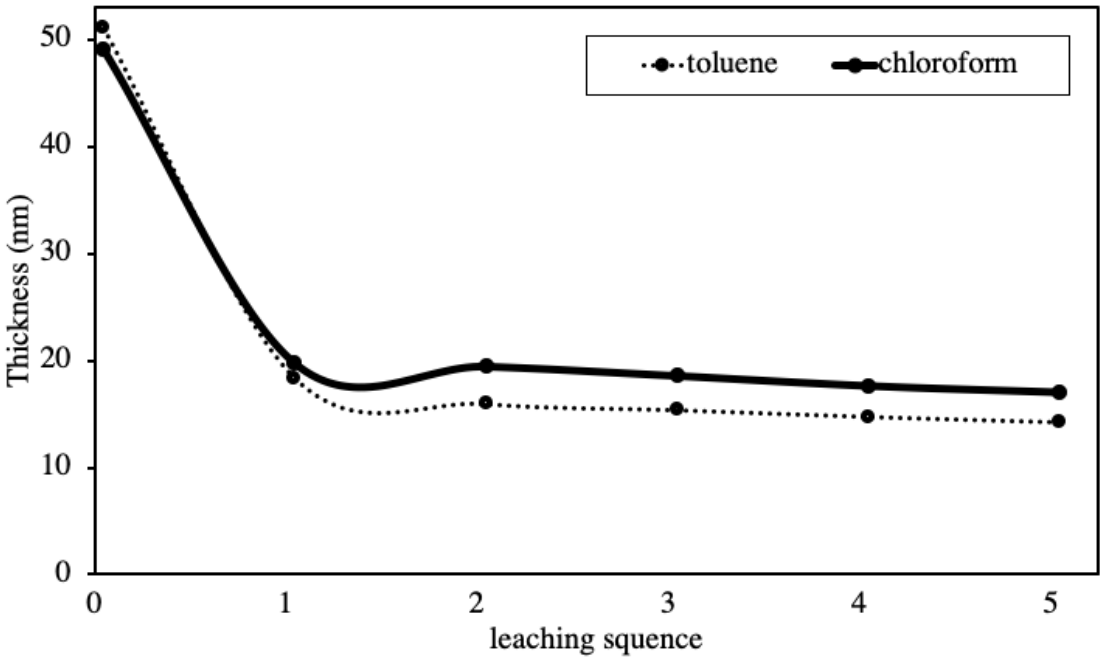

Figure 3.29. Variation of thickness as a function of number of leaching steps for centipede PS layer on SiH upon leaching with toluene (dash line) and chloroform (solid line).

Further leaching is usually required to remove loosely adsorbed polymer chains for reaching to flattened polymer layer. Gin et al., claimed that 120 days of toluene leaching is necessary to obtain only flattened layer [54]. Jiang et al. on the other side reported that the flattened layer can be obtained after shorter period of chloroform leaching [56]. Personal conversations with Jiang pointed out that only two weeks of chloroform leaching is sufficient to reach flattened layer but the same results are not reproduced in our lab. Therefore, prolonged leaching in both solvents is tested for linear PS, 4-arm star PS, comb PS and centipede PS on SiH adsorbed layers obtained after 120 h annealing. Comparing the layer thicknesses up to 7 days demonstrated that toluene leaching removes more adsorbed chains and remaining adsorbed layer is always thinner after toluene leaching. Because of this reason further leaching experiments are only done using toluene. Thickness change upto 36 days of leaching is monitored by ellipsometer (Figure 3.30). Desorption kinetics of linear PS and 4-arm star PS seem to be very similar. Comb PS and centipede PS have similar desorption kinetics as well. It's a remarkable observation because their desorption kinetics show a similar trend to their adsorption kinetics. After extensive leaching in toluene adsorbed

centipede PS remains to be the thickest layer and adsorbed linear PS forms the thinnest layer between all the samples.

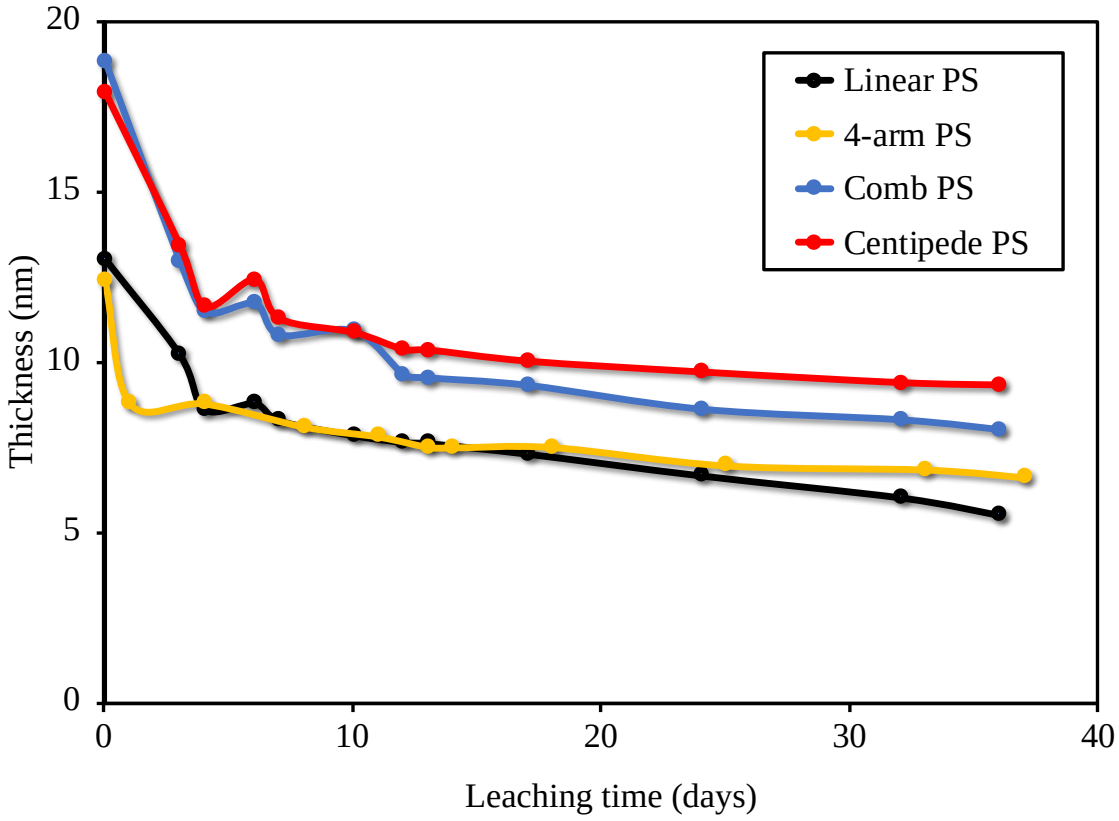

Figure 3.30. Adsorbed layer thickness change of 120 h annealed linear, 4-arm star PS, comb PS and centipede PS adsorbed layer on SiH during prolonged leaching time.

XR data (Figure 3.31) and SLD profiles (Figure 3.32) are shown for linear PS after first and prolonged leaching. Thickness of adsorbed layer is 11.6 nm after 50 minutes of toluene leaching and 4 nm after 36 days. SLD profile shows that there is a single layer with bulk-like density after first leaching but two layer structure become more dominant as leaching time increases.

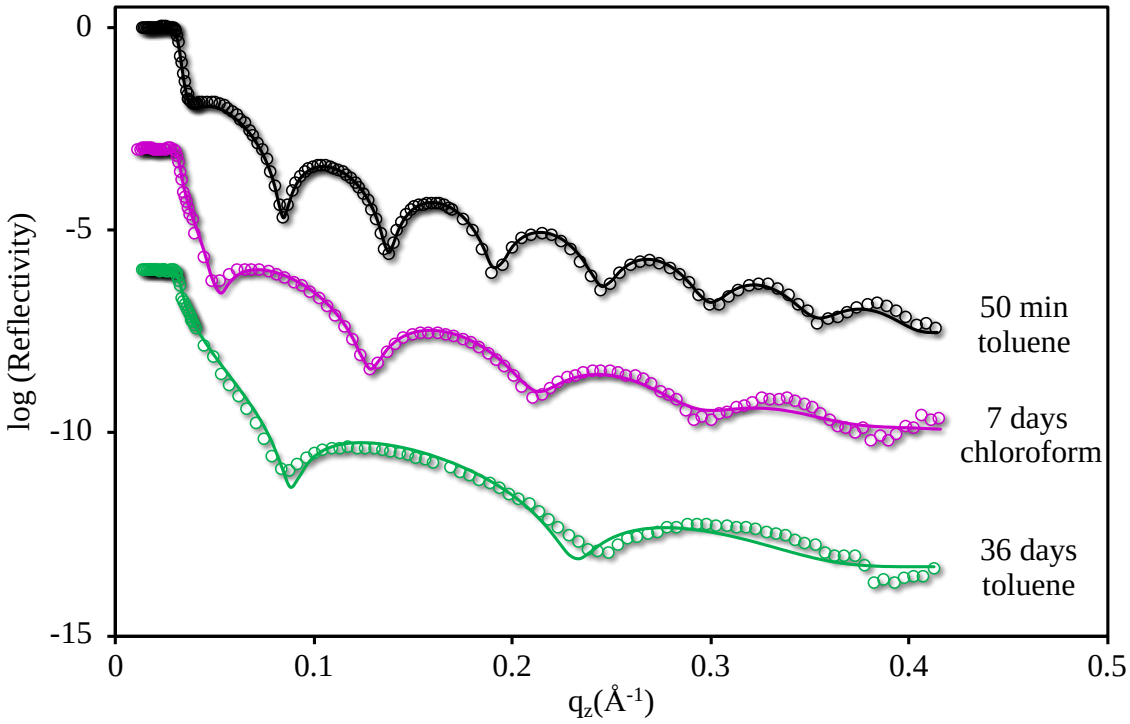

Figure 3.31. X-Ray Reflectivity data and best fit model curves as a function of wavevector in the direction of normal to the surface, (q_z) for linear PS on SiH for 120 h annealed linear PS adsorbed layer on SiH, after 50 min, 7 days chloroform, 36 days toluene.

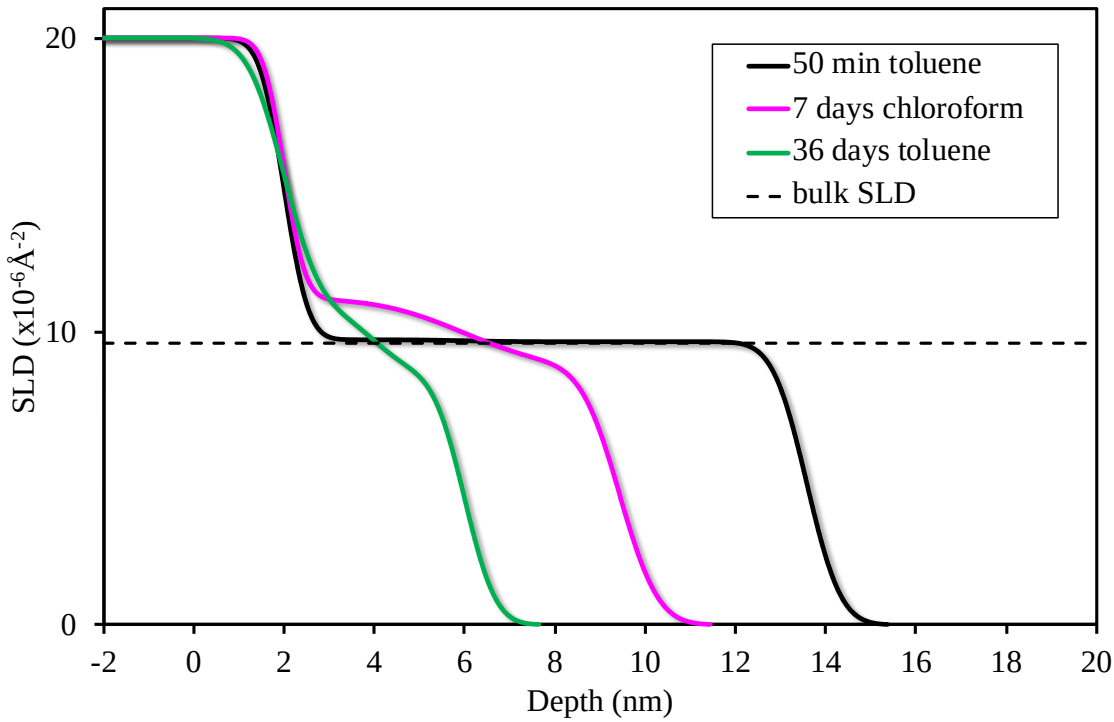

Figure 3.32. SLD profiles as a function of depth for 120 hours annealed linear PS adsorbed layer on SiH, after 50 minutes leaching with toluene, 7 days leaching with chloroform and 36 days leaching with toluene.

AFM images of linear PS after 50 minutes of toluene (a), 7 days of chloroform (b) and 36 days of toluene (c) leaching are shown in Figure 3.33. The surface of adsorbed layer is very smooth after 50 min of toluene leaching and 7 days of chloroform leaching. Lots of holes are observed after 36 days of toluene leaching with maximum 2 nm depth.

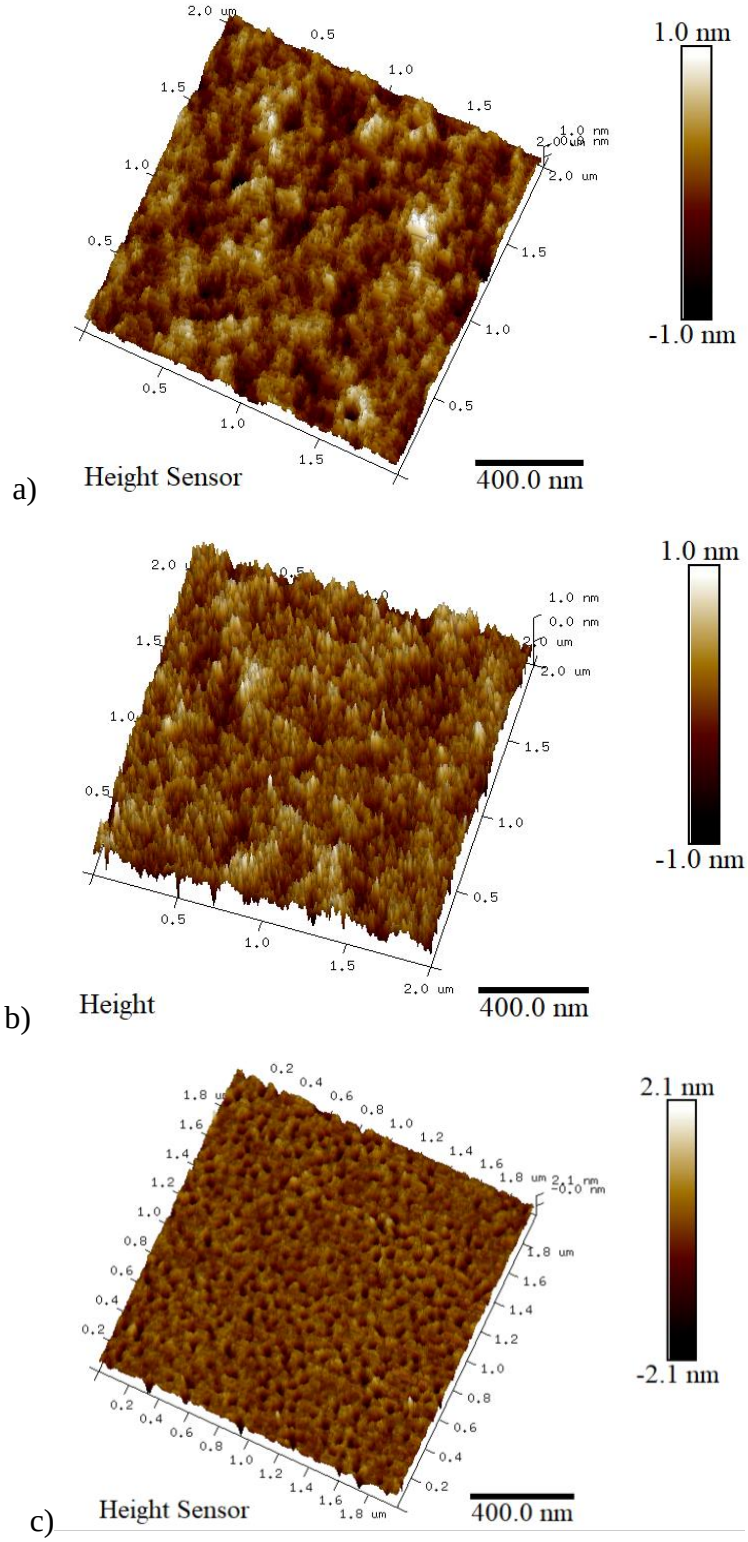

Figure 3.33. 3D AFM images of 120 hours annealed Linear PS on SiH a) 50 min toluene leached b) 7 days chloroform leached and c) 36 days toluene leached.

XRR data and best model fits for adsorbed centipede PS layers after 50 min toluene, 7 days of chloroform and 36 days of toluene leaching are shown in Figure 3.34. The increase in fringe spacing clearly reveals that most of the loosely adsorbed polymer chains are washed away.. After first toluene leaching for 50 min, 16.1 nm thick adsorbed layer remains from originally 50 nm thick centipede PS film. Chloroform leaching for 7 days decreases the adsorbed layer thickness to 11.5 nm and after 36 days of toluene leaching only 7.9 nm thick adsorbed layer remains. SLD profiles given in Figure 3.35 demonstrates that after each washing process the layer can be modeled using a single layer of bulk SLD. Only layer thicknesses change after each leaching and the air surface is smooth in each case. Comparison with adsorbed linear PS, adsorbed centipede PS has more stable structure.

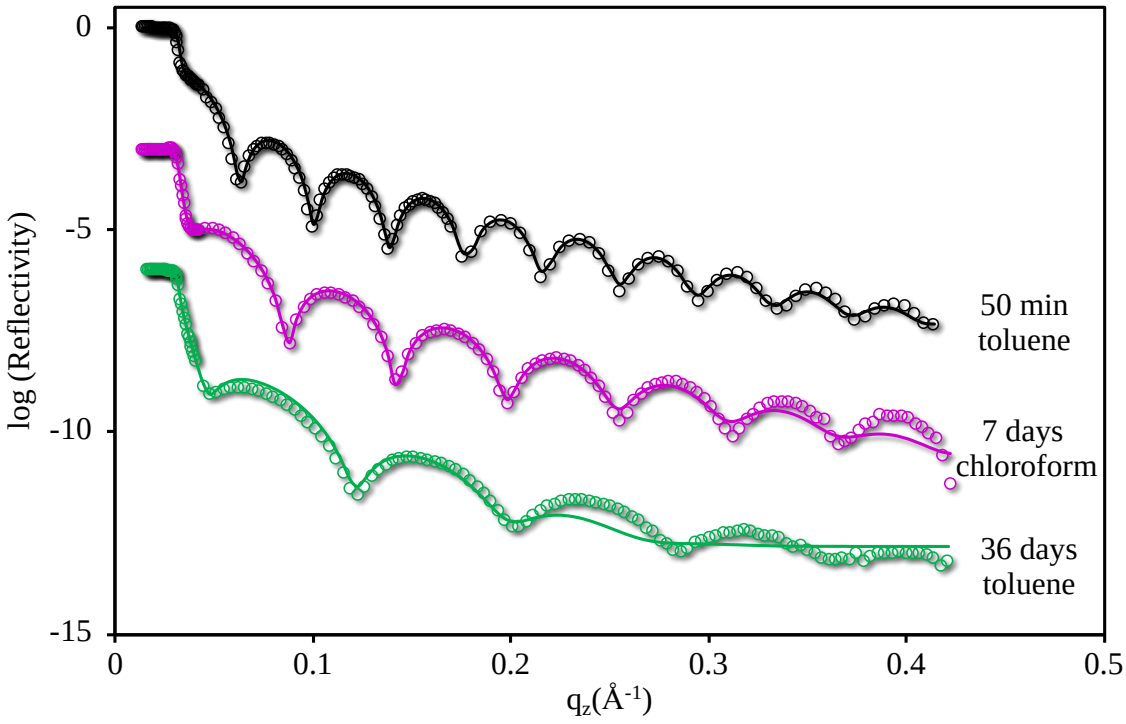

Figure 3.34. X-Ray reflectivity data (open symbols) and best fit model curves (solid curves) as a function of q_z for adsorbed centipede PS on SiH after 50 min leaching with toluene (black line), 7 days leaching with chloroform (red line) and 36 days leaching with toluene (green line). Adjacent curves have been shifted vertically by log (10)$^{-3}$ for clarity.

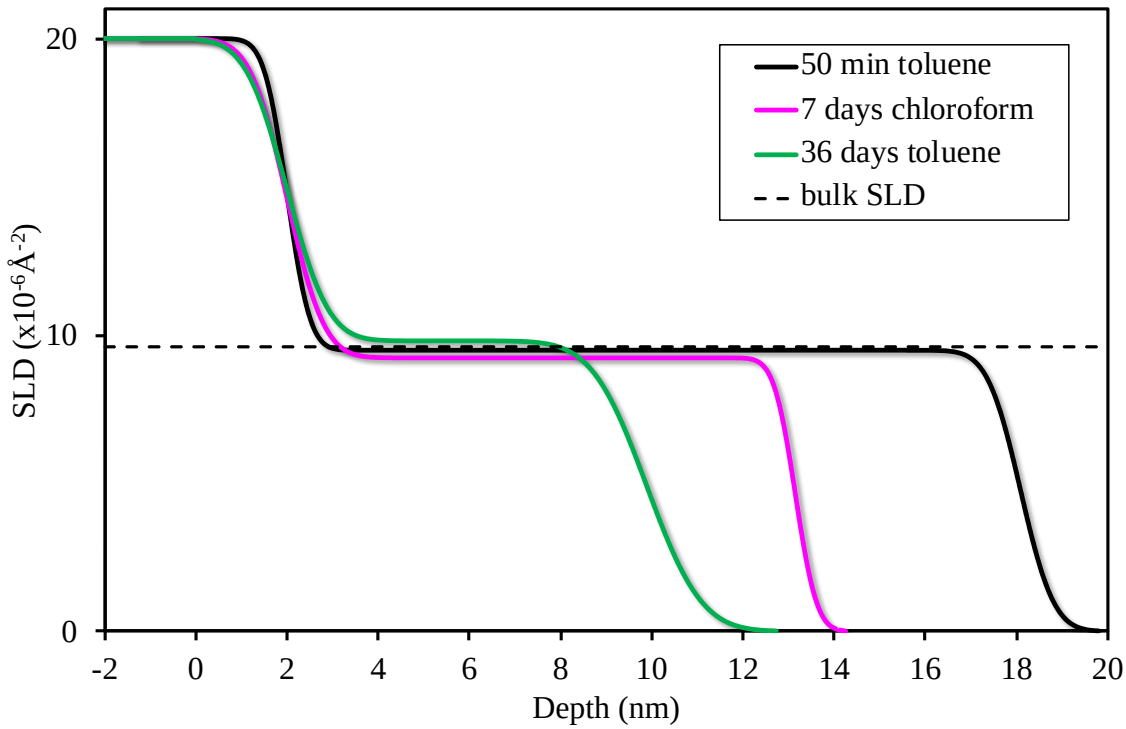

Figure 3.35. SLD profiles as a function of depth for 120 hours annealed centipede PS adsorbed layer on SiH, after 50 min leaching with toluene (black line), 7 days leaching with chloroform (red line) and 36 days leaching with toluene (green line).

AFM images of adsorbed centipede PS after 50 minutes of toluene leaching (a), 7 days of chloroform (b) and 36 days of toluene (c) is shown in Figure 3.36. Consistent with XR data, AFM images show very smooth surfaces after each leaching process.

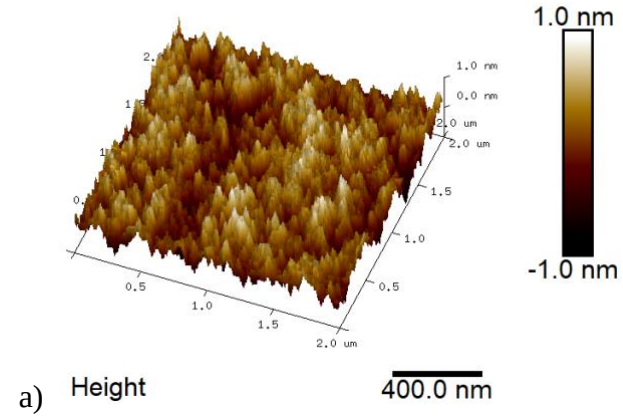

a)

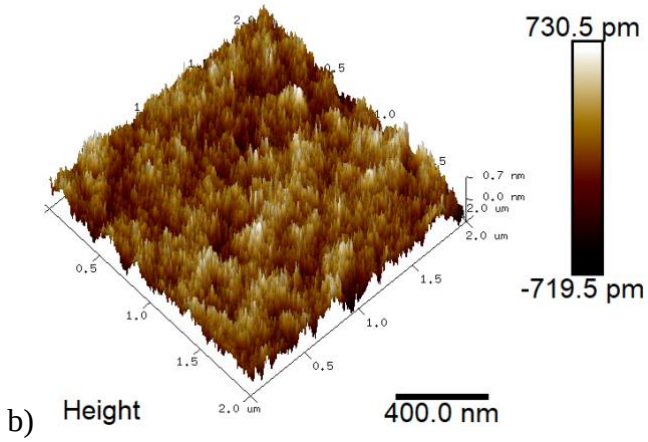

b)

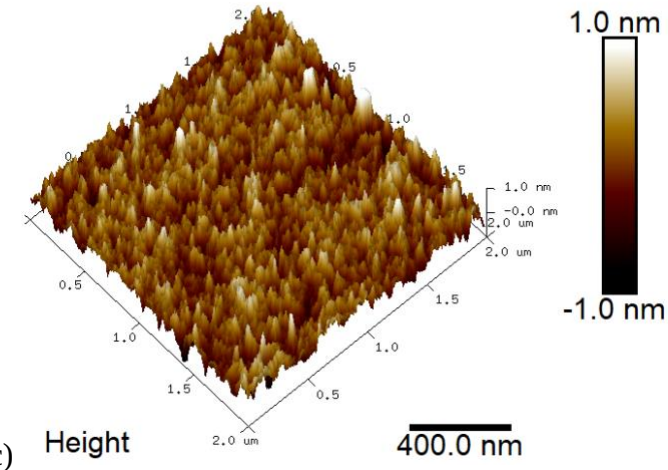

c)

Figure 3.36. 3D AFM images of 120 h annealed centipede PS on SiH a) 50 min toluene leached b) 7 days chloroform leached and c) 36 days toluene leached.

5. CONCLUSIONS

The most important result of this work is to prove that adsorbed layer formation and structure can be changed by modifying polymer architecture. Being able to control the character of the adsorbed layer with changes in entropic part paves the way for new pathways to tune the physical properties of thin polymer films.

Ellipsometry measurements on the time evolution of adsorbed PS layers showed that shape of the growth curves and overall adsorbed layer thickness depends on the architecture of the polymer. Equilibrium adsorbed layer thickness increases with increasing branching. Centipede PS yields the thickest adsorbed layers on hydrophilic and hydrophobic surfaces. Centipede adsorbed PS layer has twice as much thicker than the linear PS adsorbed layer on SiOx surface. Our results demonstrated that the adsorbed layer thickness increases in the following order: linear PS < 4-arm star PS< comb PS < centipede PS. When one moves from linear to centipede, conformational entropy of the polymer decreases in bulk and during the adsorption process centipede polymer does not lose as much entropy as a linear polymer does. Even though the enthalpic gain per segment is identical, the differences in the entropic loss get smaller for more branched architectures and hence, branched polymers adsorb to form thicker layers. The number of contacts a polymer can make also depends on the architecture of the polymer as shown by Kosmas et al. theoretically [35]. However, in this study we are not able to extract any experimental information about the number of contacts each polymer can make.

Variation in surface energy of the substrate has a significant effect on the adsorbed layer. Adsorbed layer thickness is always larger on SiH surface than on SiO_x surface. This is not surprising since hydrophobic PS chains have a stronger segment-surface interactions with SiH surface compared to hydrophilic SiO_x surface. Adsorption kinetics is also different on these surfaces. On SiH surface, adsorption is very fast, slope of the growth curve is very steep, and equilibrium adsorbed layer is formed after 8 h to 16 h of annealing. However, on SiO_x adsorption process is slower, growth curve shows a gradual increase of thickness over 64 h to 100 h before reaching equilibrium value. Surfaces of the adsorbed layers are always smoother on SiOx compared to on SiH.

Independent of the polymer architecture, adsorbed layer after long annealing times always modeled with a single layer of uniform and bulk-like density on both surfaces. This is at least not consistent with the earlier literature. However, at earlier annealing times we have observed the existence of second layer next to the substrate on SiH. This layer is formed by the mixture of adsorbed PS chains and islands of growing SiOx. Once the surface sites are all covered by adsorbed PS chains we haven't detected the presence of SiO_x and single layer is sufficient to describe our data. It is important to note that at intermediate annealing times when the SLD of this mixed layer decreases, one can assume this is an adsorbed layer with higher density. On SiO_x surface, XR data is always modeled using a single layer of bulk density for each architecture. Despite all of the different architectures almost have the same structure, their overall thicknesses and growth kinetics are different.

Lastly, it is found that solvent quality plays an important role in desorption process. Although it is claimed in the literature that chloroform can extract the loosely adsorbed chains in a few days where toluene leaching requires months, our experiments demonstrate that toluene extracts much more non-adsorbed and loosely adsorbed chains compared to chloroform under the same conditions. This fact is confirmed for each architucture and each annealing time on both hydrophilic and hydrophobic surfaces.

REFERENCES

[1] J. Nunzi, “Organic photovoltaic materials and devices,” *C. R. Phys.*, vol. 3, pp. 523–542, 2002.

[2] B. Jeong *et al.*, “Interfacial polymerization of thin film nanocomposites : A new concept for reverse osmosis membranes,” vol. 294, pp. 1–7, 2007.

[3] E. Ostuni, R. t G. Chapman, R. E. ik Holmlin, S. Takayama, and G. M. Whitesides, “A Survey of Structure-Property Relationships of Surfaces that Resist the Adsorption of Protein,” vol. 17, no. 9, pp. 5605–5620, 2001.

[4] S. Jegadesan, S. Sindhu, and S. Valiyaveettil, “Easy Writing of Nanopatterns on a Polymer Film Using Electrostatic Nanolithography,” vol. 1, pp. 481–484, 2006.

[5] X. Liu and P. X. Ma, “Polymeric Scaffolds for Bone Tissue Engineering,” *Ann. Biomed. Eng.*, vol. 32, no. 3, pp. 477–486, 2004.

[6] A. Silberberg, “Adsorption of flexible macromolecules. IV. Effect of solvent-solute interactions, solute concentration, and molecular weight,” *J. Chem. Phys.*, vol. 48, no. 7, pp. 2835–2851, 1968.

[7] C. A. J. Hoeve, “On The General Theory of Polymer Absorption at a Surface,” *J. Polym. Sci., Part C*, vol. No. 30, no. 3, pp. 361–367, 1970.

[8] R. J. Roe, “Multilayer theory of adsorption from a polymer solution,” *J. Chem. Phys.*, vol. 60, no. 11, pp. 4192–4207, 1974.

[9] J. M. H. M. Scheutjens and G. J. Fleer, “Statistical Theory of the Adsorption of Interacting Chain Molecules. 1. Partition Function, Segment Density Distribution, and Adsorption Isotherms,” *J. Phys. Chem.*, vol. 83, no. 12, pp. 1619–1635, 1979.

[10] N. Jiang *et al.*, “Nanoscale adsorbed structures as a robust approach for tailoring polymer film stability,” *Soft Matter*, vol. 12, no. 6, pp. 1801–1809, 2016.

[11] E. P. Enriquez, H. M. Schneider, and S. Granick, “PMMA Adsorption Over Previously Adsorbed PS Studied by Polarized FTIR-ATR,” *J. Polym. Sci. Part B Polym. Phys.*, vol. 33, pp. 2429–2437, 1995.

[12] Granick, H. Johnson, and D. Leonhardt, “Adsorption Isotope Effect for Protio- and Deuteropolystyrene at a Single Solid Surface,” *Macromolecules*, vol. 39, pp. 2723–2725, 2006.

[13] M. A. Cohen Stuart, G. J. Fleer, and J. M. H. M. Scheutjens, “Displacement of Polymers Theory . Segmental Adsorption Energy from Polymer Desorption in Binary Solvents,” *J. Colloid lnterface Sci.*, vol. 97, no. 2, pp. 515–525, 1984.

[14] G. P. van der Beek, M. A. Cohen Stuart, G. J. Fleer, and J. E. Hofman, “A Chromatographic Method for the Determination of Segmental Adsorption Energies of Polymers. Polystyrene on Silica,” *Langmuir*, vol. 5, no. 5, pp. 1180–1186, 1989.

[15] P. Franz and S. Granick, “Kinetics of Polymer Adsorption and Desorption,” *Am. Phys. Soc.*, vol. 66, no. 7, pp. 899–902, 1991.

[16] N. Jiang *et al.*, “Effect of CO2 on a mobility gradient of polymer chains near an impenetrable solid,” *Macromolecules*, vol. 48, no. 6, pp. 1795–1803, 2015.

[17] D. E. Martinez-Tong, B. Vanroy, M. Wübbenhorst, A. Nogales, and S. Napolitano, “Crystallization of Poly (L-lactide) Confined in Ultrathin Films : Competition between Finite Size Effects and Irreversible Chain Adsorption,” *Macromolecules*, vol. 47, pp. 2354–2360, 2014.

[18] T. Koga *et al.*, “Impact of an irreversibly adsorbed layer on local viscosity of nanoconfined polymer melts,” *Phys. Rev. Lett.*, vol. 107, no. 22, pp. 1–5, 2011.

[19] H. K. Nguyen, M. Labardi, M. Lucchesi, P. Rolla, and D. Prevosto, “Plasticization in Ultrathin Polymer Films : The Role of Supporting Substrate and Annealing,” *Macromolecules*, vol. 46, no. 2, pp. 555–561, 2013.

[20] M. J. Burroughs, S. Napolitano, D. Cangialosi, and R. D. Priestley, “Direct measurement of glass transition temperature in exposed and buried adsorbed polymer nanolayers,” *Macromolecules*, vol. 49, no. 12, pp. 4647–4655, 2016.

[21] Y. Zhang, K. K. Gangwani, and R. M. Lemert, “Sorption and swelling of block copolymers in the presence of supercritical fluid carbon dioxide,” *J. Supercrit. Fluids*, vol. 11, pp. 115–134, 1997.

[22] T. Koga *et al.*, “Dynamics of polymer thin films in supercritical carbon dioxide,” *Europhys. Lett.*, vol. 60, no. 4, pp. 559–565, 2002.

[23] M. L. Braatz, L. Infantas Meléndez, M. Sferrazza, and S. Napolitano, “Unexpected impact of irreversible adsorption on thermal expansion: Adsorbed layers are not that dead,” *J. Chem. Phys.*, vol. 146, no. 20, 2017.

[24] B. Vanroy, M. Wübbenhorst, and S. Napolitano, “Crystallization of thin polymer layers confined between two adsorbing walls,” *ACS Macro Lett.*, vol. 2, no. 2, pp. 168–172, 2013.

[25] Z. Yang, Y. Fujii, F. K. Lee, C.-H. Lam, and O. K. C. Tsui, “Glass Transition Dynamics and Surface Layer Mobility in Unentangled Polystyrene Films,” *Science (80-.).*, vol. 328, pp. 1676–1679, 2010.

[26] R. D. Priestley, C. J. Ellison, L. J. Broadbelt, and J. M. Torkelson, “Structural Relaxation of Polymer Glasses at Surfaces , Interfaces , and In Between,” *Science (80-.).*, vol. 309, no. 5733, pp. 456–459, 2005.

[27] K. Fukao and Y. Miyamoto, “Glass transitions and dynamics in thin polymer films : Dielectric relaxation of thin films of polystyrene,” *Phys. Rev. E*, vol. 61, no. 2, pp. 1743–1754, 2000.

[28] E. Glynos, B. Frieberg, H. Oh, M. Liu, D. W. Gidley, and P. F. Green, “Role of Molecular Architecture on the Vitrification of Polymer Thin Films,” vol. 128301, no. March, pp. 3–6, 2011.

[29] S. Napolitano, A. Pilleri, P. Rolla, and M. Wübbenhorst, “Unusual deviations from bulk behavior in ultrathin films of poly(tert-butylstyrene): Can dead layers induce a reduction of Tg?,” *ACS Nano*, vol. 4, no. 2, pp. 841–848, 2010.

[30] S. Napolitano and D. Cangialosi, “Interfacial Free Volume and Vitri fi cation: Reduction in T,” 2013.

[31] Y. Grohens, M. ice Brogly, C. Labbe, M. ie-O. David, and J. acques Schultz, “Glass Transition of Stereoregular Poly(methyl methacrylate) at Interface,” vol. 14, no. 8, pp. 1996–1999, 2002.

[32] C. Housmans, M. Sferrazza, and S. Napolitano, “Kinetics of irreversible chain adsorption,” *Macromolecules*, vol. 47, no. 10, pp. 3390–3393, 2014.

[33] D. N. Simavilla, W. Huang, P. Vandestrick, J. P. Ryckaert, M. Sferrazza, and S. Napolitano, “Mechanisms of Polymer Adsorption onto Solid Substrates,” *ACS Macro*

Lett., vol. 6, no. 9, pp. 975–979, 2017.

[34] C. J. Durning, B. O. Shaughnessy, and U. Sawhney, "Adsorption of Poly (methyl methacrylate) Melts on Quartz," pp. 6772–6781, 1999.

[35] M. K. Kosmas, "Ideal Polymer Chains of Various Architectures at a Surface," *Macromolecules*, no. 8, pp. 2061–2065, 1990.

[36] M. Kawaguchi and A. Takahashi, "Ellipsometric Study of the Adsorption of Comb-Branched Polystyrene Onto a Metal Surface.," *J. Polym. Sci. Part A-2, Polym. Phys.*, vol. 18, no. 5, pp. 943–950, 1980.

[37] C. C. van der Linden, F. A. M. Leermakers, and G. J. . Fleer, "Adsorption of Comb Polymers," *Macromolecules*, no. 29, pp. 1000–1005, 1996.

[38] J. S. Y. Chia, T. T. T. Michelle, J. K. Chin, P. S. Khiew, and H. Lee, "A Parametric Study on the Synthesis of Graphene Using Piranha-like Thermal Exfoliation," *2012 2nd Int. Conf. Environ. Sci. Biotechnol. IPCBEE*, vol. 48, pp. 143–147, 2014.

[39] V. Datsyuk *et al.*, "Chemical oxidation of multiwalled carbon nanotubes," *Carbon N. Y.*, vol. 46, no. 6, pp. 833–840, 2008.

[40] J. R. Vig and J. W. L. Bus, "UV/Ozone Cleaning of Surfaces," *IEEE Trans. Parts, Hybrids, Packag.*, vol. 12, no. 4, pp. 365–370, 1976.

[41] P. Ponath, A. . B. Posadas, and A. A. Demkov, "Ge(001) surface cleaning methods for device integration," *Appl. Phys. Rev.*, vol. 4, no. 2, p. 021308, 2017.

[42] V. A. Burrows, Y. J. Chabal, G. S. Higashi, K. Raghavachari, and S. B. Christman, "Infrared spectroscopy of Si(111) surfaces after HF treatment: Hydrogen termination and surface morphology," *Appl. Phys. Lett.*, vol. 53, no. 11, pp. 998–1000, 1988.

[43] M. T. García, I. Gracia, G. Duque, A. De Lucas, and J. F. Rodríguez, "Study of the solubility and stability of polystyrene wastes in a dissolution recycling process," *Waste Manag.*, vol. 29, pp. 1814–1818, 2009.

[44] N. Sahu, B. Parija, and S. Panigrahi, "Fundamental understanding and modeling of spin coating process: A review," *Indian J. Phys.*, vol. 83, no. 4, pp. 493–502, 2009.

[45] D. Meyerhofer, "Characteristics of resist films produced by spinning Characteristics of resist films produced by spinning," *J. Appl. Phys.*, vol. 49, no. 7, pp. 3993–3997,

1978.

[46] N. Jiang *et al.*, “Stability of Adsorbed Polystyrene Nanolayers on Silicon Substrates,” *Macromol. Chem. Phys.*, vol. 219, no. 3, p. 1700326, 2018.

[47] S. Bhattacharjee, “Review article DLS and zeta potential – What they are and what they are not ?,” *J. Control. Release*, vol. 235, pp. 337–351, 2016.

[48] S. Ciccariello, J. Goodisman, and H. Brumberger, “On the porod law,” *J. Appl. Crystallogr.*, vol. 21, pp. 117–128, 1988.

[49] T. C. Huang, R. Gilles, and G. Will, “Thin-film thickness and density determination from x-ray reflectivity data using a conventional power diffractometer,” *Thin Solid Films*, vol. 230, no. 2, pp. 99–101, 1993.

[50] R. R. L. De Oliveira, D. A. C. Albuquerque, T. G. S. Cruz, F. M. Yamaji, and F. L. Leite, “Measurement of the Nanoscale Roughness by Atomic Force Microscopy: Basic Principles and Applications,” in *Atomic Force Microscopy - Imaging, Measuring and Manipulating Surfaces at the Atomic Scale*, 2012, pp. 147-.

[51] H. Su, C. Lee, M. Lin, and T. Huang, “A Comparison Between X-ray Reflectivity and Atomic Force Microscopy on the Characterization of a Surface Roughness A comparison of X-ray reflectivity (XRR) and atomic force microscopy (AFM) on measuring the surface morphology is studied in this work .,” *Chinese J. Phys.*, vol. 50, no. 2, pp. 291–300, 2012.

[52] Y. Fujii, Z. Yang, J. Leach, H. Atarashi, K. Tanaka, and O. K. C. Tsui, “Affinity of polystyrene films to hydrogen-passivated silicon and its relevance to the Tgof the films,” *Macromolecules*, vol. 42, no. 19, pp. 7418–7422, 2009.

[53] P. A. Kienzle, K. V. O’Donovan, J. F. Ankner, N. F. Berk, and C. F. Majkrzak, “NCNR Reflectometry Software,” *http://www. ncnr.nist.gov/reflpak.*, 2006. .

[54] P. Gin *et al.*, “Revealed architectures of adsorbed polymer chains at solid-polymer melt interfaces,” *Phys. Rev. Lett.*, vol. 109, no. 26, pp. 1–5, 2012.

[55] D. P, “CRC Handbook of Chemistry and Physics,” *Journal of Molecular Structure*, vol. 268, no. 1–3. p. 320, 1992.

[56] N. Jiang, J. Shang, X. Di, M. K. Endoh, and T. Koga, “Formation mechanism of high-density, flattened polymer nanolayers adsorbed on planar solids,” *Macromolecules*,

vol. 47, no. 8, pp. 2682–2689, 2014.

[57] A. Beena Unni *et al.*, “Solvent Assisted Rinsing: Stability/Instability of Ultrathin Polymer Residual Layer,” *Macromolecules*, vol. 49, no. 5, pp. 1807–1815, 2016.